CAPSULE ENDOSCOPY SYSTEM WITH NOVEL

IMAGING ALGORITHMS

A Thesis Submitted to the

College of Graduate Studies and Research

in Partial Fulfillment of the Requirements

for the degree of Doctor of Philosophy

in the Department of Electrical and Computer Engineering

University of Saskatchewan

Saskatoon, Saskatchewan, Canada

By

Tareq Hasan Khan

PERMISSION TO USE

In presenting this thesis in partial fulfilment of the requirements for a Postgraduate degree from the University of Saskatchewan, I agree that the Libraries of this University may make it freely available for inspection. I further agree that permission for copying of this thesis in any manner, in whole or in part, for scholarly purposes may be granted by the professor or professors who supervised my thesis work or, in their absence, by the Head of the Department or the Dean of the College in which my thesis work was done. It is understood that any copying or publication or use of this thesis or parts thereof for financial gain shall not be allowed without my written permission. It is also understood that due recognition shall be given to me and to the University of Saskatchewan in any scholarly use which may be made of any material in my thesis.

Requests for permission to copy or to make other use of material in this thesis in whole or part should be addressed to:

Head of the Department of Electrical and Computer Engineering

University of Saskatchewan,

57 Campus Drive, Saskatoon,

Saskatchewan, S7N 5A9,

Canada.

ABSTRACT

Wireless capsule endoscopy (WCE) is a state-of-the-art technology to receive images of human intestine for medical diagnostics. In WCE, the patient ingests a specially designed electronic *capsule* which has imaging and wireless transmission capabilities inside it. While the capsule travels through the gastrointestinal (GI) tract, it captures images and sends them wirelessly to an outside *data logger* unit. The data logger stores the image data and then they are transferred to a personal computer (PC) where the images are reconstructed and displayed for diagnosis. The key design challenge in WCE is to reduce the area and power consumption of the capsule while maintaining acceptable image reconstruction.

In this research, the unique properties of WCE images are identified by analyzing hundreds of endoscopic images and video frames, and then these properties are used to develop novel and low complexity compression algorithms tailored for capsule endoscopy. The proposed image compressor consists of a new YEF color space converter, lossless prediction coder, customizable chrominance sub-sampler and an efficient Golomb-Rice encoder. The scheme has both lossy and lossless modes and is further customized to work with two lighting modes – conventional white light imaging (WLI) and emerging narrow band imaging (NBI). The average compression ratio achieved using the proposed lossy compression algorithm is 80.4% for WBI and 79.2% for NBI with high reconstruction quality index for both bands. Two surveys have been conducted which show that the reconstructed images have high acceptability among medical imaging doctors and gastroenterologists.

The imaging algorithms have been realized in hardware description language (HDL) and their functionalities have been verified in field programmable gate array (FPGA) board. Later it was implemented in a 0.18 μm complementary metal oxide semiconductor (CMOS) technology and the chip was fabricated. Due to the low complexity of the core compressor, it consumes only 43 μW of

power and 0.032 mm^2 of area. The compressor is designed to work with commercial low-power image sensor that outputs image pixels in raster scan fashion, eliminating the need of significant input buffer memory.

To demonstrate the advantage, a prototype of the complete WCE system including an FPGA based electronic capsule, a microcontroller based data logger unit and a Windows based image reconstruction software have been developed. The capsule contains the proposed low complexity image compressor and can generate both lossy and lossless compressed bit-stream. The capsule prototype also supports both white light imaging (WLI) and narrow band imaging (NBI) imaging modes and communicates with the data logger in full duplex fashion, which enables configuring the image size and imaging mode in real time during the examination. The developed data logger is portable and has a high data rate wireless connectivity including Bluetooth, graphical display for real time image viewing with state-of-the-art touch screen technology. The data are logged in micro SD cards and can be transferred to PC or Smartphone using card reader, USB interface, or Bluetooth wireless link. The workstation software can decompress and show the reconstructed images. The images can be navigated, marked, zoomed and can be played as video. Finally, ex-vivo testing of the WCE system has been done in pig's intestine to validate its performance.

ACKNOWLEDGEMENTS

TABLE OF CONTENTS

LIST OF FIGURES

LIST OF TABLES

LIST OF ABBREVIATIONS

ASIC	Application Specific Integrated Circuit
BMP	Bitmap
CR	Compression Ratio
CRC	Cyclic Redundancy Check
CS	Compressed Sensing
DCT	Discrete Cosine Transform
DPCM	Differential Pulse Code Modulation
DVP	Digital Video Port
ECG	Electrocardiogram
EEPROM	Electrically Erasable Programmable Read-Only Memory
FIFO	First In First Out
FPGA	Field Programmable Gate Array
FPS	Frames per Second
FSM	Finite State Machine
GUI	Graphical User Interface
JPEG-LS	Joint Photographic Experts Group - Lossless
JTAG	Joint Test Action Group
LCD	Liquid Crystal Display
LED	Light Emitting Diode
LUT	Lookup Table
MCU	Microcontroller
MICS	Medical Implant Communications Service
MOS	Mean Opinion Score
MSB	Most Significant Bit
NBI	Narrow Band Imaging
PCB	Printed Circuit Board
PSNR	Peak Signal to Noise Ratio
QVGA	Quarter Video Graphics Array
RAM	Random Access memory
RF	Radio frequency
RTV	Real Time View
SD	Secure Digital
SPI	Serial Peripheral Interface
SSIM	Structural Similarity
USART	Universal Synchronous/Asynchronous Receiver/Transmitter
USB	Universal Serial Bus
VIF	Visual Information Fidelity

VSNR	Visual Signal to Noise Ratio
WCE	Wireless Capsule Endoscopy
WLI	White Light Imaging

Part I: **Preface**

Chapter 1: Introduction

1.1   Overview of Wireless Capsule Endoscopy

The commonly used flexible endoscopes enable diagnosis inside esophagus, stomach and some part of small intestine, however, the largest portions of the small intestine are still difficult to reach. The pain and discomfort caused by the flexible endoscope reduces the interest of many patients to undergo for such a procedure.

The recently introduced   wireless capsule endoscopy (WCE)) [1][2][3][4][5][6][7][8] technique has a major impact in the field of endoscopy as it can greatly reduce the level of patients discomfort and also can reach the small intestine of the gastrointestinal (GI) tract. Before the introduction of WCE, it was impossible for medical doctors (gastroenterologists) to examine tissues of the small intestine without performing a surgical operation.

In WCE, after several hours of fast, the patient ingests a vitamin-sized electronic pill, which passes through the GI tract by peristalsis. While travelling through the GI tract, the pill takes images and transmits image data wirelessly to a portable data logger unit attached to a belt, around the patient's waist. During the procedure, patients are free to conduct their daily activities such as walking, sitting, driving etc. However, the patient should avoid strenuous physical activity, especially if it involves sweating, and should not bend or stoop during the procedure. After 8 - 10 hours, the battery life of the capsule runs out and the image data stored in the data logger are transferred to a workstation or a personal computer (PC) where the images are reconstructed and displayed for

medical diagnosis. Generally, the capsule comes out from the body naturally after two to three days [9]. The typical WCE system is shown in Figure 1.1.
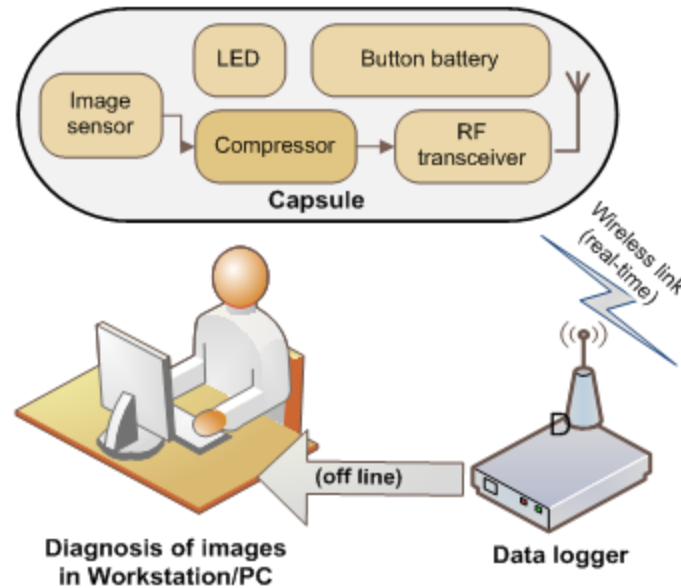
Figure 1.1 A typical wireless capsule endoscopy system

In some flexible wire endoscopy, several changeable light modes are used, such as white light imaging (WLI) and narrow band imaging (NBI). The WLI, where white light is used to illuminate the GI surface, is the most commonly used imaging mode. In the NBI mode, two discrete bands of lights are generally used – one blue and one green, with center wavelength at 415 nm and at 540 nm namely. Narrow band blue light displays superficial capillary networks, while green light displays the vessels and when combined, offer an extremely high contrast image of the tissue surface [10][11][12].

1.2   Motivation

Our key focus in this research project is mainly on the design of the image compressor of the capsule. The capsule runs on button batteries that need to supply power for about 8-10 hours [1]. Without image compression, the radio frequency (RF) transmission generally consumes more than 60% of the total power budget of the capsule [13]. An efficient image compressor can reduce the

amount of data that need to be sent and thus save the RF transmission power. However, the image compressor itself should be low-complexity hardware, so that it does not consume a significant amount of power and area. The smaller the area of the compressor, the smaller the size of the capsule can be made and small capsule is more comfortable for the patients to swallow. Saving power will also provide longer battery life, which helps to prevent incomplete examination [1] of the GI tract. Moreover, saving area and power will give the opportunity to add additional features (such as robotic capability [14][15][16][17][18], 3D imaging [19], multi-camera [20], increasing the captured image size and rate, etc.) to the capsules. This is why a low-cost (area and power) compressor is essential for endoscopic capsule.

To evaluate the performance of the compressor in a realistic scenario, animal testing of the capsule is required. For this reason, a working prototype of the capsule, (where the proposed compressor is implemented) is necessary. The complete WCE system will give the opportunity to examine the performance of different components of the system and understand their behaviour such as compatibility or any unknown issues. In this work, a prototype of the WCE system consisting of the electronic capsule, data logger unit and workstation software is developed and tested in animal intestine.

1.3   Thesis Objective

The key design challenge of endoscopy capsule is to reduce the area and power consumption of the hardware while maintaining acceptable image quality. The main goals in this research project are to develop low-complexity image compression algorithms on the basis of analyzing the unique properties of endoscopic images and validate their performance in real world by developing a WCE system prototype.

Considering the existing literature and application need, the following research objectives are set.

- To develop a compression algorithm that must be low complexity and should consume ultra low area and power as the battery life is limited.

- To design a compression algorithm which must be able to reduce the data sufficiently in order to fit into the limited bandwidth of the RF transceiver and to save power.

- To tune the compression algorithm to support both WLI and NBI imaging modes.

- To design the image compressor that should be able to produce output bit stream in both lossy and lossless modes.

- To measure the quality of the lossy reconstructed images using objective or mathematical methods [21] and they should have good quality indexes. Along with mathematical methods, the quality of the reconstructed images need to be assessed by professional medical imaging doctors visually for acceptability.

- To develop a compete WCE system consisting of an electronic capsule, a data logger unit and a PC software in order to demonstrate the advantage of the system in real-world environment and also to test the system in animal intestine.

- To investigate the performance of different components (such as image sensor, LED, RF transceiver, battery etc.) of the WCE system and to understand their behaviour such as compatibility, any unknown issues, etc.

1.4   Thesis Organization

The thesis is structured in five parts with nine chapters. A brief description of each of the parts and the chapters are given below.

Part I: Preface includes:

Chapter 1: *Introduction* presents the overview of wireless capsule endoscopy system, the motivation of the thesis, thesis organization and contributions.

Chapter 2: *Research Background* discusses the related literature works on compressor design of endoscopy capsule and prototype development of different units of WCE system.

From this point, the thesis presents the original research.

Part II: Image Compressor Design for Capsule Endoscopy includes:

Chapter 3: *Lossy Compressor Design* analyses endoscopic images and proposes a novel color space for better WCE image compression. Then a lossy image compressor is proposed, its computational complexity and simulation results are presented and compared with other literature works. The results of two subjective evaluation surveys participated by several professional medical imaging doctors on the quality of the reconstructed images are also presented. The hardware architecture of the proposed compressor, its verification in FPGA board and its ASIC implementation results are also discussed in this chapter.

Chapter 4: *Lossless Compressor Design* discusses a lossless version of the proposed compressor. The complexity analysis, simulation results, and hardware architecture of the lossless compressor are also discussed.

Part III: Prototype Design includes:

Chapter 5: *Endoscopy Capsule* discusses the complete design of a miniature FPGA based capsule prototype, where the proposed image compressors are implemented. The design criteria of the capsule, its architecture, and results are presented in this chapter.

Chapter 6: *Data Logger* discuses the design of a data logger for WCE application. This chapter also discusses about the design criteria, the data logger's hardware and software architecture and results.

Chapter 7: *Workstation Software* presents the architecture of the PC software where the images are decoded and displayed as video.

Chapter 8: *Animal Testing* presents the experiments conducted in pig's intestine with the developed WCE prototype. The captured intestine images taken by the capsule prototype are also shown in this chapter.

Part IV: Conclusion includes:

Chapter 9: *Summary and Future Work* presents the summary and discussion of this research and also points some related future works.

1.5   Research Contribution

In this research,   a low-complexity image compression algorithm for capsule endoscopy is developed. It consists of a novel color space, referred as YEF, and differential pulse coded modulation (DPCM) followed by optimized Golomb-Rice coding. Based on the nature of endoscopic images, several sub-sampling schemes on the chrominance components are applied. The proposed compressor is tuned to work with both white light imaging (WLI) and narrow band imaging (NBI). Both lossy and lossless version of the algorithm are presented. The average compression ratio achieved using the proposed lossy compression algorithm is 80.4% for WBI and 79.2% for NBI with high reconstruction quality index for both bands. Two surveys have been conducted which show that the reconstructed images have high acceptability among medical imaging doctors and gastroenterologists.

The imaging algorithms have been realized in hardware description language (HDL) and their functionalities have been verified in field programmable gate array (FPGA) board. Later it was implemented in a 0.18 μm complementary metal oxide semiconductor (CMOS) technology and the chip was fabricated. Due to the low complexity of the core compressor, it consumes only 43 μW of power and 0.032 mm^2 of area. The compressor is designed to work with any commercial low-power image sensor that outputs image pixels in raster scan fashion, eliminating the need of significant input buffer memory.

A prototype of the complete WCE system including an FPGA based electronic capsule, a microcontroller based data logger unit and a Windows based image reconstruction software have been also been developed in this work. The capsule contains the proposed low complexity image compressor and can generate both lossy and lossless compressed bit-stream. The capsule prototype also supports both WLI and NBI modes and communicates with the data logger in full duplex fashion, which enables configuring the image size and imaging mode in real time during the examination. At the time of writing this thesis, the commercial capsules [22][23][24] does not support NBI mode and communicates with data logger in half duplex fashion (data transfer from capsule to data logger only), thus real time configuration of image size, mode, light intensity etc. by sending command to the capsule are not possible during examination. The developed data logger is portable and has a high data rate wireless connectivity including Bluetooth, graphical display for real time image viewing with state-of-the-art touch screen technology. The data are logged in micro SD cards and can be transferred to PC or Smartphone using card reader, USB interface, or Bluetooth wireless link. The workstation software can decompress and show the reconstructed images. The images can be navigated, marked, zoomed and can be played as video. Finally, ex-vivo testing of the WCE system has been done in pig's intestine and several images have been captured by the prototype system to validate its performance.

A list of publications and patent applications is shown in **Appendix** A and B which are generated from the research during the program.

Chapter 2: Research Background

The promise of WCE has sparked the interest among several industries and university research groups in order to advance the technology. The first commercial WCE system, *PillCam*, was developed by *Given Imaging* in the year 2000 [22]. It was approved by the Food and Drug Administration (FDA) [25] in 2001. For the detection of damage or disease in esophagus, small intestine and colon, *Given Imaging* introduced *PillCam ESO, PillCam SB* and *PillCam COLON* namely [22]. Several other products [23][24] also came to market recently.

There have been significant amount of works reported on image compression algorithms for endoscopy capsule and on WCE prototype development. They are briefly discussed below.

2.1   Compressor design

In [26][27][28][29][30][31][32][33], Discrete Cosine Transform (DCT) based image compressors are proposed. In DCT based image compressors, 4×4 or 8×8 pixel blocks need to be accessed from the image sensor. However, commercial CMOS image sensors [34][35][36] send pixels in a row-by-row (i.e., raster-scan) fashion and do not provide buffer memory. So, to implement these DCT-based algorithms, buffer memory needs to be implemented inside the capsule to store an image frame. In order to start processing of the first 8×8 block of a 256×256 size image, the compressor has to wait until the first 8×8 block is available, that is $256 \times 7 + 8 = 1800$ pixels (assuming progressive scan). Hence, a 5.3 kB buffer memory may seem enough (assuming 24 bits per pixel for a color image). However, without the full size buffer memory (i.e., 192 kB), the image sensor needs

to be stopped (or paused) until the stored pixels are processed, as the image compressor would still be busy processing those pixels and there would be no additional memory available to store new pixels. The feature to pause in operation of sensors in the middle of a frame transmission is not commonly found in commercial image sensors. A possible solution to the problem is to use two buffer memory of size 5.3 kB, so that while the compressor works with pixels of one buffer, the new pixels continuously coming from the image sensor are stored in the other buffer. However, one needs to make sure that there is no timing violation between the compression time and input data-rate. Besides, the buffer memory takes large area and consumes sufficient amount of power which can be a noticeable overhead. For instance, a 256 kB customer owned tooling (COT) memory consumes 60 mW of power [37]. Moreover, the computational cost associated in such transform coding (i.e., multiplications, additions, data scheduling, etc.) results in high area and power consumption.

Other compression algorithms such as LZW [38] need *content addressable memory* (CAM) to build, as well as store the coder dictionary [39]. In [40], the design of an image compressor based on prediction and Huffman coding is discussed. To implement Huffman compression algorithm, memory is also required for Huffman table [41]. In [42], a compressor based on *compressed sensing* theory is described, which is a subset of transform coding; as a result, the issues with transform coding still remain. In [43], a lossless electrocardiogram compressor based on prediction and Golomb-Rice [44] coding is described. In [45], a DPCM and Wavelet based compression algorithm is proposed. The Wavelet transform needs to access pixels in blocks, therefore the issue of buffer memory is there, and also Wavelet transform is computationally expensive for capsule endoscopy application.

Among many image compression standards, JPEG-LS [46][47] can be a good choice for compression for endoscopic capsule application, because it can work with pixels coming in raster-

scan fashion, it does not need to buffer the whole image in memory and it is simpler to implement in hardware. In [13][48], design of image compressors based on JPEG-LS algorithm are described. However, it needs memory to store at least one row of the image to support for various prediction modes. Besides, it needs approximately 1.9 kB register arrays to store other key control parameters and contexts of JPEG-LS [49][50].

There are some commercial image sensors available which have built-in compression engine [51][52]. However, the physical size and power consumption of these products are still high. For instance, the typical current consumption of [51] and [52] are from 80 to 100 mA, which is extremely high for capsule endoscopy application. There are some commercially available ASICs [53] which supports compression engine. However, still they consume power in the range of 40 mW to 230 mW which is not good enough for capsule endoscopy application. Note that, for a capsule to run for 8 hours with 195 mAh button battery, the entire capsule hardware (which includes image sensor, compressor, control unit, LED, RF transceiver etc.) can maximum consume total 24 mA current.

From the above discussion, it is found that the compressors presented in the literature are still computationally expensive for capsule endoscopy application. In order to save area and power, research needs to conducted on designing a low complexity and ultra low power compressor which is customized for capsule endoscopy application.

2.2 Prototype development

A complete WCE system prototype consists of an endoscopic capsule, a data logger and workstation/PC software. The related works of these three units are briefly described below.

2.2.1 Endoscopy capsule

In the literature, several capsule prototype works are reported based on field programmable gate array (FPGA) and application specific integrated circuit (ASIC) technology. The work in [54] presents a development system based on FPGA that was specifically designed for testing the entire electronics to be integrated in an endoscopic capsule. The implemented compressor is based on integer version of discrete cosine transform (DCT) and it needs the buffering of the entire image frame in an external SRAM which will consume significant amount of area and power in real world implementation. In [55], a demo prototype of a wired-endoscopy is developed using a commercial CMOS image sensor connected with a FPGA board by 1.5 meter cable. The prototype is then tested during *ex-vivo* and *in-vivo* experiments on a porcine model. A prototype with six cameras, FPGA and flash memory is presented in [20]. The captured image data are saved in the flash memory inside the capsule instead of being transmitted outside human body wirelessly. Storing image data inside capsule flash makes the system less attractive from practical implementation. The doctor needs to wait for an uncertain amount of time to get the image data. Capsule retention problem may cause even 15 days to evacuate the capsule naturally [56]. Moreover, the receiving of the capsule from human dropping is not a hygienic and efficient way. In [13], an ASIC based capsule prototype is discussed. However, the work does not provide any animal testing results to evaluate the actual performance of the prototype in the real world. In [57], an NBI image sensor for CE application is proposed. The work in [58] proposes a capsule prototype focusing on the design of a 20 Mbps RF transceiver.

Several capsule prototype works are also found based on commercial microcontrollers and other off-the-shelf components. The work in [59] discusses a basic level capsule prototype using CMOS analog video camera, a TV modulator IC, a helical antenna, and a lighting system with 4 white LEDs. In [60], a wireless endoscope system is developed with embedded Linux technology

and the ARM microprocessors. A digital CCD image sensor (MT9D111) is used to acquire images, and an image compressor (ADV202) is used to compress the acquired images to JPEG2000 format. In [32], a capsule prototype made of commercially available components such as CMOS image sensor with an integrated JPEG compression engine, ARM 32-bit Cortex™-M3 micro-controller, and an RF transceiver module is presented. In [61], a capsular endoscopy prototype with autofocus function is developed with a microcontroller (CC2430), a commercial camera (MO-S588) and IEEE 802.15.4 compliant transceiver. A liquid lens (ARCTIC 416) is used to adjust the overall focal length. However, these microcontroller based systems make the prototype bulky and power hungry, which does not meet the key design challenges of the capsule hardware.

At the time of writing this thesis, the commercial capsules [22][23][24] does not support NBI mode and communicates with data logger in half duplex fashion (data transfer from capsule to data logger only), thus real time configuration of image size, mode, light intensity etc. by sending command to the capsule are not possible during examination.

From the above discussion, it is found that there is lack of work on the design and development of capsule prototype, which is modular, programmable, small size and suitable for doing animal testing. So, research needs to be conducted on designing a fully functional prototype which is flexible in design so that various imaging algorithms can be tested, supports several imaging modes such as WBI and NBI, configurable during examination in real time, and can be tested in animal intestine to validate its performance.

2.2.2   Data logger

In the literature, several works are found related to data logging for medical applications. Many works are found for logging electrocardiogram (ECG) signals. In [62], the design of a data logger is discussed which converts the analog ECG signals to digital and stores them in 20 MB flash memory cards. An ECG signal data logger with custom designed ASIC controller for multimedia card

(MMC) is discussed in [63]. In [64], the design of a microcontroller based portable data-logger for medical application is described which contains three-electrode ECG circuit, three accelerometers, a pressure sensor and a temperature sensor. The module can store data in 4 Mbit flash memory in real-time or can send data to PC by a wired serial interface. A low power and small size design of an ECG signal recorder is described in [65] for the purpose of long-term portable recording. Data are stored in SD card and can be transferred to PC by an isolated RS232 interface. The work in [66] presents an IP core for FPGA-based ECG data transmission using wired telephone line through modem interface. Note that, the above discussed data loggers receive data from body sensors using wired connections which is not comfortable for patients. In [67], an ARM microcontroller based wearable heart rate monitor system is described. It gathers ECE data and sends the data to a nearby PC wirelessly using Bluetooth. It does not have internal storage memory and thus the patient's movements are restricted near the host PC.

In [68], a fetal and maternal heart beat signal recorder is discussed which detects signals using skin electrodes, converts them to digital and stores in temporary SRAM for later transfer to PC by RS232 interface. In [69], fetal movements are recorded continuously on several pregnant patients using fetal movement acceleration measurement (FMAM) recorder to study its suitability in long-term home monitoring application.

In [70], a data logger unit for storing galvanic skin response (GSR) for autistic patients is discussed. The data logger receives data using RS232 interface and stores it in 16 MB EEPROM. A portable data logger with three body-fixed inertial sensors for monitoring the physical activities of Parkinson's disease (PD) patients is proposed in [71]. In [72], a microcontroller based data-logger is implemented by using a four-channel ADC to measure sweat activity. Data are stored in an EEPROM with the capability of storing data for over two days when one measurement is taken per minute. An RF transceiver is used to export the data to a monitoring host PC. A wireless data logger

for recording human movements is discussed in [73]; however the data logger is not portable as it takes power from house AC line supply, thus restricts the patient's movement near to the data logger. In the work of [74], a Java2 based software for cell phone is developed to store laboratory data, such as blood pressure, BUN (blood urea nitrogen), creatinine, Hb A1c (glycosylated hemoglobin), and other pertinent comments, into a cell phone memory. However, the cell phone does not have any sensor connected with it for automatic data acquisition.

Most of the data loggers presented in the literature have wired connection with bio-sensors, which is not comfortable for patients. Moreover, due to absence of sufficient storage capacity, wireless link, and graphical display unit, these loggers cannot be efficiently used for logging data of wireless capsule endoscopy. So, there is a opportunity for doing research in designing data loggers for capsule endoscopy which should have all the necessary resources for such application.

2.2.3   Workstation software

After endoscopy image data are transferred to PC, then data are decoded and displayed. In [75][76], automatic segmentation and detection of endoscopic video is discussed. An image enhancement method, referred as Fuji Intelligent Color Enhancement (FICE) technology [77], decomposes images by wavelength, then directly produces enhanced and high contrast pseudo mucosal images.

The related works provide some algorithms for image segmentation and enhancement without providing a complete architecture of the workstation software. In this thesis, a software architecture for WCE system is proposed and developed. Further research on image segmentation and enhancement are left for future work.

Part II: Proposed Image Compression Algorithms for Capsule Endoscopy

Chapter 3: Lossy Compression Algorithm

3.1   Introduction

The key design challenge in WCE is to reduce the area and power consumption of the capsule while maintaining acceptable reconstructed image quality. The main goal in this research is to construct low-complexity image compressors on the basis of analyzing the unique properties of endoscopic images. Based on the analysis, both lossless and lossy compression algorithms for capsule endoscopy have been introduced. In this chapter, the proposed lossy compression algorithm is discussed.

3.2   Design requirements

Considering the existing literature and the application need, in this work, the following design requirements for the compressor have been set:

- The capsule must consume low power as the battery life is limited while it travels through the intestine. Hence, focus is made on compression algorithms with low complexity and low power. Saving power will also provide longer battery life, which helps to prevent incomplete examination [1] of the GI tract. Moreover, saving power will give the opportunity to increase the resolution of the image and the frame per second (FPS) of the sensor.

- The area is a critical issue for the capsule. Memory consumes significant silicon area and power. Here, focus is made on algorithms that do not require buffering of the image in memory.

- The compressor should be able to work with commercially available CMOS image sensors [34][35][36] which send data in raster-scan fashion.

- For an accurate diagnosis, the quality of the reconstructed image is important. It has been reported that a minimum *peak-signal to noise ratio* (PSNR) of 35 dB in the reconstructed image quality is required for accurate diagnosis [78][79]. A new evaluation criterion, known as *structural-similarity index* (SSIM) [80], tells about the shape and has become popular in these days. Among other image quality assessment indexes, *visual information fidelity* (VIF) [81] and *visual signal to noise ratio* (VSNR) [82] are reported to have performed well in assessing texture[21]. Therefore, the image processing algorithm to be used in the capsule should be able to reconstruct images with high PSNR, SSIM, VIF, and VSNR indexes.

- The reconstructed images should be considered acceptable when evaluated (visually) by professional medical imaging doctors.

- The compression algorithm must be able to reduce the data to be sent by the transmitter in order to fit into the bandwidth of the transceiver and save power.

- Finally, the compression algorithm should support both imaging modes – WLI and NBI, and equally produce high quality reconstruction with high degree of compression.

3.3 Analysis of endoscopic images

In order to develop an efficient and low-cost image compression algorithm tailored for capsule endoscopy, first investigate the unique properties of WCE images are investigated first. 100 WLI (taken from 20 different positions from larynx to anus of the GI tract) and 15 NBI endoscopic test images [83] have been analysed to find the properties of the images. Moreover, several video sequences [2] (consisting of total 1,698 frames) are also used in this study. The conclusions of the several analyses are drawn from the average results of the test images.

3.3.1　Color space conversion

In this section, a novel color space, YEF, is introduced which is suitable for WCE image compression and efficient for hardware implementation. In YEF, the luminance is stored in Y component, E stores the difference between luminance and green component, and F stores the difference between luminance and blue component. The relationships are shown (3.1), (3.2) and (3.3).

$$Y = \frac{R}{4} + \frac{G}{2} + \frac{B}{4} \tag{3.1}$$

$$E = \frac{Y}{2} - \frac{G}{2} + 128 = \frac{R}{8} - \frac{G}{4} + \frac{B}{8} + 128 \tag{3.2}$$

$$F = \frac{Y}{2} - \left(\frac{3B}{8} + \frac{G}{8} \right) + 128 = \frac{R}{8} + \frac{G}{8} - \frac{B}{4} + 128 \tag{3.3}$$

From (3.1), (3.2) and (3.3), it is observed that the conversion between color spaces involves only a few additions and divisions by numbers which are powers of 2, which can be implemented by shift operations in digital hardware. In Figure 3.1, a typical WLI and a NBI endoscopic image are shown. In Figure 3.2, the 3D plots of all component values (i.e., red, green and blue) for different pixel positions of both the WLI and the NBI endoscopic images are shown. From the plots, it can be seen that in RGB plane, the changes in pixel values are high, which means that there is more information contained in the three components. Figure 3.3 shows the intensity distribution after converting to YEF. It can be seen from Figure 3.3 that there is less change in pixel values in chrominance components (E and F), which indicates that less information is contained there [84][85].

20
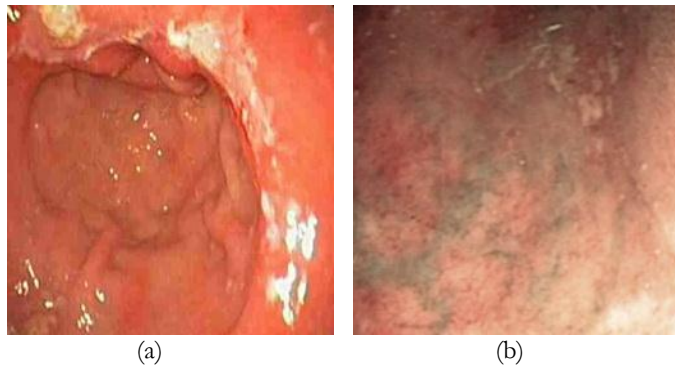
Figure 3.1 A typical endoscopy image (a) WLI; (b) NBI
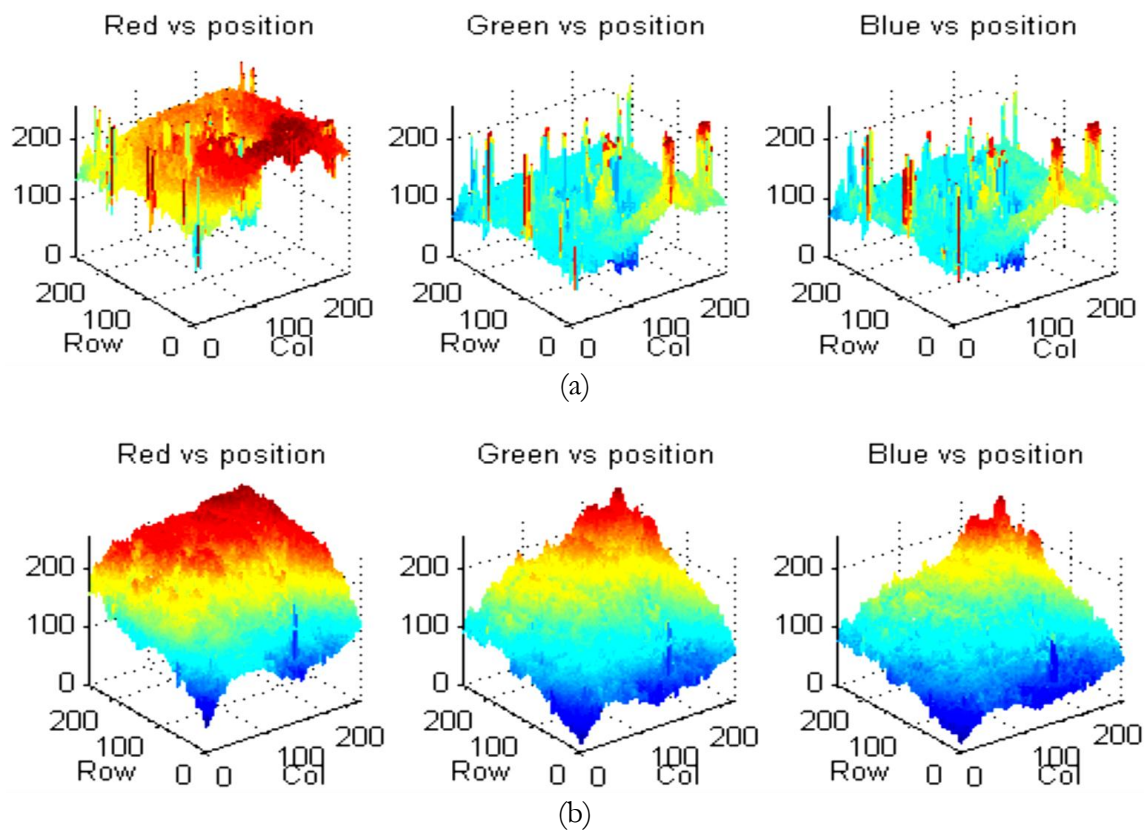
Figure 3.2 Intensity distribution of R, G, and B components: (a) WLI; (b) NBI
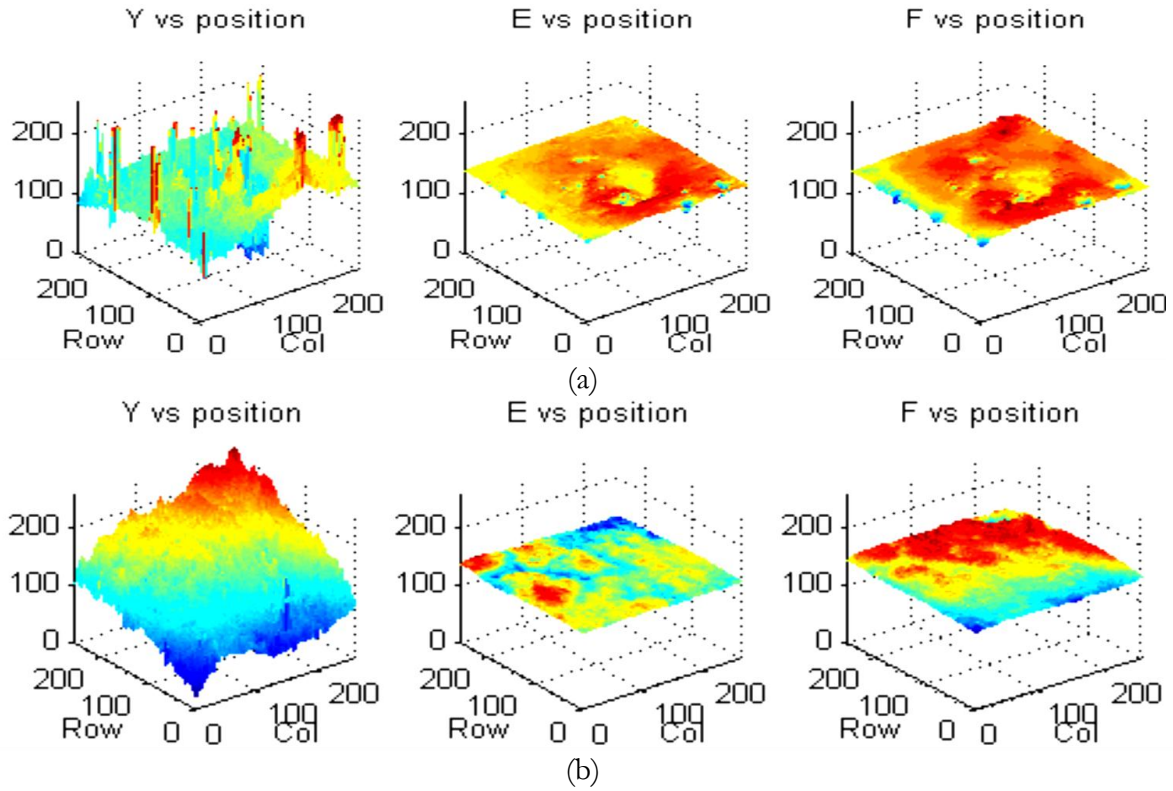
Figure 3.3 Intensity distribution of Y, E, and F components: (a) WLI; (b) NBI

The motivation for the YEF color space comes from the fact that, endoscopic images generally exhibit dominance in red color with the absence of significant green and blue components. As it have been seen in our experiment that, in most cases, the intensity distribution of green in endoscopic images is very similar to that of blue component (as seen in Figure 3.2). The experiment has also shown that the intensity distribution of luminance (Y) has similar pattern of green and blue components (as seen in Figure 3.2 and Figure 3.3) – thus, subtracting green and blue components form the luminance will produce differential pixel values of almost equal numbers. The minimum and maximum values of YEF color space for different RGB values are shown in Table 3.1.

Table 3.1: YEF ranges

	Min	Max
Y	0 *when R = 0, B = 0, G = 0*	255 *when R = 255, B = 255, G = 255*
E	64.25 *when R = 0, B = 255, G = 0*	191.75 *when R = 255, B = 0, G = 255*
F	64.25 *when R = 0, B = 0, G = 255*	191.75 *when R = 255, B = 255, G = 0*

In Table 3.2, the average standard deviation and entropy [84] for both WLI and NBI endoscopic images for several color components are shown. 100 WLI and 15 NBI images have been used in this experiment. From Table 3.2, it is seen that the YEF color space has the lowest standard deviations and entropy in chrominance components which indicate that YEF color space is a strong candidate for the compression of WCE images. In Table 3.3, the average standard deviation and average entropy of YEF color components for several WCE video sequences (consisting of total 1,698 frames) are shown; these results are similar to Table 3.2.

Table 3.2 Average standard deviation and entropy of color components

Color space	Component	Avg. StdDev		Avg. Entropy (bits/pixel)	
		WLI	NBI	WLI	NBI
RGB	R	46.6	44.1	7.1	7.2
	G	39.4	39.6	7.0	7.0
	B	34.7	36.1	6.7	6.9
YUV [86]	Y	34.3	34.6	6.8	6.8
	U	7.0	3.0	4.4	3.2
	V	9.6	5.6	4.9	4.1
YCoCg [87]	Y	38.8	39.5	7.0	7.0
	Co	13.9	7.0	5.5	4.5
	Cg	5.3	3.3	4.1	3.6
YEF	Y	38.8	39.5	7.0	7.0
	E	2.7	1.7	3.2	2.6
	F	4.7	2.1	3.9	2.8

Table 3.3: Average standard deviation and entropy of WCE video in YEF color components

Mode	Video	Avg. StdDev			Avg. Entropy (bits/pixel)		
		Y	E	F	Y	E	F
WLI	Video-1 (99 frames)	30.4	1.7	3.3	6.8	2.7	3.6
	Video-2 (97 frames)	22.7	1.1	3.2	6.5	2.2	3.6
	Video-3 (97 frames)	25.4	1.5	3.3	6.5	2.5	3.6
	Video-4 (97 frames)	21.7	1.3	2.6	6.3	2.4	3.3
	Video-5 (97 frames)	27.1	2.4	4.2	6.6	3.1	3.9
NBI	Video-1 (889 frames)	32.3	1.3	2.2	6.9	2.2	3.1
	Video-2 (322 frames)	46.3	1.7	2.1	7.4	2.7	2.9

Note that, the proposed color space does not neglect the chrominance information. The YEF color space is just another representation of the RGB color space which is more suitable for compression and theoretically lossless. YEF color components can be brought back to RGB color components using (3.4).

$$\begin{bmatrix} R \\ G \\ B \end{bmatrix} = \begin{bmatrix} 1 & 3.33 & 2.67 \\ 1 & -2 & 0 \\ 1 & 0.67 & -2.67 \end{bmatrix} \begin{bmatrix} Y \\ E-128 \\ F-128 \end{bmatrix} \qquad (3.4)$$

When (3.1), (3.2) and (3.3) are implemented in digital hardware, minor variations in the pixel values may occur due to the rounding of fractions to integers. The YEF color space can be made fully reversible (i.e. reconstructed image is numerically identical with original image) by adding 3 more extra bits for storing fraction along with the 8 bits for integer as shown in Table 3.4. Here overall PSNR is calculated using (3.15).

Table 3.4: Average image quality index for different data bit length

Number of bits (Integer+Fraction)	Overall PSNR (dB)	VSNR (dB)	VIF	SSIM
9 (8+1)	58.13	75.63	0.9932	0.9989
10 (8+2)	98.60	97.83	0.9972	0.9997
11 (8+3)	∞	∞	1.0000	1.0000

3.3.2 Sub-sampling

Next, the characteristics of both WLI and NBI endoscopic images have been analyzed so that the advantages of the unique features can be used and accordingly develop an efficient compression algorithm. For this purpose, three images of different types: a standard image ("mandrill"), a WLI endoscopic image and an NBI endoscopic image (as shown in Figure 3.1) are analyzed. The histograms are shown in Figure 3.4 and Figure 3.5. Now, comparing Figure 3.4 with Figure 3.5 and also from the results of Table 3.2 and Table 3.3, it is seen that the variations of E and F components in endoscopic images are narrower than that of the standard image. It is due to the color homogeneity of the endoscopic images. This observation leads to the choice of sub-sampling [88][89]. From this analysis, it is found that the E and F components can be heavily sub-sampled (e.g., YEF811, YEF812, etc.) for achieving higher compression ratio without losing the image quality. For example, YEF812 sub-sampling means that for every eight Y components, one E

component and two F components are sampled as shown in Figure 3.6. Sub-sampling is done in horizontal direction only. It should be noted that, sub-sampling to Y component would lead to heavy loss in the reconstruction of final image; hence Y is not sub-sampled in any stage of the algorithm.
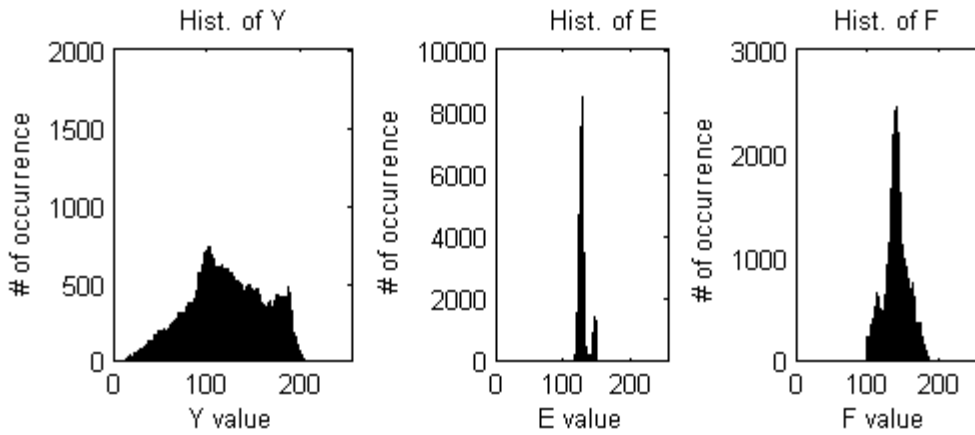
Figure 3.4 Histogram of standard "mandrill" image

(a)
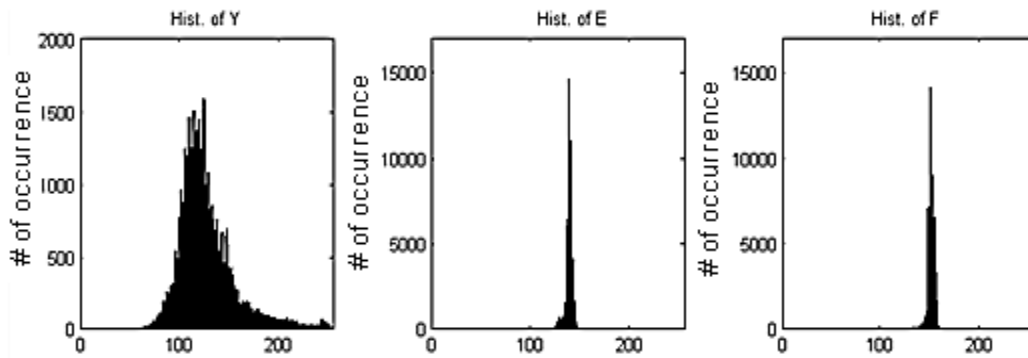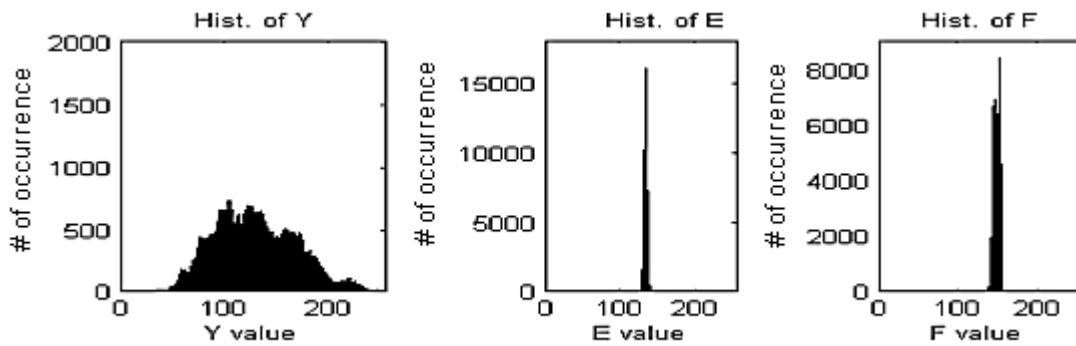
Figure 3.5 Histogram of an endoscopic image: (a) WLI; (b) NBI
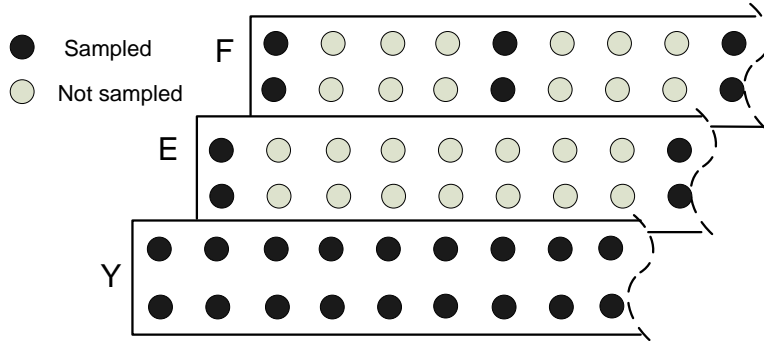
Figure 3.6 YEF812 sub-sampling scheme

In addition, the endoscopic images are analyzed by human doctors visually. The human eye is very sensitive to small changes in brightness (Y) but not to small changes in color. Thus, losing information in the chrominance components compresses the image while introducing distortions to which the eye is not sensitive [85].

3.3.3 Differential pulse coded modulation (DPCM)

In endoscopic images, the component values change gradually and slowly. The difference between the component values of two consecutive pixels is generally small as sharp edges are rare in endoscopic images. The change in component values (dX) with respect to its adjacent left pixel in any row is given by (3.5):

$$dX_{r.c} = X_{r,c} - X_{r,c-1} \qquad (3.5)$$

where, $X_{r,c}$ is the pixel value at row r and column c, and $X_{r,c-1}$ is its adjacent left pixel value. X can represent Y, E, or F component values. Figure 3.7 shows the changes in dX for a standard image and as well as for an endoscopic image. From Figure 3.7, it is seen that small changes in pixels values

occur in endoscopic images. Here, the average absolute difference (AAD) is used as shown in (3.6) as the statistical measure of dX.

$$dX_{avg,image} = \frac{\sum_{n=1}^{N}\sum_{m=1}^{M-1}\left|(x_{m+1,n} - x_{m,n})\right|}{M \times N} \qquad (3.6)$$

where, M and N are the image width and height namely; x is the original component value. The average AAD for 100 test WCE images are also shown in Table 3.5. The results are consistent with Figure 3.7, as it is found that in general, the difference in pixel (dX) with respect to the adjacent left pixel is very small in endoscopic images compared to that of standard images. As a result, the DPCM is a good choice [85]. The block diagram of DPCM is shown in Figure 3.8. It should be noted that, DPCM (no quantization is used) is a lossless encoding scheme with little computational complexity, which will reduce both power and area consumption.

(a)

(b)
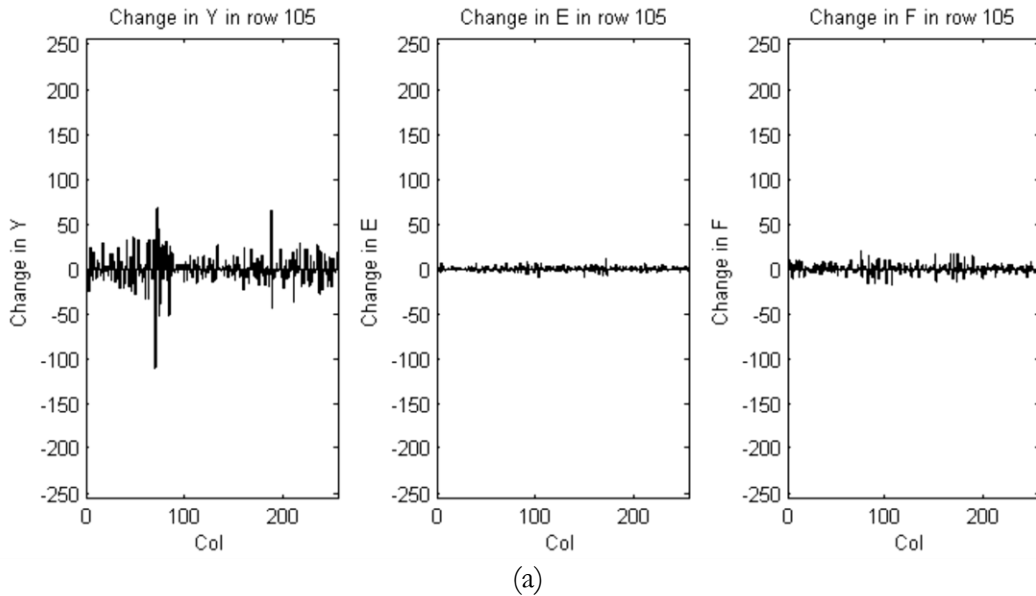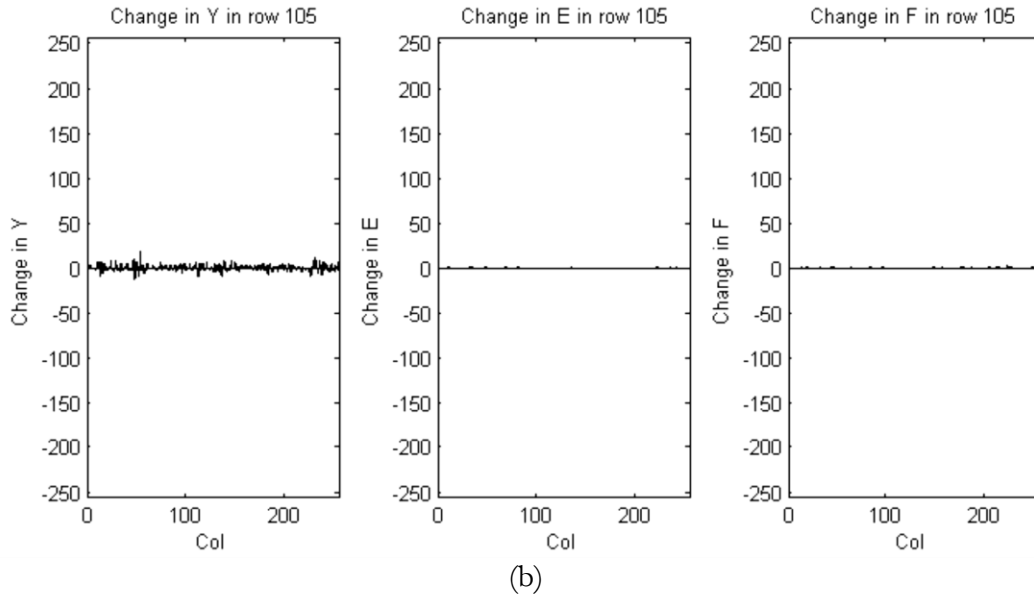
Figure 3.7 Changes in pixel values (dX) with respect to its adjacent left pixel (a) in standard "mandrill" image; (b) in an

endoscopic image

(a)

(b)
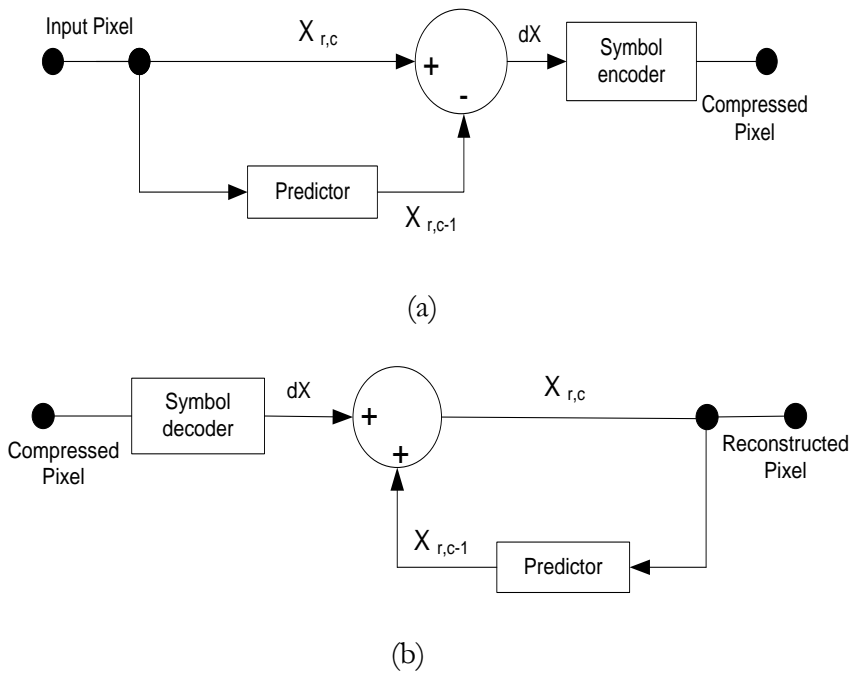
Figure 3.8 Block diagram of DPCM (a) encoder; (b) decoder

Table 3.5: Avg. absolute difference in consecutive pixel values

	WCE image #1	Baboon	Lena	100 WCE images
dY	2.87	15.23	8.28	4.21
dE	0.30	1.56	0.97	0.19
dF	0.26	2.99	1.30	0.19

3.3.4 Variable length coding

The next step is to find a suitable variable-length encoding scheme which is efficient in coding and also less error-prone. For this purpose, the *dX* values of Y, E, and F components are analyzed. The histograms of *dY*, *dE* and *dF* of one WLI and one NBI endoscopic image are shown in Figure 3.9. These plots show a two sided geometric distribution. In the case of geometric distribution, the Golomb code gives the optimum code length [44].
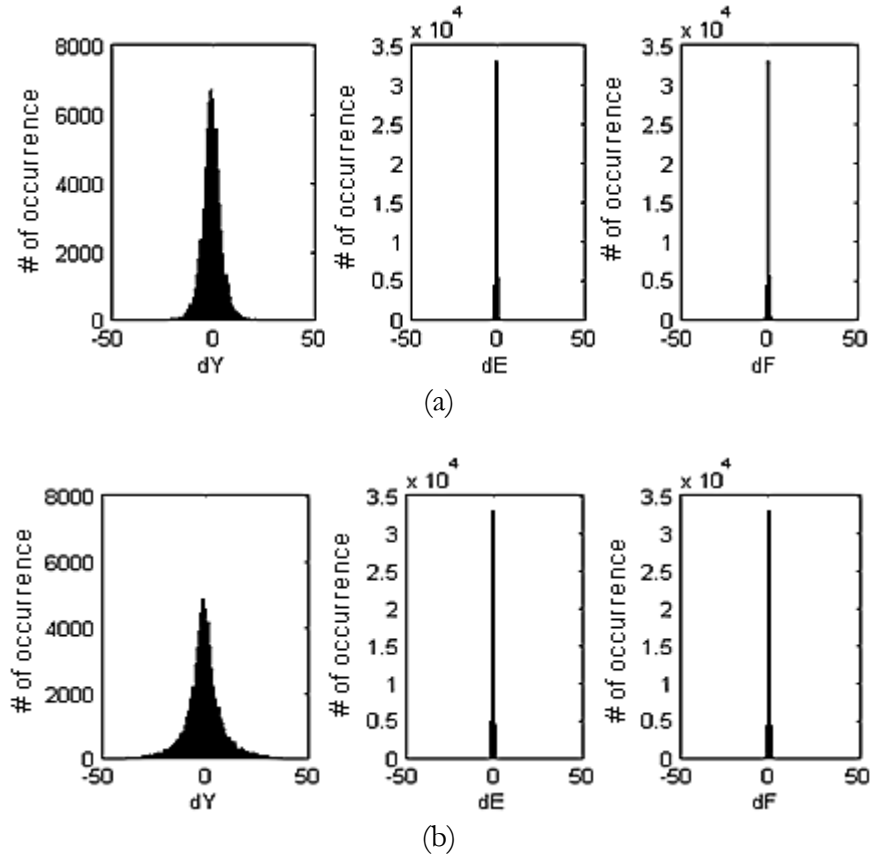
Figure 3.9 Histogram of *dX* for an endoscopic image: (a) WLI; (b) NBI

The *Golomb-Rice* code is a simpler version of the Golomb code, which is easier to implement in hardware than the original version, but has similar compression efficiency [85]. Hence, it have been chosen to encode *dX*. Since, *dX* can be either positive or negative, and Golomb-Rice code can work only with positive integers, the field of positive *dX* are mapped to *even integers* and negative *dX* to *odd integers* using (3.7).

$$m\_dX = \begin{cases} 2dX, & \text{when } dX \geq 0 \\ 2|dX|-1, & \text{when } dX < 0 \end{cases} \qquad (3.7)$$

More experiments have been conducted to further customize the encoding. The experiments show that the values of *dY* do not generally exceed the range from +127 to -128 due to the absence of sharp changes between two consecutive pixels in endoscopic images, whereas the *dE* and *dF* values vary in a narrower range. So, it can be assumed that, the mapped positive integers (*m_dX*) will range from 0 to 255, which can be expressed in binary using 8 bits. Our proposed optimized Golomb-Rice coding is as follows:

- First define: $I = 2^8 = 256$

- *M* is a predefined integer and a power of 2 as expressed in (3.8) where *k* is a non negative integer.

$$M = 2^k \qquad (3.8)$$

- Then *m_dX* is divided by *M* as shown in (3.9) and (3.10):

$$q = \text{Integer}\left(\frac{m\_dX}{M}\right), \qquad (3.9)$$

$$r = m\_dX \mod M \qquad (3.10)$$

- The quotient (q) is expressed in unary in $q + 1$ number of bits. Then the remainder (r) is concated with the unary code, and r is expressed in binary in k number of bits. It is desirable to limit the size of the Golomb-Rice code as it becomes very long for larger values. This is done by using a parameter named, g_{limit}. If $q >= j$, as j is defined in (3.11), then the unary code of j is prepared. This acts as an escape code for the decoder and is followed by the binary representation of $m\_dX - j \times M$ in $log_2 I$ bits.

- The maximum length of Golomb-Rice code (g_{limit}) is chosen among the numbers that are multiple of 8 and it is chosen as 32 because it gives the best compression ratio when conducting simulations. The length of a Golomb-Rice code (*gr_len*) can be calculated using (3.11) and (3.12):

$$j = g_{limit} - \log_2 I - 1 \tag{3.11}$$

$$gr\_len = \begin{cases} q + 1 + k, \text{when } q < j \\ g_{limit}, \text{when } q \geq j \end{cases} \tag{3.12}$$

A flowchart of Golomb-Rice coding algorithm is shown in Figure 3.10. Figure 3.11 shows the length of Golomb-Rice code for different values of k. It has been noticed from Figure 3.9 that the most occurred value of *dE* and *dF* is zero and others are very close to zero. Hence, to get a good compression, smaller length codes for zero and near-zero values need to be assigned. So, $k = 1$ for encoding the mapped integers for *dE* and *dF* is chosen. For *dY*, a wider range of values occurs. So, $k = 2$ for encoding the mapped integers of *dY* is chosen. It has been noticed from Figure 3.9 (a) and (b), that *dY* generally spans wider in NBI images than WLI images due to the presence of sharper edges. To get the best compression ratio, the k parameters for the mapped *dX* are set as summarized in Table 3.6.
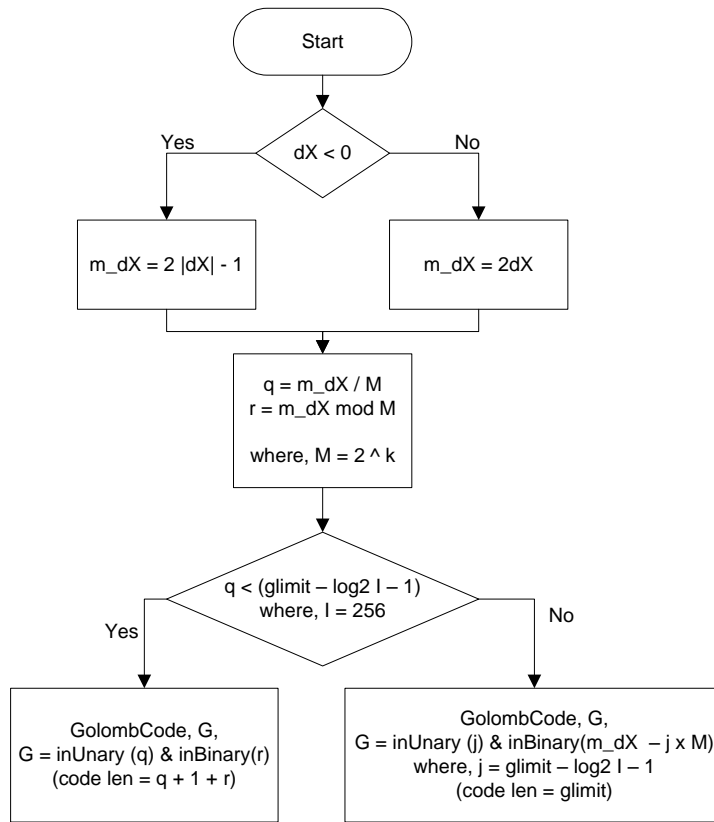
Figure 3.10 Flowchart of Golomb coding algorithm
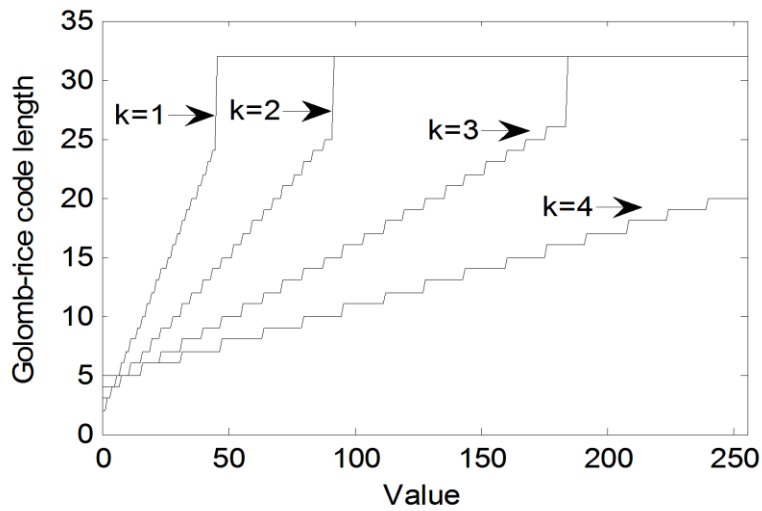
Figure 3.11 The length of Golomb-Rice code

33

Table 3.6: k parameter for WLI and NBI images

Mode	m_dY	m_dE	m_dF
WLI	2	1	1
NBI	3	1	1

3.3.5 Corner clipping

In wireless endoscopy, the corner areas in a captured image are blacked out in commercially available WCE images [2][22]. In this work, advantage is taken from this fact and add another level of compression by implementing a corner clipping algorithm. The image processor in the capsule may discard these corner pixels during compression and thus achieve higher compression ratio. From the implementation point of view, it is easier to cut the four corners diagonally instead of cutting the image in a circular fashion. Figure 3.12 (a) and (b) show a typical capsule endoscopy image [22] and the calculation of L respectively. For a square of length W, the maximum length (L) is calculated, where no pixels would be discarded inside the circle of maximum radius W/2. Considering the geometric relationships (from Figure 3.12 (b)): $\sin 45° = \dfrac{h}{L} = \dfrac{1}{\sqrt{2}}$, $h = d - \dfrac{W}{2}$, and

$d = \sqrt{\left(\dfrac{W}{2}\right)^2 + \left(\dfrac{W}{2}\right)^2} = \dfrac{W}{\sqrt{2}}$, L in terms of W (image width) is calculated as shown in (3.13). For example, the value of L is 75 for a 256 × 256 image.

$$L = W\left(1 - \frac{1}{\sqrt{2}}\right) = 0.29W \qquad (3.13)$$

Once, L is determined, the clipping algorithm can be implemented in hardware with few combinational logic blocks. As seen from the pseudo code as shown in Figure 3.13, the column and row pixel positions are checked to see whether they fall into the desired visual region; if the position is inside, it is sampled; if not, the pixel is ignored (i.e., not sampled). In Figure 3.13, cX and cY hold the column and row positions of the current pixel namely.
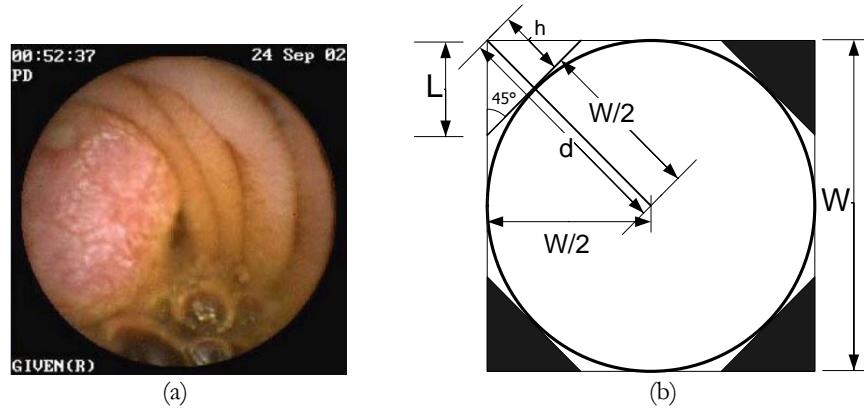
Figure 3.12 (a) A typical endoscopy image (Pillcam SB, courtesy: Given Imaging); (b) Maximum length calculation

```
1.    Is_inside_visual_area := False
2.     If ( cY < L )   {
3.        If cX >=(L-cY) And cX <(W-(L-cY))
4.             Is_inside_visual_area := True }
5.     Else if cY >= (W - L) {
6.        If cX >=((cY-(W-L))+1) And cX<(W-((cY-(W-L))+1))
7.             Is_inside_visual_area := True }
8.     Else
9.        Is_inside_visual_area := True
```

Figure 3.13 Pseudo code for corner clipping algorithm

3.4   Proposed lossy compression algorithm

The block diagram of the lossy compression algorithm is shown in Figure 3.14. Note that, the loss mainly occurs due to sub-sampling and finite precision implementation of the color space conversion. The DPCM and Golomb-Rice encoder are lossless modules. The compressor accepts the original WCE image data in RGB format as input and reads the pixel in a raster-scan fashion. Then it compresses the data and generates the compressed bit-stream as output.
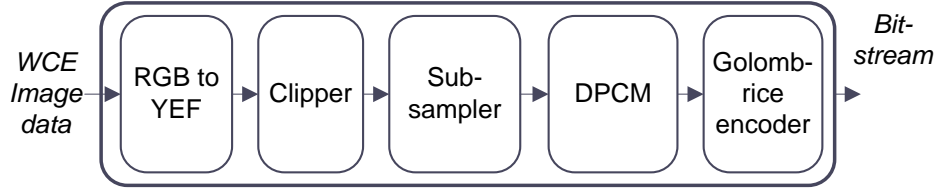
Figure 3.14 Block diagram of the proposed lossy compression algorithm

In hardware implementation, the proposed dual-band compressor can be directly interfaced with any digital-video-port (DVP) compatible commercial RGB image sensors [34][35][36] that output pixels in a raster scan fashion, eliminating the need of significant buffer memory, as well as temporary storage.

3.5   Complexity analysis of the proposed algorithm

In Table 3.7, a comparison of the complexity of the proposed scheme with other works is shown. For an image of n pixels, the proposed algorithm has lowest computational complexity $O(n)$, and does not need any memory buffer. On the other hand, the DCT-based algorithms [26][27][28][32][31][30]   have complexity of $O(n \log n)$ and need memory buffer to store image frame. Compared with the JPEG-LS scheme in [13], the presented algorithm implements simpler prediction scheme and works on YEF plane that enables sub-sampling. There is no need to implement the "Run mode" due to fact that endoscopic images do not contain long runs. The work in [45] uses a wavelet-based coding; although the complexity of wavelet transform is $O(n)$, the actual implementation takes more power and area than the proposed DPCM-based scheme. The work based on sensing theory[42] has the highest computational complexity, $O(n^3)$.

Table 3.7: Comparison of complexity with other works

	Compression Algorithm			Need of Buffer memory?	Complexity
	Type	Block size	Color plane		
Chen *et al.* [13]	JPEG-LS (with run mode)	_	RGB	Yes	$O(n)$
Wahid *et al.* [26]	Transform coding (DCT)	4 × 4	RGB	Yes	$O(n \log n)$
Turcza *et al.* [27]	Transform coding (DCT)	4 × 4	YCbCr	Yes	$O(n \log n)$
Lin *et al.* [28]	DCT and LZ77 encoding	8 × 8	RGB	Yes	$O(n \log n)$
JPEG-FP [26][32]	Transform coding (DCT)	4 × 4	RGB	Yes	$O(n \log n)$
Hu *et al.* [45]	Wavelet coding	_	RGB	Yes	$O(n)$
Wu *et al.* [42]	Block-based Compressed Sensing	8 × 8	YUV	Yes	$O(n^3)$
Dung *et al.* [31]	H.264 based DCT	4 × 4	RGB	Yes	$O(n \log n)$
Proposed	Differential coding (DPCM)	_	YEF	No	$O(n)$

3.6   Simulation results

In order to assess the image quality of the proposed scheme in YEF plane, the performance is measured in terms of SSIM [80], VIF [81], PSNR, and VSNR [82]. Table 3.8 and Table 3.9 show the average data of these indexes for all the tested WLI and NBI sample images.

Table 3.8: Quality of the reconstructed WLI images after sub-sampling

Sub-sample scheme	Luminance (Y)				Chrominance	
	SSIM	VIF	PSNR(dB)	VSNR(dB)	PSNR(dB) E	PSNR(dB) F
YEF888	0.999	0.988	57.3	58.0	60.2	60.5
YEF422	0.998	0.986	57.0	55.5	57.8	58.9
YEF412	0.998	0.984	56.5	54.7	54.6	58.8
YEF814	0.998	0.977	55.3	52.5	51.0	58.3
YEF822	0.998	0.978	55.9	53.2	54.6	55.0
YEF812	0.998	0.972	54.7	51.4	51.0	54.8
YEF811	0.998	0.957	53.6	46.1	51.0	50.4
YEF16.1.2	0.997	0.952	52.3	43.9	47.9	50.4

Table 3.9: Quality of the reconstructed NBI images after sub-sampling

Sub-sample scheme	Luminance (Y)				Chrominance	
	SSIM	VIF	PSNR(dB)	VSNR(dB)	PSNR(dB) E	PSNR(dB) F
YEF888	0.998	0.989	57.1	69.2	60.7	60.0
YEF422	0.998	0.989	57.1	66.2	58.3	59.2
YEF412	0.998	0.988	57.0	66.2	55.1	59.2
YEF814	0.998	0.987	56.9	66.2	51.8	59.1
YEF822	0.998	0.986	56.7	66.4	55.1	56.7
YEF812	0.998	0.985	56.8	66.5	51.8	56.7
YEF811	0.998	0.980	56.5	59.4	51.8	53.5
YEF16.1.2	0.998	0.978	56.5	59.3	49.4	53.5
YEF16.1.1	0.998	0.973	56.2	52.1	49.4	50.9

It can be seen from Table 3.8 and Table 3.9 that YEF888 scheme yields the best performance as expected since no sub-sampling is performed. The YEF16.1.2 scheme (that means for every 16 Y components, one E and two F components are taken) produces the poorest result

since it is heavily sub-sampled. In case of NBI, it is YEF16.1.1 that exhibits poorest results. In this work, to support both band imaging, YEF812 have been chosen for the VLSI implementation. Table 3.10 shows the comparisons of compression ratio (CR) and overall PSNR with other related works. Here, the CR and the overall PSNR considering all three color components are calculated using (3.14) and (3.15) respectively:

$$CR = \left(1 - \frac{\text{Total Bits After Compression}}{\text{Total Bits Before Compression}}\right) \times 100 \tag{3.14}$$

$$PSNR_{overall} = 20 \times \log_{10} \frac{255}{\sqrt{\dfrac{1}{M \times N \times 3} \sum_{c=1}^{3} \sum_{n=1}^{N} \sum_{m=1}^{M} \left(x_{m,n,c} - x'_{m,n,c}\right)^2}} \tag{3.15}$$

where, M and N are the image width and height namely. C represents the color components (red, green, and blue), x and x' are the original and reconstructed component values namely. It should be noted that, all previously reported works so far are based on white light imaging (WLI). Hence, the results of WLI only are presented in Table 3.10 . Here, the CR is broken into three categories – sub-sampling only, sub-sample with encoding, and sub-sample with encoding and clipping – for better assessment. For instance, when YEF812 scheme is used, the scheme achieves an average compression ratio of 80.4% (with sub-sampling + encoding + clipping) and average PSNR is 43.7 dB. It can be seen that, with the addition of a simple clipping algorithm, the achieved CR is improved by around 4%. Note that the results shown here are the average CR of all 100 WLI images. The overall PSNR is calculated without clipping. The errors between original and reconstructed images are generated due to sub-sampling and color space transformation. Note that the encoding and decoding procedure are lossless. Clipping does not have any impact on the quality of the image in the visual region, and hence only affects the CR.

Table 3.10: Comparison of performance with other works (WLI only)

	SS scheme	CR %			Overall PSNR (dB)
		SS (only)	SS + G	SS + G + C	
Proposed	YEF888	0.00	62.9	69.2	51.3
	YEF422	33.3	71.2	76.1	49.3
	YEF412	41.7	73.3	77.8	47.3
	YEF814	45.8	74.4	78.7	41.4
	YEF822	50.0	75.4	79.5	45.9
	YEF812	54.2	76.5	80.4	43.7
	YEF811	58.3	77.5	81.3	42.2
	YEF16.1.2	60.4	78.2	81.8	40.4
X. Chen *et al.*[13]				56.7	46.4
X. Xiang *et al.* [48]				72.7	46.8
K. Wahid *et al.* [26]				87.1	32.9
P. Turcza *et al.* [27]				32.0	36.5
M. Lin *et al.* [28]				79.6	32.5
JPEG-FP [32]				81.5	31.5
C. Hu *et al.* [45]				72.0	39.6
J. Wu *et al.* [42]				50.0	31.0
L. Dung *et al.* [31]				82.0	36.2
J. Li *et al.* [33]				75.4	47.7
M. Lin *et al.* [30]				82.3	40.7

SS – sub-sampling; G – Golomb encoding; C - clipping

When compared with other existing works targeted towards capsule endoscopy (for WLI), the proposed scheme produces competitive CR with higher image reconstruction quality. The proposed algorithm for YEF812 sub-sampling outperforms in CR and competitive PSNR compared to [27][28][42][13][48][45] and[33]. Compared to the works from [26][32][31] and[30], the proposed algorithm has competitive CR and higher PSNR. It should be noted that these works use DCT-based approach, which is computationally expensive. Moreover, the reconstructed images may contain blocking artifacts due to the inherent nature of DCT-based algorithms. Note that, our proposed algorithm does not produce any blocking artifacts in the reconstructed images. Thus, considering the compromise of CR and PSNR, the proposed algorithm outperforms all other schemes by a good margin. From Table 3.8, it is also seen that the reconstructed images of the

proposed algorithm have medically acceptable PSNR (over 35 dB) [79][78][90] in all schemes. In Figure 3.15, the original and reconstructed WLI images using the proposed algorithm for YEF814 and YEF812 sub-sampling scheme are shown.

| (a) Original | (b) YEF814
PSNR = 48.3,
CR = 78.2% | (c) YEF812
PSNR = 47.7,
CR =80.3% | (d) YEF812 (clipped)
PSNR = 47.7,
CR = 82.0% |
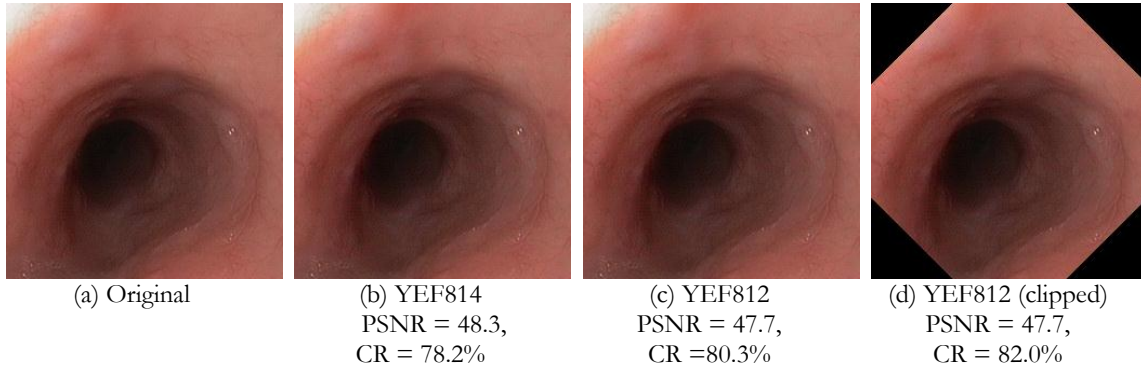
Figure 3.15 Original WLI image (a) and reconstructed WLI images (b)-(d)

The results for NBI images are shown in Table 3.11. Due the presence of sharper edges in luminance component in NBI images, the compression ratio gets slightly less than WLI images. However, chrominance (E and F) components in NBI images vary less than WLI images (as shown earlier in Table 3.2), which enables heavily sub-sample (such as YEF16.1.1) color components without losing image quality. Figure 3.16 shows the original and reconstructed NBI images for YEF16.1.1 sub-sampling scheme.

The average compression ratio and image quality of several endoscopic video sequences for YEF812 sub-sampling scheme (both WLI and NBI) are shown in Table 3.12. The results in Table 3.12 are better (higher CR and PSNR) than that of Table 3.10 and Table 3.11.

Table 3.11: Results for NBI endoscopic images

SS Scheme	Compression ratio (CR) %			Overall PSNR (dB)
	SS (only)	SS + G	SS + G + C	
YEF888	0.00	61.2	67.8	51.3
YEF422	33.3	69.5	74.7	49.8
YEF412	41.7	71.6	76.5	47.7
YEF814	45.8	72.8	77.4	44.8
YEF822	50.0	73.7	78.2	46.9
YEF812	54.2	74.9	79.2	44.4
YEF811	58.3	75.9	80.1	43.4
YEF16.1.2	60.4	76.6	80.6	41.7
YEF16.1.1	62.5	77.2	81.1	40.8

SS – sub-sampling; G – Golomb encoding; C – clipping
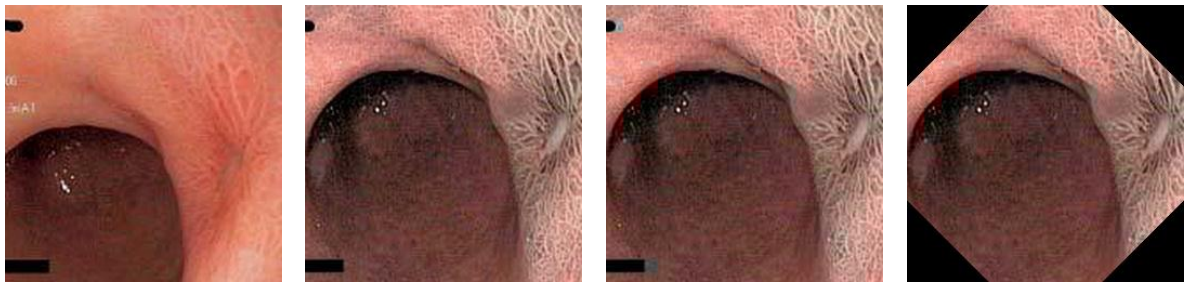
| (a) Original WLI | (b) Original NBI of (a) | (c) YEF16.1.1 PSNR = 40.8, CR = 76.1% | (d) YEF16.1.1 (clipped) PSNR = 40.8, CR = 80.6% |

Figure 3.16 Original images (a)-(b), and reconstructed NBI images (c)-(d)

Table 3.12: Average compression ratio and image quality in WCE video for YEF812 sub-

sampling

Mode	Video	Avg. CR %	Avg. Overall PSNR (dB)	SSIM	VIF	VSNR
WLI	Video-1 (99 frames)	86.1	47.2	0.9965	0.9551	44.2
	Video-2 (97 frames)	86.0	47.6	0.9965	0.9527	41.8
	Video-3 (97 frames)	85.6	47.5	0.9966	0.9510	43.8
	Video-4 (97 frames)	86.1	47.6	0.9964	0.9441	40.9
	Video-5 (97 frames)	85.7	46.4	0.9963	0.9592	44.6
NBI	Video-1 (889 frames)	82.3	46.3	0.9972	0.9718	52.4
	Video-2 (322 frames)	81.7	46.3	0.9977	0.9800	52.3

Images with different pathological conditions will show different texture; for example, a polyp aspect is different than a Crohn's disease. To evaluate the performance of our scheme for these cases, another simulation has been conducted where several GI images with known diseases (or conditions) were used. The results are summarized in Table 3.13. The achieved reconstruction quality is high (PSNR over 41 dB in all cases) which indicates that the proposed scheme is well able to reconstruct images of pathological importance. Some of the original and reconstructed images with disease names are shown in Figure 3.17 .

Table 3.13: Performance of images with disease / medical condition

Image with condition		Number of images	Avg. CR %	Avg. overall PSNR (dB)
WLI	Polyps	10	81.7	42.9
	Crohn's disease	10	79.7	41.3
	Ulcer	10	82.4	42.9
	Cancer	10	80.0	41.8
NBI	Barrets oesophagus	5	79.3	46.1
	Rectal benign tubular adenoma	1	74.5	40.4
	Oesophageal glycogenic acanthosis	5	79.9	46.6
	Oesophageal papillomatosis	1	79.7	45.6
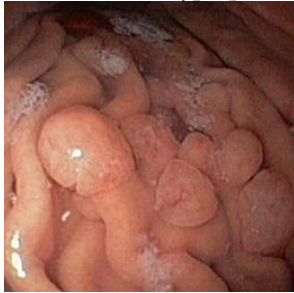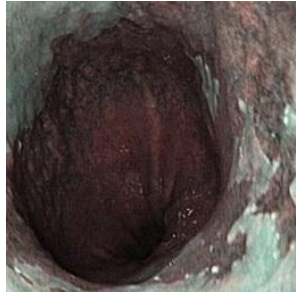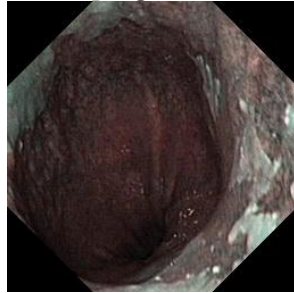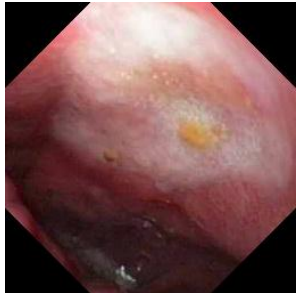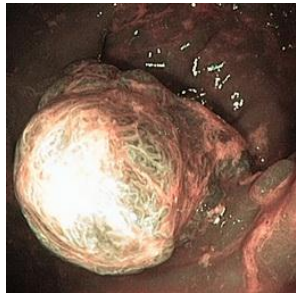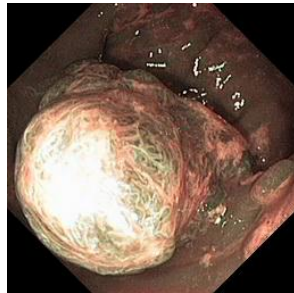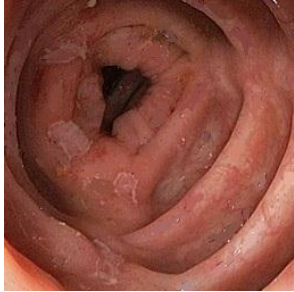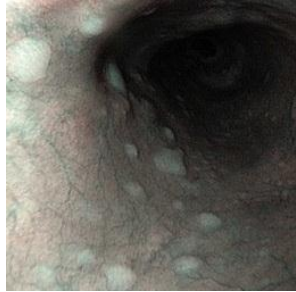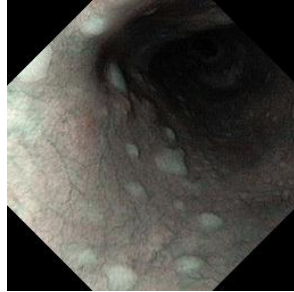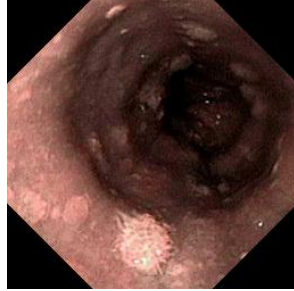
WLI	NBI
(Original at left, Reconstructed YEF812 at right)	**(**Original at left, Reconstructed YEF812 at right)
Disease 1: Hyperplastic polyps in the gastric body	**Disease 5: Barrets oesophagus**
CR: 80.34%, PSNR: 44.71	CR: 78.70%, PSNR: 45.06
Disease 2: A benign gastric ulcer at diaphragm level	**Disease 6: A large rectal benign tubular adenoma**
CR: 83.97%, PSNR: 44.79	CR: 74.58%, PSNR: 40.42
Disease 3: Crohns disease	**Disease 7: Oesophageal glycogenic acanthosis**
CR: 76.67%, PSNR: 44.70	CR: 80.01%, PSNR: 46.97
Disease 4: Cancer in the sigmoid colon	**Disease 8: Oesophageal papillomatosis**
CR: 81.25%, PSNR: 42.23	CR: 79.74%, PSNR: 45.61

Figure 3.17 Original images and reconstructed images with known medical conditions; all PSNR in dB

3.7   Subjective evaluation by medical doctors

The diagnostic process of medical images involves two basic processes: visually inspecting the image (i.e., visual perception) and come up with an interpretation (i.e., cognition) [91][92]. In general, the most important factors contributing to medical image quality are contrast, spatial resolution, and noise. Ideally high contrast, high spatial resolution, and low noise are desirable; however, these are not independent factors, as they may affect each other in many ways[93]. As part of the visual perception, in this work, two surveys have been conducted. In the first survey, several original and reconstructed (for YEF812 sub-sampling case) image pairs were shown to four professional doctors in the field of medical imaging (names are mentioned in the Acknowledgement section) and were asked to provide numerical ratings on the quality of the reconstructed images by visually comparing with the original images. The survey questions and images are shown in Appendix C.1. The results of this survey is shown in Table 3.14. Every reconstructed image has passed the test of acceptability. The average Mean Opinion Score (MOS) [79] of all images is 2.10, which can be ranked as "highly acceptable".

Table 3.14: Results of the first survey by medical doctors

	Doctor 1 S_1	Doctor 2 S_2	Doctor 3 S_3	Doctor 4 S_4	MOS
Image #1	2	2	2	2	2.00
Image #2	2	2	2	2	2.00
Image #3	3	2	2	2	2.25
Image #4	3	2	2	2	2.25
Image #5	1	2	2	3	2.00
Average Mean Opinion Score (MOS)					**2.10**

Excellent (no visual difference) = 3, Good (highly acceptable) = 2
Average (marginally acceptable) = 1, Poor (not acceptable) = 0
MOS = sum$\{S_1:S_M\}$/M, M = 4

In the second survey, several original images were used where diseases or conditions (such as polyp, cancer, etc.) were positively labeled (by Gastrolab [83]). The reconstructed images were generated using the proposed scheme (using YEF812 sub-sampling). In this survey, seven gastroenterologists (names added in the Acknowledgment section) were shown both original (with a condition labeled) and the reconstructed images, and asked to provide opinion score on the ability to detect that particular condition. The survey questionnaire was formulated with consultation with these gastroenterologists. The survey questions and images are shown in Appendix C.2. and the results are summarized in Table 3.15. The average MOS is 1.43 (i.e., categorized as "Yes, sufficiently enough information"), which indicates that the proposed lossy compression scheme is able to retain enough information to easily identify those five conditions.

Table 3.15: Results of the second survey by medical doctors

	Image	Doc 1 S_1	Doc 2 S_2	Doc 3 S_3	Doc 4 S_4	Doc 5 S_5	Doc 6 S_6	Doc 7 S_7	MOS
WLI	**Image #1** Disease: Hyperplastic polyps in the gastric body	2	2	1	2	2	1	0	1.43
	Image #2 Disease: Oesophageal lesion caused by a sharp chicken bone	2	2	1	2	2	0	1	1.43
	Image #3 Disease: Cancer in the Sigmoid Colon	1	2	1	2	2	0	2	1.43
NBI	**Image #4** Disease: Barrets oesophagus	1	2	1	2	2	1	1	1.43
	Image #5 Disease: Oesophageal glycogenic acanthosis	2	2	1	2	2	1	0	1.43
Average Mean Opinion Score (MOS)									**1.43**

Yes, no doubt = 2; Yes, sufficiently enough information = 1;
Neutral, unsure = 0; No, not enough information = -1; No, not at all = -2;
MOS = sum{S_1:S_M}/M; M = 7

In this work, compression algorithm has been proposed for capsule endoscopy and done some initial assessments (both objective and subjective) which shows some positive and encouraging results. However, more exhaustive experimentation and clinical trials need to be done in future to draw a final conclusion. In order to strengthen the performance of visual assessment on clinical diagnostic's point of view, in the future, it is planned to conduct animal testing followed by a "task-based" approach [94] where the doctors would attempt to perform a specific diagnosis and the accuracy of their decision would be measured using statistical tools (such as Receiver Operating Characteristics (ROC) analysis [95]).

3.8   Hardware implementation

From the results of Section 3.6, it is seen that the compression ratio and image quality are inversely proportional (i.e. if compression ratio is increased, then image quality is decreased and vise - versa) and a compromise need to be made between the two. Among them YEF812 scheme is chosen for conducting survey and for the hardware implementation of the compressor. The reason for choosing YEF812 is that it provides a good compression ratio, which will significantly reduce the bandwidth and power requirements of the RF transceiver. Moreover, the reconstructed image quality in YEF812 scheme is above the requirements for medically acceptable PSNR and the images also passes the subjective evaluation by professional medical doctors as discussed in Section 3.7.

3.8.1   Compressor architecture

The compression algorithm with YEF812 sub-sampling is implemented in Very high speed integrated circuits Hardware Description Language (VHDL) and the functionality is verified. The overall block diagram of the proposed image compressor is shown in Figure 3.18. Most commercial CMOS image sensors [34][35][36] send image data bytes in raster-scan fashion using a common Digital Video Port (DVP) parallel output interface[35]. The input lines of the proposed compressor

implements the DVP interface so that commercial CMOS image sensors can be directly interfaced with the proposed compressor. In a DVP interface, the *VD (or VSYNC)* and *HD* (or *HSYNC*) pins indicate the *end of frame* and *end of row* respectively. The image compressor samples the RGB pixel bytes from *DATA_BUS(7:0)* bus on each positive edge of *DCLK* and then generates the compressed variable length codes on the *CODE_DATA(31:0)* bus and its end bit index on *CODE_LEN (4:0)* bus within a single clock cycle (cc) of *DCLK*. Thus, the latency of the proposed design is 1 cc. Whenever a new code appears on the data bus, the *IS_NEW_CODE* signal goes from low to high.
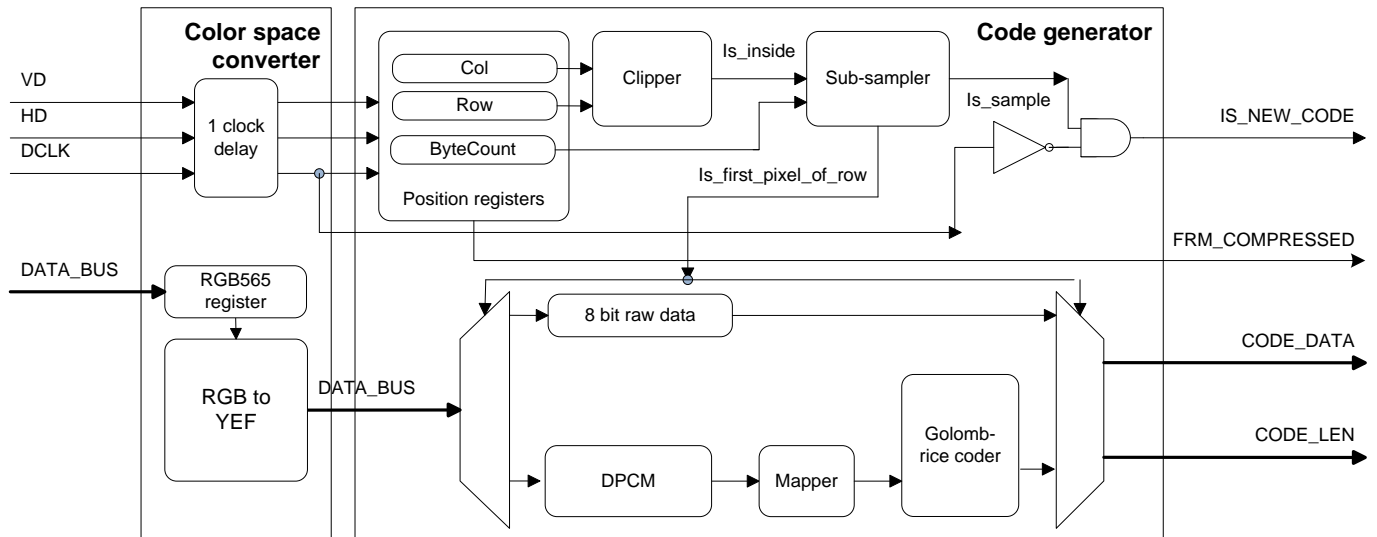
Figure 3.18 Block diagram of the compressor

The overall design is divided into three major components. The description of these components is given below.

3.8.1.1 Color space converter

This block converts the RGB pixel data to YEF according (3.1), (3.2) and (3.3). The image sensor sends the RGB data for a pixel in RGB565 format using 2 clock cycles; so a 16 bit (2 bytes) register is implemented to store the RGB data for one pixel. The *RGB to YEF* block converts the data to

49

YEF422 format and the output is fed to the *Code generator* block. The *VD*, *HD* and *DCLK* signals are delayed 1 cc as the conversion from RGB to YEF is only possible from the second cycle.

3.8.1.2 Code generator

In the *code generator* block, the position registers such as the *Col*, *Row*, and *ByteCount* stores the column, row, and the byte-position in the row of the currently sampled pixel namely. From the *Col* and *Row*, the *Clipper* module decides whether clipping is necessary. If the pixel is inside the set visual region, the pixel byte-position is further checked by the *Sub-sampler* module where YEF812 scheme is implemented. The *DPCM* module calculates the change of pixel value with respect to its left pixel value. The *Mapper* maps the changes to non-negative integers and then the *Golomb-Rice coder* generates the variable length code on *CODE_DATA* bus along with its code length on *CODE_LEN*. The first pixel of the row is transmitted in raw 8-bit format. The compressor generates the variable length code in a single clock cycle, thus it can produce output at the same rate of the input pixels coming from the image sensor. So, it does not need any significant input buffer memory. After a complete frame is compressed, the *FRM_COMPRESSED* signal is asserted.

3.8.1.3 Parallel to serial converter (P2S)

A parallel to serial (P2S) converter, as shown in Figure 3.19, is needed to connect the compressor to RF transceiver which accepts data serially using any serial protocol. Compressed output bit-stream is available for sampling at the *SERIAL_DATA* bus at each positive edge of *SERIAL_CLK*.

The P2S block samples the *CODE_DATA* and *CODE_LEN* buses at the low to high transition of the *IS_NEW_CODE* and then sends the *CODE_LEN* number of bits serially (starting MSB first) using the *SERIAL_DATA* and the *SERIAL_CLK* pins. The *DCLK_32* is the input clock signal for this module that has at least 32 times higher frequency than the *DCLK* frequency, so that in one clock cycle of *DCLK*, all the coded bits (which can be maximum 32) can be

safely transmitted serially. At each positive edge of *SERIAL_CLK,* the RF transceiver can sample the bits from the *SERIAL_DATA* pin.
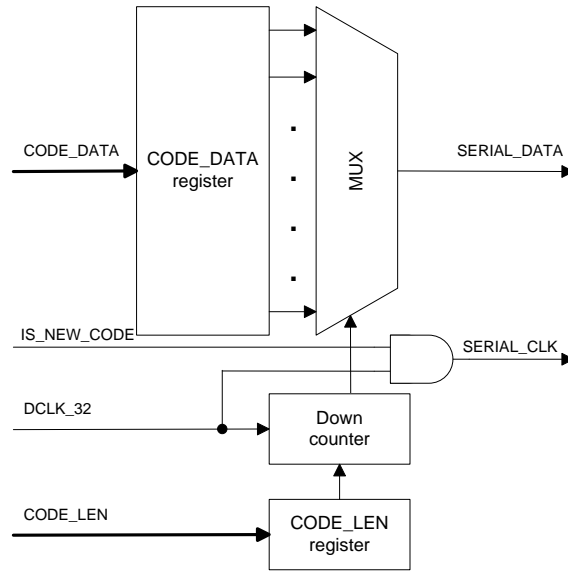
Figure 3.19 Block diagram of the parallel to serial converter (P2S)

3.8.2 Design verification in FPGA

The overall compression system as shown in Figure 3.18 is then verified in Altera DE2 board (having Cyclone II FPGA). The block diagram and the experimental setup are shown in Figure 3.20. A commercial image sensor [34] is used to capture images and it is connected with the DE2 board using GPIO ports. The compressor compresses the captured images and the compressed bit-stream is stored in the on-board SRAM of the DE2 board. Then the compressed bit-stream in the SRAM is read by a PC using USB port. The stream is then decoded in the PC software and the image is reconstructed.
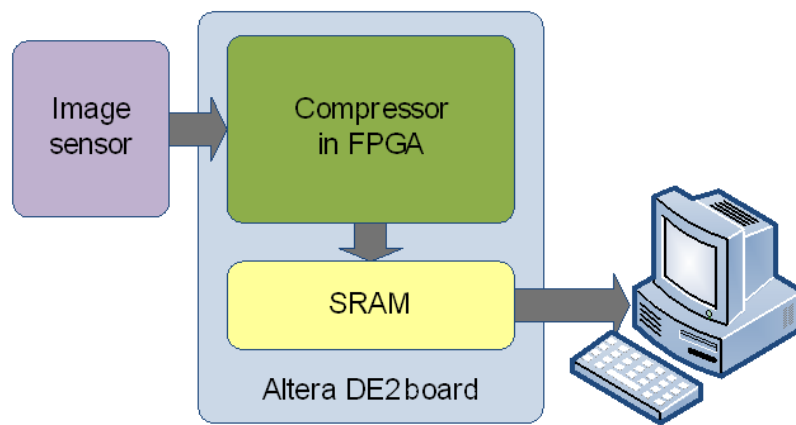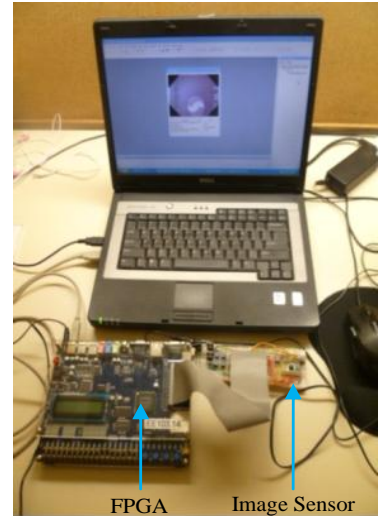
(a)   (b)

Figure 3.20 (a) FPGA verification diagram; (b) FPGA verification setup

3.8.3   ASIC chip fabrication of the compressor

The proposed design (lossy compressor) is later synthesized using 0.18 µm CMOS technology using standard Artisan library cells. CMOS 0.18 µm technology (CMOSP18) is chosen because due to its availability in the lab. The compressor consumes 995 cells and 0.33 mW of power (estimated by simulation using *Synopsys design analyzer*) at 2 FPS. It should be noted that, the P2S block only helps to interface the compressor with serial RF transceiver and this block may not be considered as part of the compressor. The design without the P2S module consumes only 0.042 mW of power. The percentage area and power consumption of different blocks of the design (estimated by simulation using *Synopsys design analyzer*) is shown in Figure 3.21. The P2S module consumes the major portion of the power as it runs at 32 times higher clock frequency than the other modules. However, the color space converter (RGB2YEF) and the code generator block consumes very low power compared to P2S. This is due to the simplicity in the compression algorithm as described in Section 3.5.
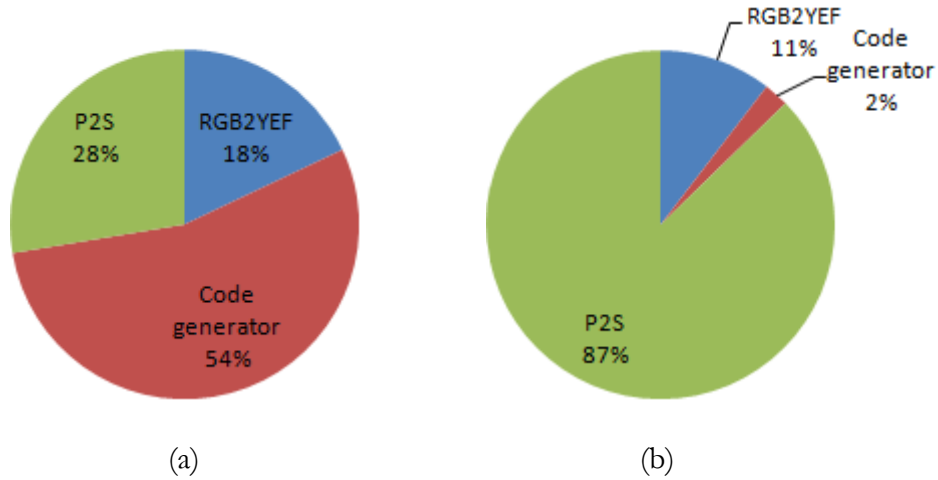
Figure 3.21 Chip details of different blocks: (a) area consumption; (b) power consumption

The image compressor including P2S unit (without RGB2YEF) is fabricated in silicon and the microphotograph of the chip is shown in Figure 3.22. For testing the chip, it is connected with an image sensor [34] and with Altera DE2 FPGA board similar with the diagram shown in Figure 3.20, the difference is that the compressor chip is outside the FPGA board. The FPGA contains blocks for initializing the image sensor, transferring the bit-stream generated by the compressor chip to the DE2's on-board RAM, clock generator etc. The actual power consumption (measured) of the chip is 0.22 mW.
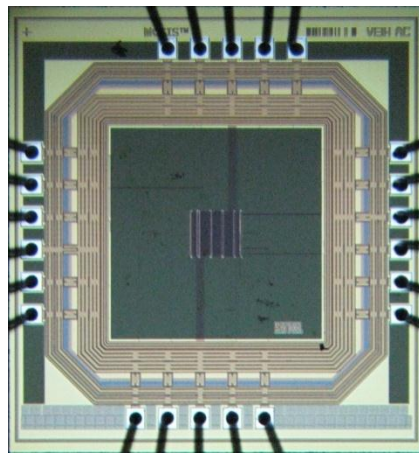
Figure 3.22 Microphotograph of the lossy compressor chip

The synthesized results are compared with other works and presented in Table 3.16. It should be noted that the results shown are only for WLI, since as of today, there is no existing work on image compression for NBI. From Table 3.16, it is seen that the proposed compressor occupies the least core area and hardware cost (i.e., gate count). It needs small size of buffer memory (only 5 bytes), which can be considered negligible, and implemented using resisters. The power consumption of the compressor is also the lowest comparing with all other works.

Table 3.16: Comparison of hardware cost with other schemes (WLI only)

Work	Type	Complexity	Die size (mm×mm)	Core area (mm²)	Cell count	Gate count	Buffer memory	Latency (cc)	Power (mW)
[13]	JPEG-LS (with run mode)	O(n)	3.4×3.3^2	11.2^2	--	19.5K	2.19 KB	w[1]	0.80
[26]	Transform coding (DCT)	O($n \log n$)	--	0.326	3,466	--	Yes	18	10.00
[28]	DCT and LZ77 encoding	O($n \log n$)	1.25×1.25	0.384	--	31K	Yes	--	14.92
[31]	H.264 based DCT	O($n \log n$)	--	--	--	60K	Yes	--	0.92
[30]	DCT and LZ77 encoding	O($n \log n$)	--	--	--	318K	Yes	--	9.17
Proposed	Differential coding	O(n)	0.67×0.71	0.032	736	2.5K	5 B	1	0.33

[1]w=width of input frame; e.g., for a 256 × 256 image, the latency is 256;
[2]includes other digital components, such as, microcontroller, I2C module, etc.;

The latency for [28] and [31] were not reported. However, these schemes use 2-D 8 × 8 DCT coding that is similar to the DCT implementation presented in [96]; as a result, the latency for [28] and [31] is estimated to be 92. Compared to all these existing designs, the proposed scheme has a latency of 1 clock cycle (cc) which is the lowest. It is noted again that the design supports both WLI and NBI modes and performs equally well for both types of images.

Therefore, the proposed algorithm meets all the design criteria set in Section 3.2 and presents itself as a strong candidate for power-efficient implantable image compressor for wireless endoscopic applications.

3.9   Summary

In this chapter, a lossy image compression algorithm is developed on the basis of analyzing the unique properties of endoscopic images. A novel and low complexity color space, YEF, has been proposed for better compression of endoscopic images. After converting the pixels from RGB color space to YEF, the proposed compressor calculates the difference of adjacent pixels using by DPCM and then encodes the differences in variable length Golomb-Rice coding. Based on the nature of endoscopic images, several sub-sampling schemes on the chrominance components are applied. The proposed compressor is tailored to work with both WLI and NBI. The compressor is designed to work with any commercial low-power image sensor that outputs image pixels in raster scan fashion, eliminating the need of memory buffer and temporary storage (as needed in transform coding schemes). An image corner clipping algorithm is also introduced.

Compared to other designs targeted to video capsule endoscopy, the proposed scheme performs strongly with a compression ratio of 80.4% for WLI and 79.2% for NBI, and a high reconstruction peak-signal-to-noise-ratio (PSNR), over 43.7 dB for both bands. The reconstructed images have been verified by several medical imaging doctors for acceptability.

The proposed design is verified in field-programmable-gate-array (FPGA) board and then implemented in a 0.18 μm CMOS technology and the chip has been fabricated. Compared with other works, the proposed compressor consumes the least silicon area and power, which makes it a strong candidate for power-efficient implantable image compressor for wireless endoscopic applications.

Chapter 4: Lossless Compression Algorithm

4.1   Introduction

Lossy image compression algorithms produce some difference between the original and reconstructed images. For medical diagnostics, the distortion of the reconstructed image can lead to inaccurate diagnostics decisions. However, lossless compression algorithms produce identical reconstructed images compared with the original images without any distortion. In this chapter, the proposed low complexity lossless compression algorithm designed for WCE is discussed.

4.2   Design requirements

In this work, the following design requirements for the compressor have been set:

- The capsule must consume low power as the battery life is limited while it travels through the intestine. Hence, focus is made on compression algorithms with low complexity and low power.

- The area is a critical issue for the capsule. Memory consumes significant silicon area and power. Here, focus is made on algorithms that do not require buffering of the image in memory.

- The compressor should be able to work with commercially available CMOS image sensors [34][35][36] which send data in raster-scan fashion.

- For an accurate diagnosis, the quality of the reconstructed image is important. So, focus is

made on lossless image compression algorithms.

- The compression algorithm must be able to reduce the data to be sent by the transmitter in order to fit into the bandwidth of the transceiver and save power.

- Finally, the compression algorithm should support both imaging modes – WLI and NBI, and equally produce high quality reconstruction with high degree of compression.

4.3   Analysis of endoscopic images

In order to develop a low-cost and lossless image compression algorithm tailored for capsule endoscopy, 100 WLI (taken from 20 different positions from larynx to anus of the GI tract) and 15 NBI endoscopic test images [83] have been analysed. Moreover, several video sequences [2] (consisting of total 1,698 frames) are also used in this study. The conclusions of the several analyses are drawn from the average results of the test images.

4.3.1   Color space conversion

The novel YEF color space is also used in this algorithm. A detailed discussion on converting RGB pixels to YEF can be found in Section 3.3.1. It should be noted that, YEF color space is reversible, thus pixels from YEF color space can be reverted back to RGB without any data loss. While reverting, a minor change in some pixel values may occur due to rounding of fractions to integer, which is negligible.

4.3.2   Differential pulse coded modulation (DPCM)

The DPCM block calculates the difference of consecutive pixel values, dX. It does not quantize the data, so no loss of data occurs at this stage. The detailed description of this stage can be found in Section 3.3.3.

4.3.3 Variable length coding

The difference of the consecutive pixels (dX) is then mapped to non negative integer using (3.7) and then they are encoded in variable length coding.

4.3.3.1 Golomb-Rice coding for dY component

The histograms of dY, dE and dF of one WLI and one NBI endoscopic image are shown in Figure 3.9. These plots show a two sided geometric distribution and in the case of geometric distribution, the Golomb-Rice code can give optimum compression. So, the difference in luminance is encoded using Golomb-Rice code.

The Golomb-Rice coding algorithm is similar to that is presented in Section 3.3.4. Figure 4.1 shows the length of Golomb-Rice code for different values of k. It has been noticed from Figure 3.9 that the most occurred value of dE and dF is zero and others are very close to zero. For dY, a wider range of value occurs. So, $k = 2$ for encoding the mapped integers of dY for WLI images is chosen.

It has been noticed from Figure 3.9 (a) and (b), that dY generally spans wider in NBI images than WLI images due to the presence of sharper edges. To get the best compression ratio, $k = 3$ for encoding the mapped integers of dY for NBI images is set.
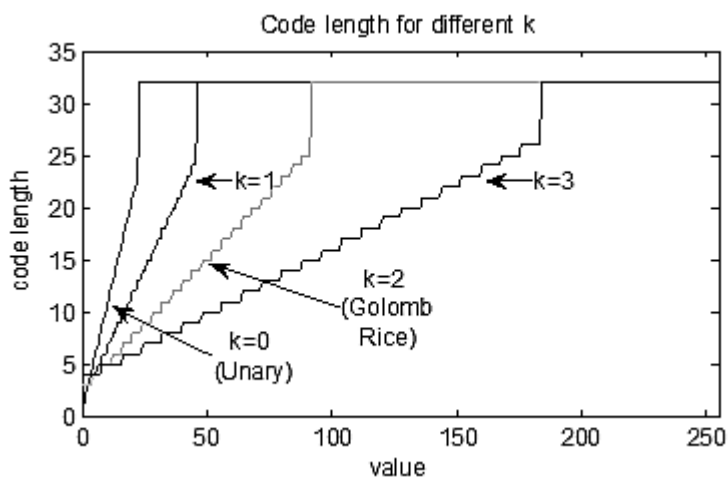
Figure 4.1 Length of Golomb-Rice and unary code

58

4.3.3.2 Unary coding for dE and dF component

The number of occurrence of *dE = 0* and *dF = 0* is very high as shown in Figure 3.9. In Golomb-Rice code for *k = 2*, it needs 3 bits to represent '0'. However, in *unary* coding, it only needs 1 bit to represent '0'. Hence, to get a good compression, smaller length codes for zero and near-zero values need to be assigned. As *dE* and *dF* values are mostly zero (others are very near to zero), unary code can be used to get better compression. Unary code can be generated by setting *k = 0* in the Golomb-Rice encoder. The maximum unary code length (u_{limit}) is set as 32 similar to g_{limit} for Golomb-Rice code. It should be noted that, unary code gets very large for larger values as shown in Figure 4.1. *dY* has wider range of values than *dE* and *dF* as shown in Figure 3.9. So, unary coding of *dY* does not improve compression ratio.

Pseudo color NBI images are reconstructed by combining two grayscale images in the workstation software. One image is captured using green light and another using blue light. As the input images are grayscale, only the luminance (Y) component is compressed and transmitted. The chrominance components are not sampled for NBI images. The coding scheme is summarized in Table 4.1.

Table 4.1: *k* parameter for encoding component differences

Mode	*dY*	*dE*	*dF*
WLI	2 (Golomb-Rice)	0 (Unary)	0 (Unary)
NBI	3 (Golomb-Rice)	Not sampled	

4.3.4   Corner clipping

In wireless endoscopy, the corner areas in a captured image are blacked out. The pixels at corner areas of the image are discarded using the corner clipping algorithm as described in Section 3.3.5 to get better compression.

4.4   Proposed lossless compression algorithm

The block diagram of the proposed lossless compression algorithm is shown in Figure 4.2. In contrast with the lossy compression algorithm, as proposed in Section 3.4, it does not sub-sample pixels, rather all pixels are sampled and encoded.
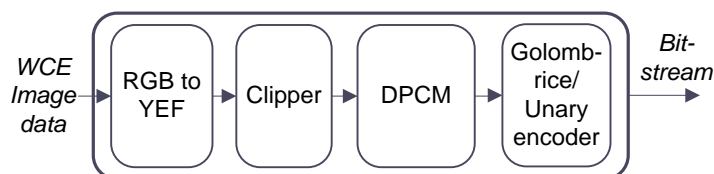
Figure 4.2 Block diagram of the proposed lossless compression algorithm

In the proposed algorithm, after converting RGB pixels to YEF color space, the compressor takes the difference of consecutive pixels using differential pulse coded modulation (DPCM) and then encode the differences in variable length coding. The differences of luminance (*dY*) component are encoded in Golomb-Rice code and the differences of chrominance (*dE* and *dF*) components are encoded in unary code. A customized corner clipping scheme is also implemented to remove uninteresting corner area of the image to increase compression ratio. The proposed lossless algorithm works in raster scan fashion and can be directly interfaced with commercial image sensors [34][35][36], eliminating the need of input buffer memory.

4.5   Complexity analysis of the proposed algorithm

A comparison between the proposed lossless algorithm and a standard lossless algorithm, JPEG-LS [46][47], is shown in Table 4.2. Here, it is seen that the proposed algorithm has lower computational complexity (such as static prediction and static k parameter) and lower memory requirement. Similar to the discussion presented in Section 3.5, the proposed algorithm has lowest computational complexity $O(n)$, and does not need any buffer memory.

Table 4.2: Comparison between the proposed lossless and standard JPEG-LS algorithm

	Proposed algorithm	JPEG-LS
Color space	YEF	RGB
Prediction	Static (left pixel)	Dynamic (based on edge detection)
Buffer memory required?	No	Yes, memory to store one row of image pixel + 1.9 kB for context register
k - parameter	Fixed	Dynamically calculated based on context array
Coding	Golomb-Rice and Unary	Golomb-Rice
Run mode	No (as long runs are rare in WCE images)	Yes

4.6   Simulation results

As the proposed compressor is lossless, the reconstructed image is identical compared with the original image and there is no degradation in the image quality. The average compression ratio (CR) of several WLI endoscopic images and video frames taken from [83][2] are summarized in Table 4.3. From Table 4.3, the proposed lossless compression algorithm produces approximately 78% average compression ratio for different types of images. Also, the proposed compression algorithm outperforms the standard JPEG-LS algorithm in compression ratio more than 17% for endoscopic images.

Table 4.3: Simulation results of WLI images

	Image description		Number of images	Avg. CR %
Proposed	Images from 20 different positions (from Larynx to Anus) of GI tract		100	74.7
	Capsule endoscopy video frames	Video -1	99	80.6
		Video -2	97	80.5
		Video -3	97	80.1
		Video -4	97	80.6
		Video -5	97	79.9
	Images containing disease condition	Ulcer	10	76.7
		Polyp	10	76.0
		Crohn disease	10	73.5
		Cancer	10	73.8
JPEG-LS	Images from 20 different positions (from Larynx to Anus) of GI tract		100	57.9

The compression ratio of luminance component (without sampling the chrominance) of several NBI images are shown in Table 4.4.

Table 4.4: Simulation results of NBI images

Image description		Number of images	Avg. CR %
Images from different positions of GI tract		15	82.4
Capsule endoscopy video frames	Video -1	889	85.3
	Video -2	322	84.8
Images containing disease condition	Barrets Oesophagus	5	82.4
	Oesophageal Glycogenic Acanthosis	5	83.0

In order to demonstrate the effectiveness of the proposed compression algorithm in endoscopic images over standard images, the proposed algorithm is applied on two standard images [85] and the compression ratios are shown in Table 4.5. Here it is seen that the proposed

compression algorithm works much better on WCE images than standard images. It is due to the fact that there are relatively large variations in E and F component in non-endoscopic images than endoscopic images. As a result, dE and dF span in wider range in non-endoscopic images and the use of unary code cannot produce good compression ratio as unary code becomes very large for large values as shown in Figure 4.1.

Table 4.5: Comparison of compression ratio between standard images and WCE images

Image type	Image name	CR %
Standard image	Lena	62.6
	Mandrill	44.9
WCE	Images from different positions of GI tract	74.7

4.7 Hardware implementation

The hardware architecture of the proposed lossless compressor is similar as described in Section 3.8 except it does not require the sub-sampling block. Also, the Golomb-code generator uses different k parameters values as mentioned in Table 4.1. The hardware described in Section 3.8 can work as both lossy and lossless compressor. To get lossless compressed data, the sub-sampling block is disabled and the k parameter values are updated according to Table 4.1.

4.8 Summary

In this chapter, a lossless image compressor tailored towards WCE images is proposed. In the proposed algorithm, after converting RGB pixels to YEF color space, the compressor takes the difference of consecutive pixels using differential pulse coded modulation (DPCM) and then encodes the differences in variable length coding. The differences of luminance (dY) component are encoded in Golomb-Rice code and the differences of chrominance (dE and dF) components are

encoded in unary code. A customized corner clipping scheme is also implemented to remove uninteresting corner area of the image to increase compression ratio. The compressor has a average compression ratio of 78% for endoscopic images and images can be reconstructed from the compressed bit stream without any data loss. The proposed compressor works in raster scan fashion and can be directly interfaced with commercial image sensors, eliminating the need of input buffer memory.

Part III: **Prototype Development and Testing**

Chapter 5: Electronic Capsule

The state-of-the-art wireless capsule endoscopy (WCE) technology offers painless examination for the patients and the ability to examine the interior of the gastrointestinal tract by a non-invasive procedure for the gastroenterologists. In this part of the thesis, a modular and programmable WCE development system platform consisting of a miniature field programmable gate array (FPGA) based electronic capsule, a microcontroller based portable data logger unit and a workstation PC software are designed and developed. Due to the flexible and reprogrammable nature of the system, various image processing and compression algorithms can be tested in the design without any hardware change. The designed capsule prototype supports various imaging modes including white light imaging (WLI) and narrow band imaging (NBI), and communicates with the data logger in full duplex fashion, which enables configuring the image size and imaging mode in real time during the examination. A low complexity image compressor based on a novel color space is implemented inside the capsule to reduce the amount of RF transmission data. The data logger contains graphical LCD for real time image viewing and SD cards for storing image data. Data can be uploaded to a workstation PC or Smartphone by SD card, USB interface or by wireless Bluetooth link. The workstation software is developed to decompress and reconstruct images for diagnostics.

5.1 The capsule endoscopy system architecture

The overall architecture of the proposed capsule endoscopy system is shown in Figure 5.1. The system mainly consists of three major units - the capsule, the data logger and the workstation (such as PC or Smartphone). In order to receive an image frame from the capsule, a command is sent

wirelessly from the data logger unit to the capsule. The command contains the required image size, imaging mode, and light intensity information, which can be changed at anytime during data recording by the user through a graphical user interface (GUI) of the data logger. After receiving the command, the capsule configures its image sensor, compressor and lighting intensity levels based on the information in the command and then starts to send data packets of an image frame in compressed form wirelessly. The data logger reads the packets, stores them in SD card and then optionally decompresses and displays images on its LCD in real-time. The *end of a frame* is detected by a special sequence of bits (32 zero bits). The data logger then sends the wireless command again and it gets the next frame and so on. After data recording is completed, data from the data logger can be transferred to a PC or Smartphone using SD card, USB interface, or by Bluetooth link. In the PC or Smartphone software, the compressed image data are decompressed and displayed for medical diagnosis. The architecture of three major units - the capsule, the data logger and the workstation (such as PC or Smartphone) are described in this part of this thesis.

Capsule (1), Wearable data recorder (2),
Data transfer by SD (3), USB (4) and Bluetooth (5),
Workstation PC (6), Smartphone (7)
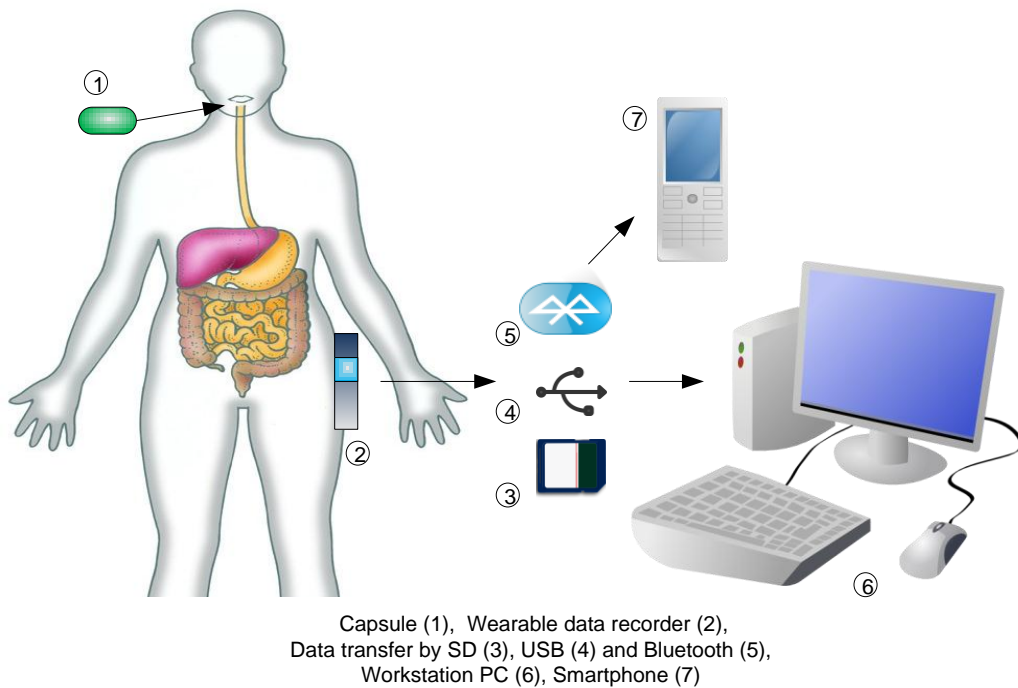
Figure 5.1 Capsule endoscopy system architecture

67

In this chapter, the design of a miniature FPGA based endoscopy capsule is discussed. The capsule hardware is designed in modular printed circuit boards (PCBs), thus any portion of the hardware can be replaced or modified without effecting the others boards. The developed capsule prototype supports various imaging modes including WLI and NBI, and communicates with the data logger in full duplex fashion, which enables configuring the image size and imaging mode in real time during the examination. The low complexity image compressors as proposed in Chapter 3 and Chapter 4 are implemented inside the capsule to reduce the amount of RF transmission data.

5.2   Design requirements of the capsule

In order to design an electronic capsule, the following design requirements are set.

- The capsule should be re-programmable, so that various image processing and compression algorithms (such as lossy and lossless) can be tested in order to find the most optimum solution, without any hardware change.

- The image sensor and the RF transceiver in the capsule should have standard interfaces enabling to test different components from different vendors.

- The capsule should support various lighting modes (such as WLI and NBI) and several types of LEDs must be present with the ability to control their intensity.

- The capsule should have an RF transceiver having sufficient bandwidth and error correction capability for proper transmission of the images. For example, for QVGA (320 × 240) resolution at 2 frames-per-second (FPS) and 80% compression ratio, the required application throughput of the wireless transceiver should be at least 722 kbps.

- The power consumption of the capsule must be low and should be able to work for more than 8 hours.

- The hardware design of the capsule should be modular, thus one board can be modified without changing the other boards.

- The size of the capsule should be small enough so that it can be swallowed in animal for *in-vivo* or *ex-vivo* animal testing.

- The capsule should communicate with the data-recorder in full-duplex fashion, so that the capsule can be configured in different settings by sending commands from the data-recorder wirelessly in real-time.

5.3   Architecture of the capsule

To make the hardware modular, the capsule is divided into four boards: *Imaging board*, *FPGA board*, *RF board* and *Power board*. The components were chosen considering performance, power requirement and physical size to fit into a miniature capsule prototype. The overall block diagram of the capsule is shown in Figure 5.2. A brief description of each of the boards are given below.
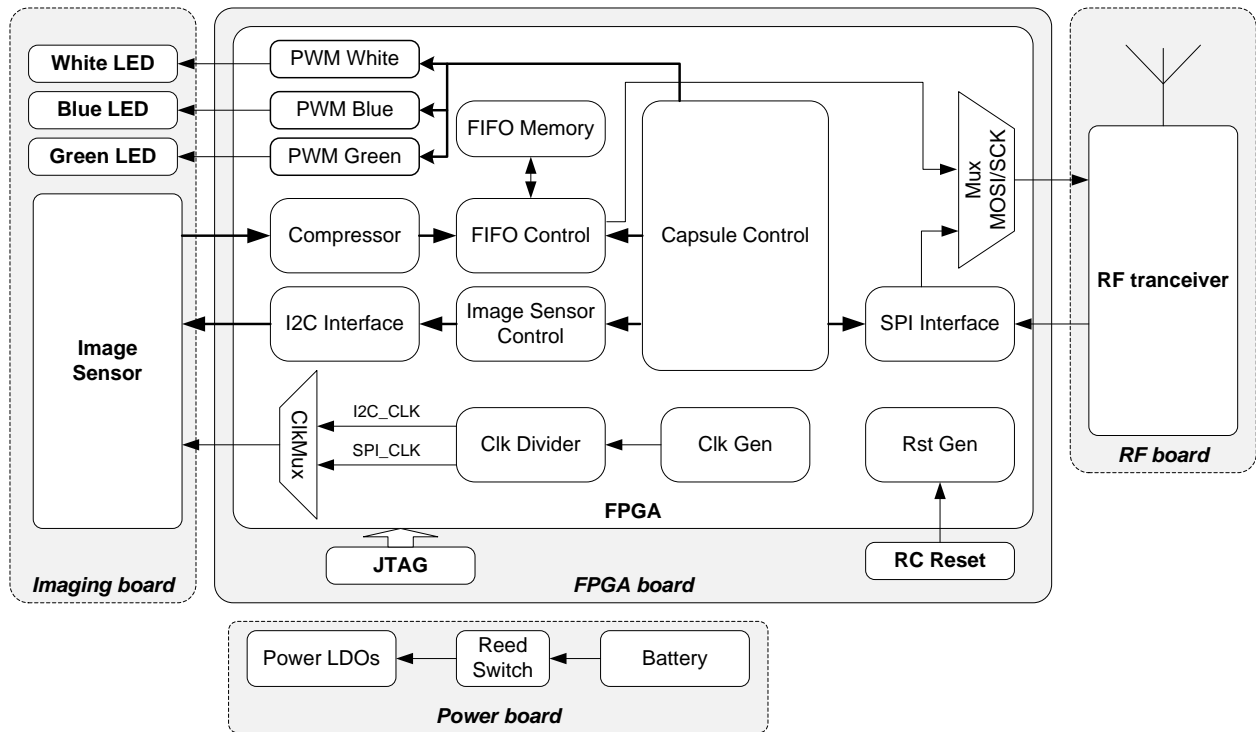
Figure 5.2 Architecture of the capsule

5.3.1 Imaging board

A commercial CMOS image sensor [34] is used in the capsule for capturing images. The image sensor sends pixel data in raster-scan fashion through a standard digital video port (DVP) parallel output interface, enabling to change the sensor with other sensors from different vendors implementing DVP interface, without major change in the design. It supports images of different size such as VGA (640 × 480), QVGA (320 × 240), QQVGA (160 × 120), subQCIF (128 × 96) etc. The sensor can be configured through two wire *I2C interface* [97]. The physical size of the sensor is 6 × 6 × 4.5 mm and a lens with adjustable focal length is placed over the pixel array.

In order to support both WLI and NBI imaging modes, two white LEDs [98], one blue LED [99] having a peak wavelength of 405 - 410 nm and one green LED [100] having a peak wavelength of 520 nm are used in the design. The white LEDs are illuminated while capturing WLI images. While capturing NBI images, one frame is captured by illuminating the blue LED and

70

another frame is captured by illuminating the green LED, and later these two frames are combined in the PC software to generate a high contrast NBI image. LEDs intensity are controlled by pulse width modulation (PWM) signals, which are generated from the FPGA.

5.3.2 FPGA board

This board contains the FPGA and an RC reset circuit. The RC reset circuit generates an active low reset signal after power up for resetting the FPGA. The FPGA contains all the custom designed digital blocks needed for the capsule operation. The chosen FPGA in [101] has physical dimension of $8 \times 8 \times 1.23$ mm and it contains 2112 lookup tables (LUTs), non-volatile RAM for storing configuration, built in clock generator, on-chip general purpose RAM blocks, 104 I/O lines etc. which makes it a suitable choice for miniature capsule endoscopy application. The board also contains JTAG interface for programming and debugging purpose. The digital blocks implemented inside the FPGA are briefly described below.

5.3.2.1 Capsule control

This block controls the overall capsule operation. An finite state machine (FSM) is implemented inside this block as shown in Figure 5.3. After getting reset signal, it initializes the RF transceiver parameters such as setting the data rate, channel frequency, packet size, auto-acknowledgment mode etc. The communication with the RF transceiver is done using the *SPI* interface block. Then it flashes the internal FIFO buffer of both the RF transceiver and the buffer of *FIFO Control block* and then sets the RF transceiver in RX (i.e. receiver) mode. The state machine then waits for a command to be sent by the data logger. After a command arrives, it reads the command from the RF transceiver and stores it in an internal register. The transceiver is then set in TX (i.e. transmitter) mode. Depending upon the command, the image sensor is then initialized with proper frame size by

the *Sensor control* block and proper LEDs are turned on based on the imaging mode (such as WLI or NBI). A request signal is sent to the *compressor* block and the compressor starts to send compressed data bits of the captured image to the *FIFO control* block. The state machine then requests the *FIFO control* block to send a complete data-packet (consists of 256 bit) to the RF transmitter directly through the *MuxMOSI/SCK* multiplexer. After a data packet is sent, it checks whether more packets needs to be sent for the current image frame or not. If more packets need to be sent, then it repeats the above procedure. When all packets for the current image frame are sent, then it turns off all the LEDs, flashes RF FIFO buffer, set the RF in RX mode and starts to wait for the next command from the data logger and so on.
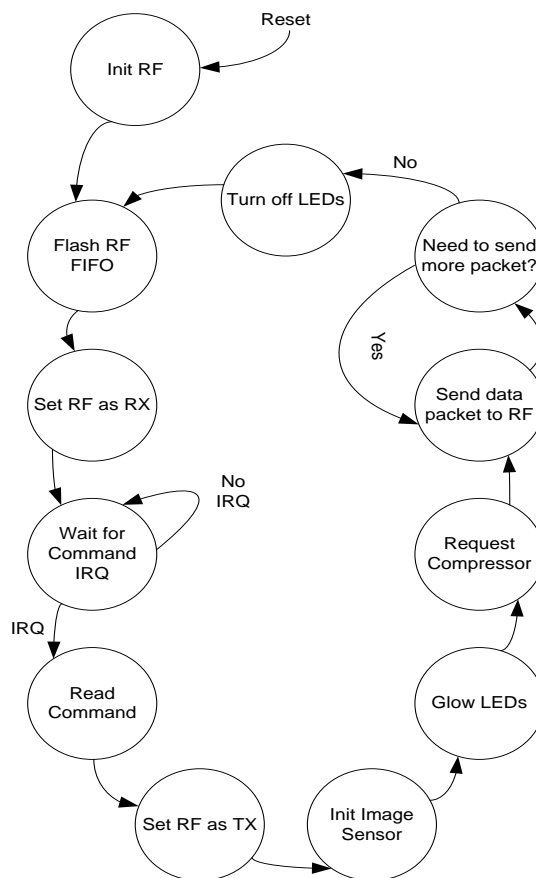
Figure 5.3 FSM inside capsule control block

5.3.2.2 Image sensor control and I2C interface

These blocks are used to configure different settings of the image sensor depending on the received command from the data-recorder unit. At the *Init Image Sensor* state as shown in Figure 5.3, the *Capsule Control* block requests *Image Sensor Control* block to set the internal configuration registers of the image sensor based on the received command. *Image Sensor Control* block communicates with the image sensor using the *I2C Interface* (master mode) [97] block. After the image sensor is configured, the clock input for these blocks are turned off by a glitch free clock gate [102] to save dynamic power.

5.3.2.3 Pulse Width Modulation (PWM) for LEDs

Three instances of PWM block are used in the design to adjust the light intensity of the white, blue and green LEDs. Each block takes a 3 bit intensity input from the *Capsule Control* block, giving the opportunity to control the light intensity at 8 different levels.

5.3.2.4 Compressor

The low complexity image compressors as proposed in Chapter 3 and Chapter 4 are implemented inside the capsule to reduce the amount of RF transmission data. The hardware architecture of the lossy and lossless compressors are described in Section 3.8 and Section 4.7 namely. In this prototype, the compressor hardware is implemented in such a way that it can reconfigure its parameters (depending on the wireless command received from the data logger) for both lossy and lossless compression and for both WLI and NBI modes.

5.3.2.5 FIFO control and memory

FIFO is used as buffering element or queuing element in a system when the rate of read operation is slower than the rate of write operation. The *Compressor* can produce bit-steam at a higher rate than the application throughput of the RF transceiver, so a FIFO is needed in the system. The *FIFO*

Control block stores the compressed data bits generated by the *Compressor* block in FIFO memory and sends the data bits to RF transceiver in first-in-first-out fashion when requested by the *Capsule Control* block. The *FIFO Memory* is a dual-port memory having a word width of one bit. The memory is synthesized in the FPGA's embedded RAM blocks [101]. The exact required size of the FIFO memory depends on the data throughput of the RF transceiver (discussed in Section 5.4.3).

5.3.2.6 Reset and clock generator

A 14 MHz built-in clock inside the FPGA is used as the primary clock source in the design. The *Clk_divider* block generates one clock output at 14 MHz (same as the input clock), and another at 777.76 kHz. The *Rst_gen* block is responsible for resetting the different blocks in the FPGA in proper order. The image sensor in [34] needs higher frequency clock input during initialization than the clock required for a low frame-per-second (FPS) capsule endoscopy application [103]. So, during initialization of the image sensor, the input clock frequency of the sensor is set with higher frequency clock and after the initialization is done, it is set with lower frequency clock. This clock switching is done by the *ClkMux* which is controlled by the *Capsule Control* block. The *ClkMux* block contains mechanisms to switch between two related clock sources without introducing glitches at the output [104].

5.3.3 RF board

This board contains the RF transceiver with other necessary passive components. The medical implantable communication service (MICS) compatible RF transceiver, which works at 402-405 MHz frequency, is the most suitable for transmitting data through the human body [105]. However, the MICS RF transceiver vendor [106] sells a low data-rate (effective data-rate around 500 kpbs [107]) transceiver (ZL70102) which is not sufficient even for 2 FPS capsule endoscopy application. A custom designed transceiver (ZL70081) having a data-rate of 2.7 Mbps, which is used in *PillCam*

[22], is not available for public purchase. So, the RF transceiver by Nordic [108] is used, which works at 2.4 GHz frequency band and having a raw data-rate of 2 Mbps. However, the theoretical effective data rate with minimum header information is 1.68 Mbps. The works in [109] and [107] show that 2.4 GHz transceivers, such as Nordic, can be effectively used to get data wirelessly through animal body.

Nordic transceiver [108] contains cyclic redundancy check (CRC) based error detection and retry with auto acknowledgement feature. In auto acknowledge mode, after receiving a data packet, the receiver checks the CRC bits and detects whether there was any error during the transmission of the packet. If there was any error, then it requests the transmitter to resend the data-packet again. This process goes on until the packet is transmitted successfully. So, in *auto acknowledgement* mode, generally no data loss happens, though the number of retries can decrease the overall application throughput. The transceiver communicates with the FPGA by *SPI Interface* [97] block. The physical size of the transceiver is 4 × 4 × 0.85 mm and it requires a 2.4 GHz chip antenna having a dimension of 6.5 × 2.2 × 1 mm.

5.3.4 Power board

As power source, three silver oxide button batteries [110], each having a rated voltage of 1.55 V and capacity of 195 mAh, are used in series in the design. The design requires 2.8 V and 1.5 V for image sensor, 1.2 V is for powering the FPGA core, and 3.3 V for RF transceiver and FPGA I/O power. These four DC voltage levels are generated using miniature low dropout regulators (LDO) [111]. A normally closed (N/C) magnetic reed switch [112] is placed between the batteries and the inputs of the power regulators in order to turn on and off power in the design from outside.

5.4 Results and discussion

5.4.1 The electronic capsule prototype

In first phase, the four boards, as outlined in Figure 5.2, are manufactured in circular PCBs each having a diameter of 43 mm as shown in Figure 5.4 for testing and troubleshooting. The PCBs are fabricated with the help of department lab.
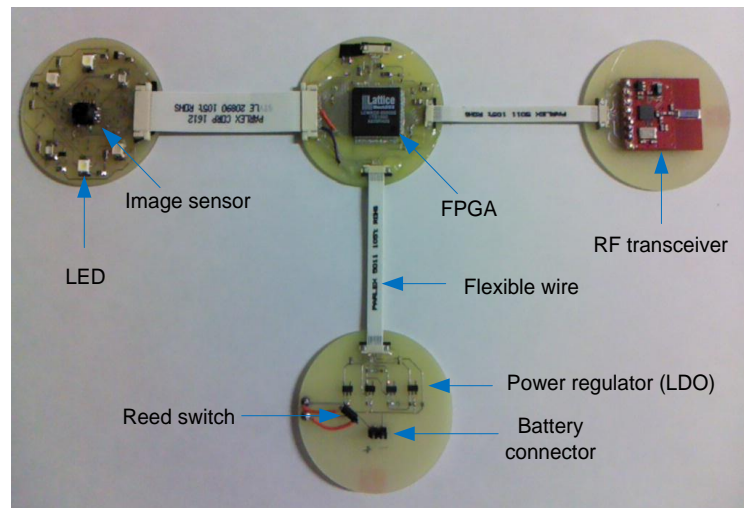
Figure 5.4 Photograph of the generation-1 capsule PCBs

In the second phase, the four PCBs are contracted out to third party for design[113], manufacturing and assembling [114] and the boards are manufactured in smaller size circular PCBs each having a diameter of 16 mm as shown in Figure 5.5. The PCBs are stacked on top of another using board-to-board connectors. The developed capsule PCBs are put inside a cylindrical casing having a length of 6 cm and diameter of 2 cm. The weight of the prototype is 20 g with casing, PCBs, and three button batteries.

<center>(a)</center> <center>(b)</center>
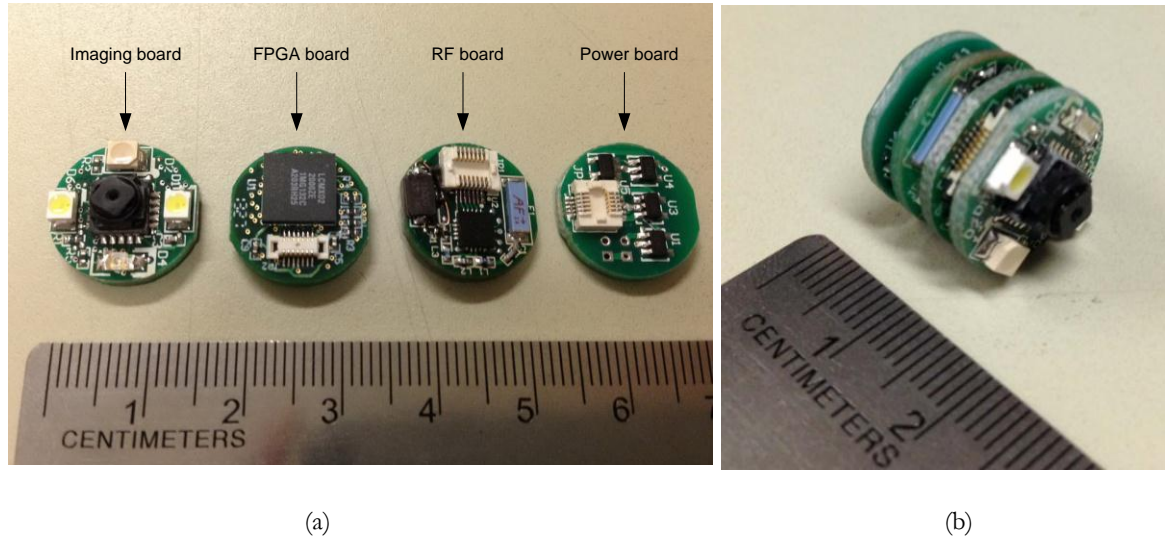
<center>Figure 5.5 Photograph of (a) The generation-2 capsule PCBs; (b) PCB's stacked together;</center>

It should be noted that, the prototypes do not contain the fabricated ASIC chip. The reason is that some of the features such as YEF color space and NBI mode came up later after the chip has been fabricated and so those features were not included in the chip. As the research is ongoing, the system is developed in flexible and programmable FPGA based platform so that design can be updated without going through the lengthy fabrication process of ASIC.

5.4.2 Resource and power consumption

The digital blocks discussed in Section 5.3.2, are modeled in VHDL and synthesized in the FPGA of the capsule prototype. The synthesis results generated by *Lattice Diamond* [115] are summarized in Table 5.1.

<center>**Table 5.1 FPGA Synthesis results**</center>

Resources	Usage
Number of registers	485 out of 2112 (23%)
Number of LUT4s	957 out of 2112 (46%)
Number of 9 Kbit block RAMs	8 out of 8 (100%)
Number of PIO	25 out of 105 (24%)
Max DCLK[1] frequency	32.5 MHz
Power consumption in FPGA at 2 FPS (Simulated)	12.42 mW

<center>[1]clock output from image sensor fed to the FPGA</center>

The measured current consumption of the entire capsule prototype in different image sizes and modes are shown in Figure 5.6.
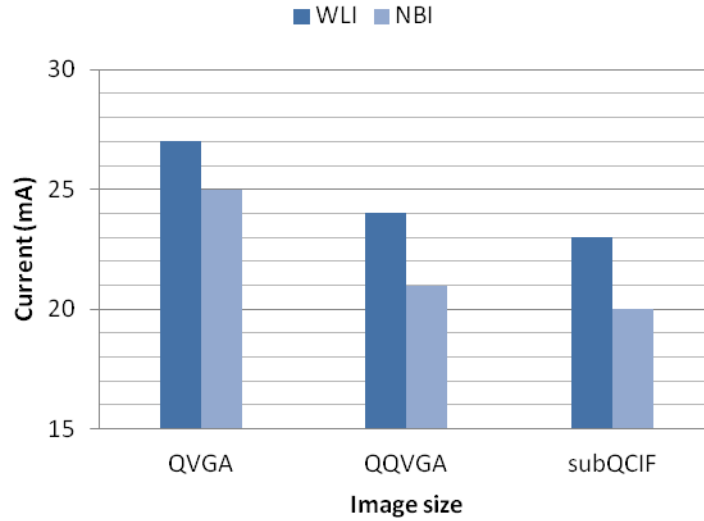
Figure 5.6 Current consumption (measured) of the capsule in different image transmission modes

For an average of 23 mA current consumption, the capsule can run for 8.5 hours with three 195 mAh button batteries [110].

5.4.3   Discussion on FPS and FIFO size

The FPS of the capsule is directly proportional to the frequency of the image sensor output clock, f_{DCLK}, as expressed in (5.1).

$$FPS = \frac{f_{DCLK}}{N} \qquad (5.1)$$

where, N = Total number of DCLK cycle needed for one image frame = 410436 (for image sensor of [34], in QVGA *full* mode)

From Table 5.1, it is seen that the maximum DCLK frequency the FPGA can support is 32.5 MHz. From (5.1), the maximum supported FPS can be calculated as 79.18 f/s.

However, it should be noted that the bottle-neck of the system is the application throughput of the RF transceiver, $RF_{AT,}$ as expressed in (5.2).

$$W \times H \times BPP \times (1 - CR\%) \times FPS \leq RF_{AT} \qquad (5.2)$$

where, W = image width = 320 (for QVGA), H = image height = 240 (for QVGA), BPP = bit-per-pixel = 24, CR = compression ratio = 80.4% (from Section 3.6). For 2 FPS image transmission rate, the minimum required application throughput of the RF transceiver can be calculated from (5.2) as 722.53 kbps.

There are several research works available in the literature about the design of low power and high data rate RF transceivers for capsule endoscopy. The work in [58] and [116] proposes design of a transmitter having data rate of 20 Mbps and 15 Mbps namely and [117], [118] and [119] proposes 2 Mbps transmitters. In [120], and ultra wide band communication channel for capsule endoscopy is proposed. For instance, if the transmitter of [116] is used in our design, then QVGA images can be sent at maximum 42 frames/second as calculated from (5.2). However, these transmitters are still in the research level and not available commercially.

The image compressor can produce bit-steam at a higher rate than the application throughput of the RF transceiver, so a FIFO is implemented for proper transmission. The required size of the FIFO, $FIFO_{Size,}$ can be calculated from (3).

$$FIFO_{Size} = \frac{B \times f_{DCLK}}{N_r} - RF_{AT(Worst)} \qquad (5.3)$$

where, B = data burst size = data size for one row of an image after compression =

$W \times BPP \times (1 - CR\%) = 1505$ bits,

Nr = Total number of DCLK cycle needed for one row = 1560 (for image sensor of [34]).

For two FPS image transmission and RF_{AT} = 722.53 kbps, the FIFO size can be calculated from (5.3) as 8 KB.

Depending upon the environmental condition (such as wireless interference from nearby electronic devices, distance of transmission, signal attenuation due to obstruction, etc.), the RF transceivers application throughput can go much lower. Several experiments with commercial capsule in [22] revealed the fact that image transmission were not at a smooth rate of 2 FPS, rather images were sometimes sent as low as 0.1 FPS due to error in transmission.

5.4.4   Comparison with other works

In Table 5.2, the proposed capsule prototype is compared with several other works. The work in [59] [32] and [121] proposes microcontroller based capsule architectures which consume significant amount of power. The battery life of these works are not mentioned in their papers. The work of [54] claims to have 19 frame/second referencing a research paper based RF transceiver (having data rate of 1.5 Mbps). However, the transceiver was not interfaced with their prototype for real-time experimentation and such high FPS will reduce the battery life of the system dramatically. The works in [57][58] are developed in ASIC platform disabling programmability and flexibility of the design. The proposed capsule prototype is programmable, modular and flexible, capable of capturing both WLI and NBI images, supports both lossy and lossless compression and real time configuration of image resolution and imaging modes through wireless commands, having a reasonable battery life of 8.5 hours.

Table 5.2: Comparison with other works

	Design platform	Image size	FPS	Imaging mode	Real time image size and mode control	Battery life (hour)
[54]	FPGA	320 × 240	19	WLI	No	1.7[2]
[32]	MCU	160 × 160	2	WLI	-	-
[121]	MCU	640 × 480	0.5	WLI (grayscale)	No	-
[57]	ASIC	512 × 512	2	WLI and NBI	Yes (only mode)	6-8
[59]	MCU	-	-	WLI	No	-
[58]	ASIC	340 × 340	10.5	WLI	No	-
Proposed	FPGA	QVGA (320 × 240), QQVGA (160 × 120), subQCIF (128 × 96)	2.21[1]	WLI (both Lossy & Lossless), NBI	Yes	8.5

[1]For 800kbps application throughput of RF transceiver; [2]assuming 195mAh battery; "-" not mentioned

5.5   Summary

In this chapter, a miniature field programmable gate array (FPGA) based electronic capsule is designed and developed. The capsule contains the proposed low complexity image compressor and can generate both lossy and lossless compressed bit-stream. The capsule prototype also supports both white light imaging (WLI) and narrow band imaging (NBI) imaging modes and communicates with the data logger in full duplex fashion, which enables configuring the image size and imaging mode in real time during the examination. The capsule prototype has 4 PCBs, each having a diameter of 16 mm and the prototype has a battery life of 8.5 hours.

Chapter 6: Data Logger

6.1　Introduction

Recent advances in miniature and portable bio-sensors, embedded processors, and wireless technologies have caused a rapid growth in sensing and recording physiological signals for medical applications. Bio-sensors convert body signals such as temperature, blood pressure, breathing [122], heartbeat, electrocardiogram (ECG) [123], etc. to electrical signals to be processed, transmitted, and recorded in electronic devices [124]. Data coming from implanted or external body sensors can be transmitted wirelessly to a portable and wearable data logger unit, thus giving the patient the freedom to do household works during continuous data recording without the hassle of cumbersome wired devices. After logging is completed, the data are transferred to a personal computer (PC) or Smartphone which may be later examined by physicians. In this chapter, a portable, battery operated data logger unit having wireless connectivity with the bio-sensor is discussed. The design of the data logger is general and can be used for several medical applications.

In this chapter, the prototype is demonstrated for video wireless capsule endoscopy (WCE). The data logger presented in this work is portable and has high data rate of 2 Mbps wireless connectivity with implantable or externally attached body sensors which eliminated the need for wires. It also has high memory capacity of 4 GB micro secure digital (SD) card, graphical display for showing images, graphs, charts in real time, keypad and touch screen based user interface. After logging, the data can be transferred to PC using a SD card reader at a speed of up to 25 MB/sec or using an USB interface. Optionally, the data can also be transferred to PC or Smartphone wirelessly

using Bluetooth technology. An illustration of a wireless body sensor data logging system using the proposed data logger is shown in Figure 6.1.
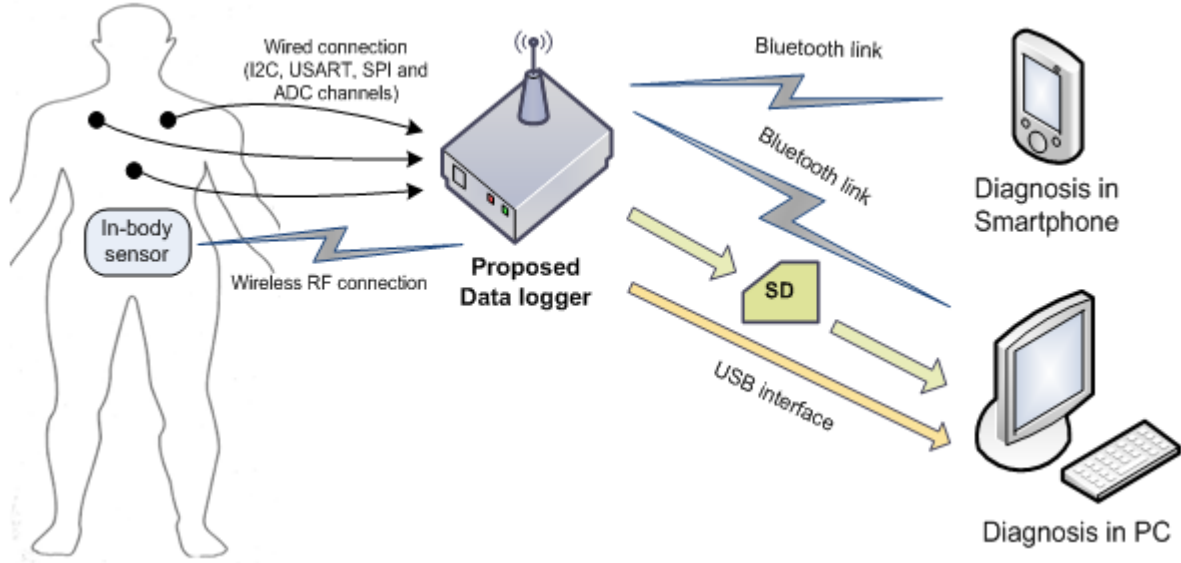
Figure 6.1 Illustration of a wireless body sensor data logging system

6.2   Design requirements

- In capsule endoscopy, images are generally transmitted in compressed form at 2 frames-per-second for about 8 to 10 hours. The storage space required, S, for this application can be expressed using (6.1), where, W is the image width, H is the image height, BPP is the bits-per-pixel, FPS is frames per second, CR is the compression ratio, and T is the duration of data logging in hour.

$$S = W \times H \times BPP \times (1 - CR) \times FPS \times T \times 3600 \qquad (6.1)$$

In order to store color QVGA (320 × 240, 24 bits-per-pixel) images transmitted at 2 FPS having 80% compression ratio for 10 hours, at least 3.1 GB memory space is required.

- The data rate of the wireless transceiver must be high enough to support the above mentioned transmission which is calculated as 720 kbps.

- It must consume low power so that battery is able to supply power continuously for at least 10 hours.

- The data logger should be able to communicate with the capsule in real-time during logging and control various features of the capsule, such as, changing image size, imaging mode (e.g., white light imaging, narrow band imaging), frame rate, etc. The interface used for this interactive control operation must be easy to use.

- Real time viewing of the images, while the capsule is in operation and the data logging is in process, is another important feature. Using it, a physician can take decision to change imaging mode, image size, or frame rate of a certain region of the GI tract for better viewing. The data logger must have necessary hardware for displaying color images and firmware to decompress and display compressed image data.

- After data logging is completed, there must be easy and fast way to transfer the data to workstation PC or Smartphone for diagnostics.

- The physical size and weight of the data logger must be as less as possible.

6.3 The data logger architecture

The data logger is designed to have four layers as shown in Figure 6.2. Each layer completes its functionality by using the resources of its lower layers. By only changing the application layer firmware, the data logger can be used in several applications, without modifying the lower level driver and hardware layers. A brief description of each layer is given below.
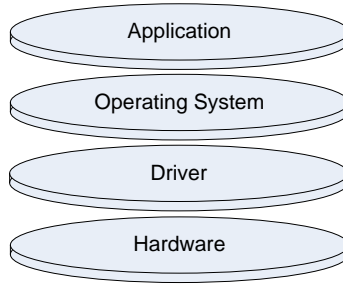
Figure 6.2 Data logger design layers

6.3.1 Hardware

The overall block diagram of the hardware is shown in Figure 6.3. The design consists of a microcontroller (MCU) and several peripherals connected with it. Each major component of the design is briefly described below.
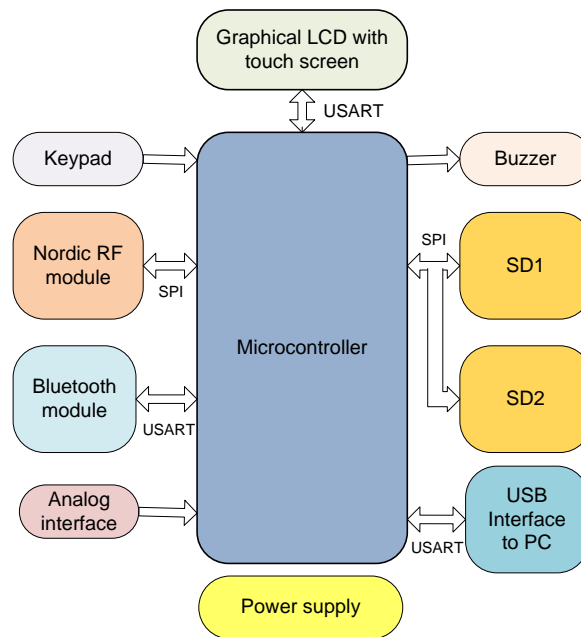
Figure 6.3 Block diagram of the data logger hardware

6.3.1.1 Microcontroller

A microcontroller from the XMEGA-A1 [125] family is chosen for this design. To increase the data sample rate and writing speed in the storage device, a high speed MCU is required. Moreover, several peripherals need to be connected with the MCU using SPI and UART protocol. The

XMEGA microcontroller can work at 32 MHz clock and it has several hardware SPI and UART ports which works faster than software SPI or UART. The chosen MCU also has 78 programmable I/O lines, 128 kB flash for program storage, 8 kB SRAM and 2 kB EEPROM to store user defined variables temporarily and permanently namely.

6.3.1.2 Data storage device

In Table 6.1, the comparisons of different permanent memory storage device [126] in a single chip are shown. Parallel EEPROMs need significant number of I/O lines to interface with MCU. Serial EEPROMs needs relatively lesser I/O lines, however their memory capacity is low and cascading several EEPROMs for increasing capacity, needs significant area and more I/O lines. MicroSD card [127] seems to be the best choice as it has high memory capacity and needs only few I/O lines. Moreover, its defect and error management unit promises reliable data read/write. In the data logger design, two 2 GB SD card is connected with the MCU using hardware SPI at 16 MHz clock speed. Note that, several SD cards may be connected as shown in Figure 6.4 and the storage capacity can be increased significantly. When one SD becomes full, data are written in another SD card automatically, and thus data logging can continue without the interruption of replacing SD card. Moreover, data can be transferred from SD card to PC using SD/MMC card reader at high speed such as 25 MB/sec.

Table 6.1: Comparison of different permanent memory storage device

	EEPROM				Micro SD
	Parallel	Serial			
		I2C	SPI	3 WIRE	
Capacity	512 kB	64 kB	64 kB	2 kB	2 GB[1]
Clock (MHz)	5	0.4	20	2	25[2]
Pins required	30	2	4	4	4
Error correction	No	No	No	No	Yes

[1] Maximum capacity for FAT16 file-system for a single SD
[2] In standard SPI mode

86
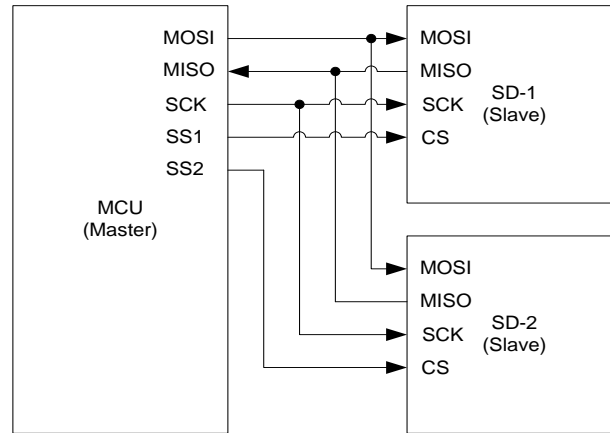
Figure 6.4 SD card connection with MCU by SPI

6.3.1.3 Graphical LCD with touch screen

To enable real time viewing of images, graphs, charts, texts etc. during data logging, a 2.4" graphical LCD [128] capable of displaying 320 × 240 pixels (QVGA) using 262,144 colors is chosen. The display also contains resistive touch area, enabling advanced and interactive user interface. The LCD connects with the MCU using hardware USART and it receives command from the MCU at a baud rate of 2 Mbps.

6.3.1.4 Wireless transceiver

The characteristics of several wireless transceiver units are shown in Table 6.2. The major challenge of any wireless link is the data corruption in the transmission channel. Nordic transceiver [108] contains cyclic redundancy check (CRC) based error detection and retry with auto acknowledgement (i.e. resend data packet until success) feature which makes the link promisingly reliable, though several retry may decrease the overall data transmission rate in a noisy environment [73]. Nordic is selected for this application and it is connected with the MCU using hardware SPI at 8 MHz speed.

Table 6.2 Comparison of different wireless transceivers

	MICS [106]	Linx [129]	Micrel [130]	Zigbee [131]	Nordic [108]
Frequency band	402 MHz	433 MHz	915 MHz	2.4 GHz	2.4 GHz
Data rate	800 kbps	10 kbps	115 kbps	250 kbps	2 Mbps
Retry and auto ack.	Yes	No	No	Yes	Yes
TX current (mA)	5	3.4	25	250	11.3
RX current (mA)	5	5.2	13.5	55	13.5

6.3.1.5 Bluetooth

A Bluetooth transceiver [132] is also connected with the MCU using hardware USART at 230 kbps baud. Data transmitted from wireless body sensor can be captured either by Nordic or by Bluetooth in the data logger and then can be uploaded wirelessly to personal computer or Smartphone using Bluetooth.

6.3.1.6 USB interface

The design also contains an USB interface (as shown in Figure 6.5) that has 1 Mbps data rate to connect with PC using wired link. This wired interface can be optionally used to transfer data to workstation PC after data logging.
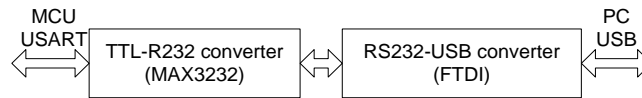

Figure 6.5 USB interface to PC

6.3.1.7 Analog interface

Analog data can also be taken in the data logger using the wired analog interface. The analog interface consists of multiplexed 8 programmable analog to digital converter (ADC) channels, 8 analog comparators, and 2 digital to analog converter (DAC) channels of the microcontroller.

Analog data such as body temperature, blood pressure can be taken using the ADC channels and then the data can be saved in SD card and its real time graphical plot can be displayed on LCD.

6.3.1.8 Power supply

As the power source of the data logger, three 3.7 V polymer lithium-ion batteries, each having 2000 mAh rating are used in parallel, thus making total battery rating of 6000 mAh. The design also contains a 200 mA having 3.3 V output voltage boost converter [133] and an under voltage protection of 2.6 V. A 500 mA constant current battery charging circuit [134] using PC's USB port is also included in the design so that recharging can be done without removing the batteries from the hardware. To indicate and monitor the charging level, the battery voltage is divided using two fixed resistors connected in series and the voltage of the common point of the resistors is fed to an analog to digital converter (ADC) channel of the microcontroller.

6.3.1.9 Other peripherals

To interact with the user, the design contains 4 push button switches. The button press is signalled to the MCU as interrupt. A buzzer is included in the design to generate small beep sounds.

6.3.2 Driver firmware and Disk Operating System

The driver layer consists of low level firmware routines for accessing different hardware peripherals such as graphical LCD, RF transceiver, SD, etc. A disk operating system (DOS) for embedded system [135] is implemented which handles file operations in SD card. The DOS implements FAT16 file system and the maximum writing speed in SD card is found to be 115 kB/s when the MCU is running at 32 MHz.

6.3.3 Application Firmware

This layer contains the firmware designed for a specific data logging application. The proposed data logger is generic that encompasses many different medical applications such as ECG, heartbeat,

capsule endoscopy, blood pressure etc. In this work, the firmware for capsule endoscopy application is implemented.

6.3.3.1 Graphical User Interface

In order to set different settings such as image size, imaging mode, enable/disable real time view, etc.; a menu based graphical user interface (GUI) is designed in the data logger as shown in Figure 6.6. User can use either 4 keys (*Up*, *Down*, *Enter* and *Escape*) or touch to select different menu options. Additional features may be added to the interface if needed.
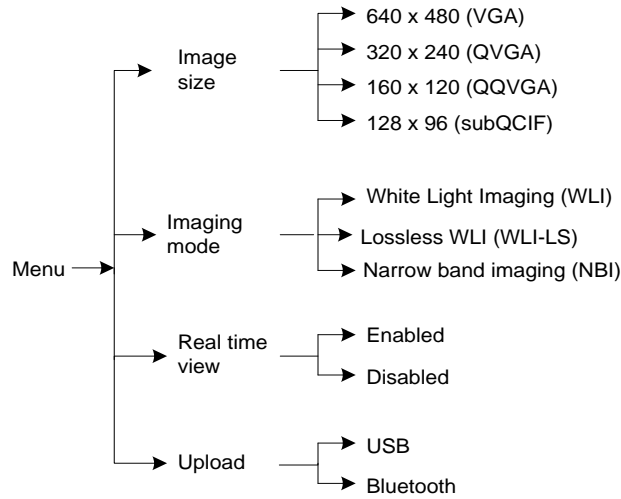
Figure 6.6 Menu tree of the data logger

6.3.3.2 Data logging

In order to receive data from the capsule, a command is sent wirelessly to the capsule from the data logger containing information of required image size and imaging mode. After receiving command, the capsule starts to send the data packets of an image frame in compressed from. The data logger reads the packets and stores them in SD card. A timer is also used to add time stamp for each image frame. The end of a frame is detected by a pattern of consecutive 4 zero bytes. The overall data logging procedure is shown in Figure 6.7.

90
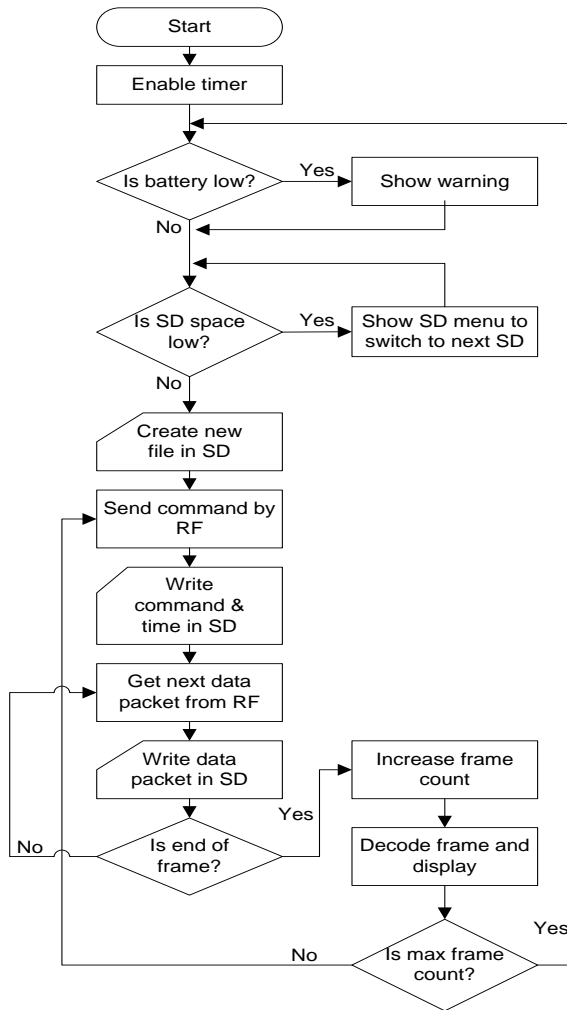
Figure 6.7 Flowchart of the data logging procedure for capsule endoscopy

6.3.3.3 Image decoding algorithm

In capsule endoscopy, image data are transmitted wirelessly from the ingested capsule in compressed form. The proposed compression algorithm discussed in Section 3.4 is implemented in the capsule. In the data logger, the de-compressor or the decoder for the proposed compression algorithm is implemented for real time viewing of images. The overall image decoding algorithm is shown in Figure 6.8.

Figure 6.8 Block diagram of the image decoding algorithm

In the compressed bit stream, the first pixel component is stored in raw 8 bit format. This is read in

X, where X is the actual pixel value. In YEF color space, X corresponds to Y, E and F components.

Xp is the next predicted pixel value. Initially,

$$Xp = X \qquad (6.2)$$

Next define,

$$I = 2^8 = 256 \qquad (6.3)$$

$$M = 2^k \qquad (6.4)$$
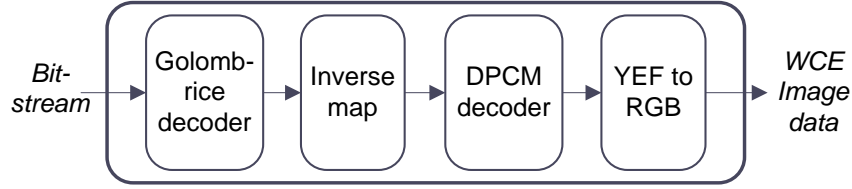
where, k is a Golomb-Rice code parameter . The maximum length of Golomb-Rice code

(g_{limit}) is chosen as 32. The pseudo code for Golomb-Rice code decoder is shown in Figure 6.9.

```
1.  q := the number of 0 in the code until a 1 is reached
2.  if q < (g_limit − log_2 I − 1) then
3.      r := next k bits in binary
4.      m_dx := q × M + r
5. else
6.      m_dx := next 8 bits in binary +  (g_limit − log_2 I − 1) × M
```

Figure 6.9 Pseudo code for Golomb-Rice decoder

The decoded m_dx is then inverse mapped to signed integer as shown in the pseudo code in Figure

6.10.

```
1. If m_dx mod 2 = 0 then
2.      dx := m_dx / 2
3. else
4.      dx := -((m_dX + 1) / 2)
```

Figure 6.10 Pseudo code for inverse mapping

The differential pulse coded modulation (DPCM) decoder then calculates the next actual pixel value using (6.5) and sets the prediction for next pixel using (6.2).

$$X = Xp + dX \qquad (6.5)$$

After the actual component values of a pixel are calculated, they are converted to RGB color space using (3.4). Then the R, G, B pixels are sent to graphical LCD for displaying the image frame.

6.3.3.4 Data uploading

After data logging, data can be uploaded to PC or Smartphone using any of the following three methods: (a) by removing the SD cards from data logger, (b) using USB interface, and/or (c) using wireless Bluetooth link. When using USB or Bluetooth link, a file transfer protocol is implemented which sends at first the filename, then the file size, and then its data bytes. A PC software is developed to receive the data from the data logger by USB or by Bluetooth. After receiving compressed data, the PC software can decode and display the images as video at any given FPS.

6.4   Results

6.4.1   Specification of data logger prototype

The proposed data logger for capsule endoscopy application is prototyped in our laboratory as shown in Figure 6.11. The size of the prototype is 10 × 10 × 2 cm. The weight of the PCB is 114 gram; each battery weighs 37 gram, making the total weight of the prototype 151 gram with one battery. With three batteries, the total weight is 114 + 3 × 37 = 225 gram. Note that, for capsule endoscopy application, minimum 10 hours battery life is required. If one battery is used instead of three batteries then the hardware can run for 11.8 hours (calculated from Table 6.3 and Table 6.4), which meets the design requirement for capsule endoscopy application. As the design of the

proposed data logger is general, three batteries are used to meet other applications which may require more data logging time.
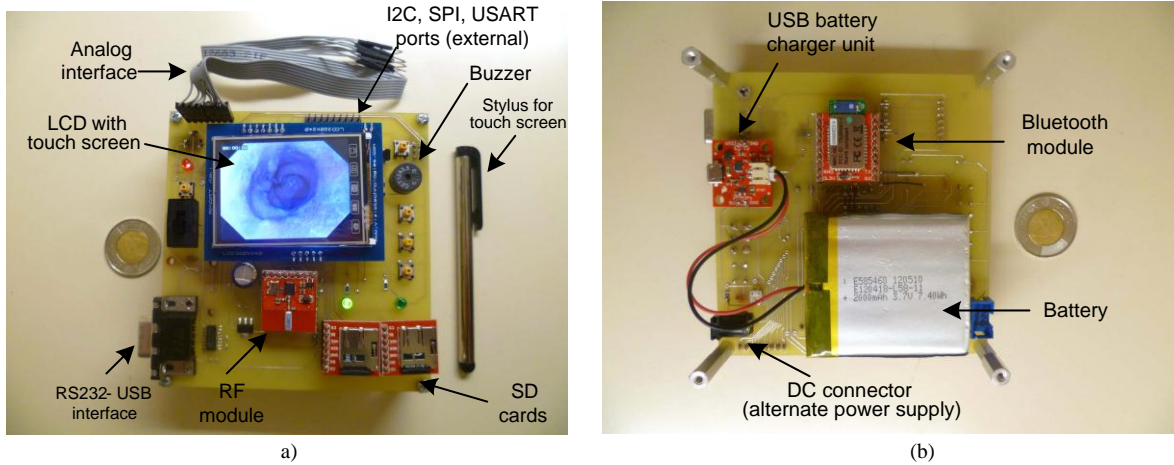

Figure 6.11 Photograph of the prototype (a) top view (compared with a Canadian $2 coin); (b) bottom view

6.4.2 Experimental results for RF channel selection

Experiments have been conducted to observe the interference of other frequencies (such as Wi-Fi, Smartphone, medical instruments etc.) in both hospital (Royal University Hospital, Saskatoon, SK, Canada) and home environment [73] on the Nordic transceiver in its different frequency channels. Several experiments showed that using duck antenna [136] instead of chip antenna improves the RF transmission quality. In Figure 6.12, the number of retry required by the transceiver to send 100 data packets (each packet contains 32 bytes) in different frequency channels in several environments using duck antenna is shown. As the data logger is wearable, the distance between the sensor and the logger should be less than 1 meter (taking a conservative approach).
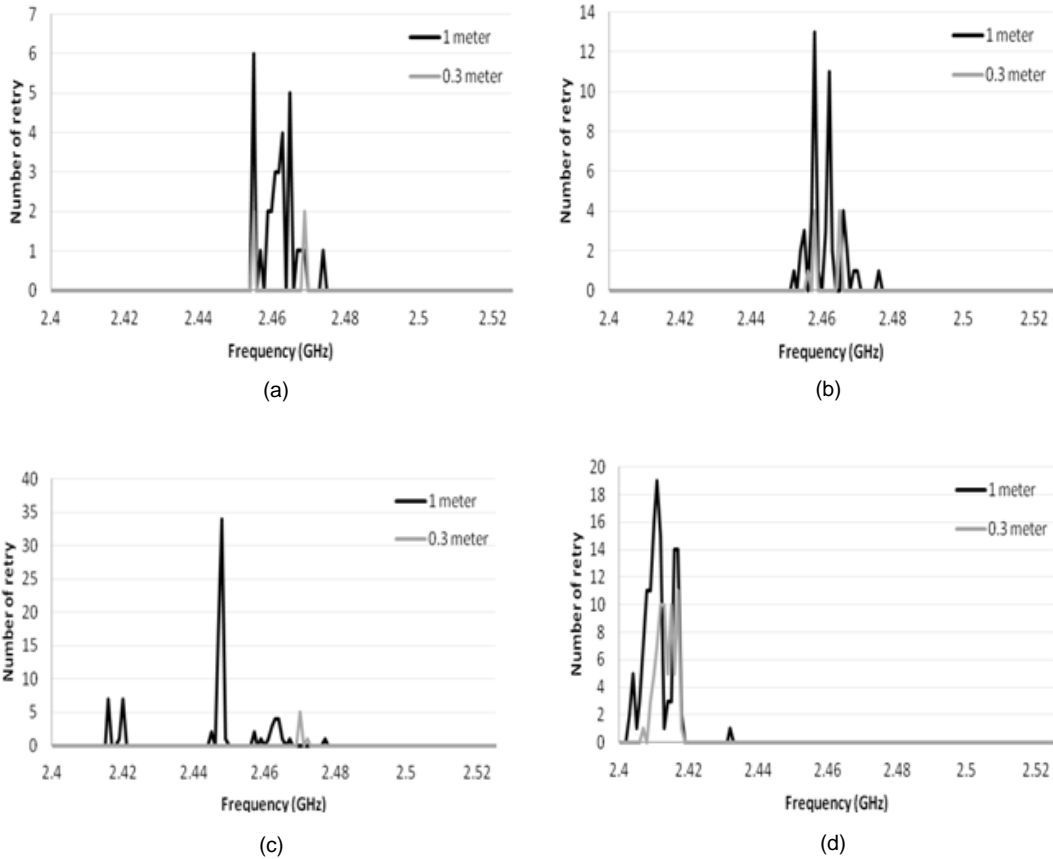
94

Figure 6.12 Number of retry required in different frequency channels (a) in home environment; (b) in home environment near Smartphone in use; (c) in hospital environment near medical imaging department; (d) in hospital environment near cancer department.

From Figure 6.12, it is observed that several retries are required from 2.4 GHz to 2.48 GHz channels due to interference in different environments. So, decision have been made to operate the transceiver in a clear channel at 2.5 GHz which will cause minimum number of retries during data transmission. Note that, the Bluetooth device will not have any interference effect on Nordic transceiver as they work in a mutually exclusive way.

It is possible to select the best channel dynamically during data logging for ambulatory diagnostics. To do that, the data-logger will go to *channel selection mode* every after 30 minutes, or by user at anytime from selecting a menu option. The data logger will send a command to the capsule to set its transceiver at the first channel and the data logger will also set its transceiver to the first

channel. Then the data logger will send some data packets to the capsule and log the number of retry required for that channel. This step will be done for all the available channels. (In Nordic transceiver, total 126 channels starting from 2.4 GHz to 2.526 GHz are available). Then the channel which has minimum retries will be selected and the data logger will send a command containing the channel number to the capsule so that both data logger and capsule communicates at the same channel. The flow chart for this procedure is shown in Figure 6.13.
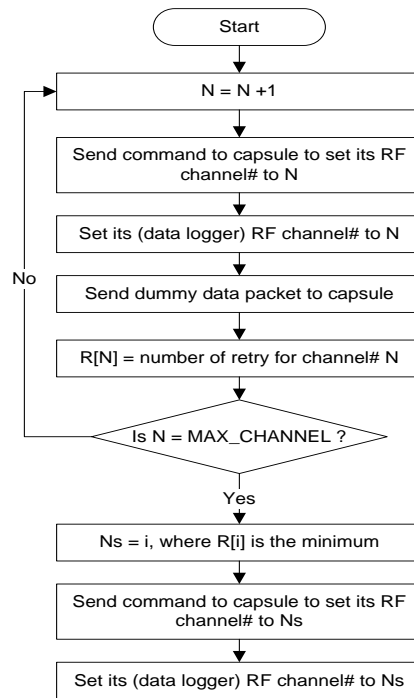
Figure 6.13 Flowchart for selecting best RF frequency channel

6.4.3 Power consumption

The power consumption of the data logger in different modes is shown in Table 6.3. When real time viewing (RTV) is disabled, the graphical LCD is taken to sleep mode to save power. In Figure 6.14, the percentage power consumption of different hardware components during data logging (using Nordic RF link, in RTV enabled mode) is shown. It is seen that, the LCD consumes the majority of power (54%) if the RTV is enabled. It should be noted that the RTV mode is not a normal mode of

96

operation, rather a special feature that a physician may use if desired. After the data logging is completed, it can be transferred to PC by removing the SD card, which costs no power for the data logger. When transferring data using Bluetooth, the LCD and Nordic RF are taken to sleep mode to save power. During data transfer by USB interface, the Bluetooth is also taken to sleep mode.

Table 6.3 Power consumption in different modes

Mode		Current (mA)	Power (mW) @ 3.3 V
Display menu		160	528
Data logging in SD card	RTV enabled	170	561
	RTV disabled	90	297
Data transfer to PC	Using SD card reader	0	0
	Bluetooth	140	462
	USB interface	93	307
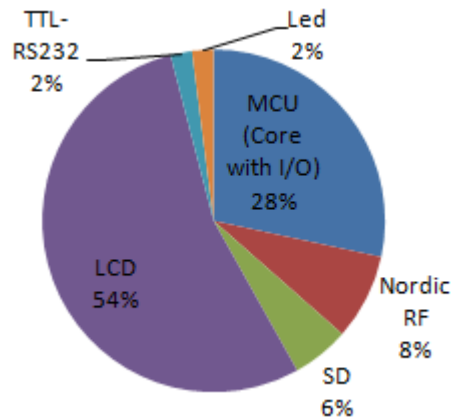
Figure 6.14 Percentage power consumption of different hardware components

6.4.4 Comparison with other works

The overall specification of the designed data logger and its comparison with other works are shown in Table 6.4. Comparing with other works on data loggers in the literature, the proposed data logger has high speed wireless connectivity including Bluetooth, contains graphical LCD for real time data viewing and touch screen. The storage space is sufficient for many other medical applications; moreover, it can be increased easily by connecting more SD cards as shown in Figure 6.4 or

97

implementing FAT32 file system in the firmware which can support higher capacity SD card (8 GB or higher) than FAT16. The writing speed and RF bandwidth of the data logger is sufficiently high to capture and store data at high sampling rate. Thus the proposed data logger fulfills all the design requirements as discussed in Section 6.2 for capsule endoscopy application. From Table 6.4, it is also seen that the data loggers in other literature works are intended for different applications and they cannot be used for wireless capsule endoscopy application efficiently. The proposed data logger is mainly designed for capturing capsule endoscopy images. However, because of using high capacity components (such as, 2 Mbps RF link, 4 GB storage space, graphical LCD, etc.), it can also be used in many other medical applications such as, monitoring and logging of heartbeat, blood pressure, body temperature, etc.

Table 6.4: Comparison with other data loggers

	Intended data logging application	Memory capacity	Sampling rate (Writings Speed)	Wireless	Graphical LCD	Touch input	Battery life (hour)	Is usable for WCE?
[70]	GSR	16 MB	13.2 kHz	No	No	No	50	No (no wireless link available)
[62]	ECG	20 MB	200 Hz	No	No	No	-	
[68]	Fetal and maternal heart beat	-	500 Hz	No	No	No	24	
[63]	ECG	512 MB	33 kS/s	No	No	No	72	
[137]	ECG	1 GB	250 Hz	No	No	No	924	
[73]	Human movements	-	60 Hz	250 kbps	No	No	-[1]	Partially (low bandwidth, low memory capacity, no graphical LCD for RTV)
Pro-posed	WCE	4 GB[3]	192 k pixel/s [2] (115 kB/s)	2 Mbps link and Bluetooth	Yes	Yes	35.3	Yes

[1] not battery operated; [2] for 80% compression ratio; [3] expandable

6.5   Summary

In this chapter, the design of a data logger for capsule endoscopy application is discussed. The data logger is portable and its battery can supply power for more than 35 hours. It has high data rate wireless connectivity including Bluetooth, graphical display for real time data viewing with state-of-the-art touch screen technology. The data are logged in micro SD cards and can be transferred to PC or Smartphone using card reader, USB interface, or Bluetooth wireless link. A fast and low cost image decoding algorithm for real time viewing of endoscopic images is also presented. Experiments have also done in both hospital and home environment for testing RF interference and an algorithm for choosing the best RF frequency channel dynamically for ambulatory diagnostics is also presented.

Chapter 7: Workstation Software

7.1   Introduction

In WCE, data are transferred from data logger unit to a workstation or PC, where the images are decoded, reconstructed and displayed for medical diagnostics. In this chapter, the design of a workstation or PC software for WCE system is discussed.

7.2   Design requirements

In a Windows based PC software, the following functionalities need to be implemented:

- The software should be able to receive data from SD card, USB interface and also from wireless Bluetooth interface of the data logger.

- The software should contain the decompression or the decoding algorithms (for both lossy and lossless) to reconstruct images from the compressed data for both WLI and NBI modes.

- In NBI mode, the capsule prototype takes two grayscale images of the same location of the tissue. One image is captured using green light and other using blue light. The software should have the functionality to generate a single high contrast NBI image by combining the two grayscale images.

- It should be able to store the reconstructed images in standard format, such as JPG or BMP.

- It should have a display interface, where the reconstructed images can be displayed, zoomed, marked, navigated to any frame, and the sequence of images can be played as video at any given FPS.

7.3   Architecture of the workstation software

The overall architecture of the workstation software is shown in Figure 7.1. Its main components are briefly described below.
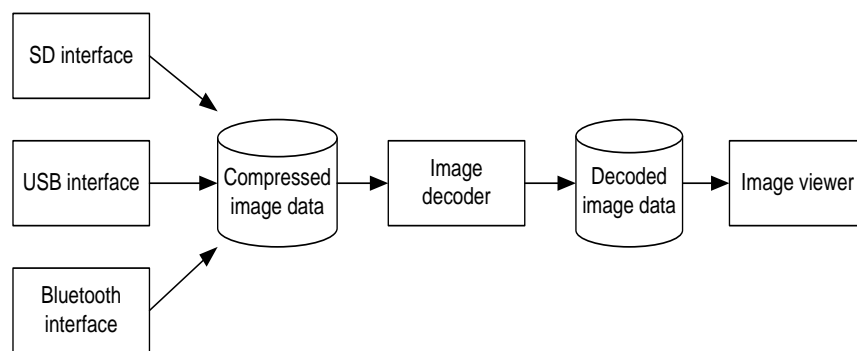

Figure 7.1 The architecture of the workstation software

7.3.1   Input interface

Compressed data files from the data logger are transferred to the workstation by SD card, USB interface, or by Bluetooth link. The software uses necessary driver routines for accessing USB and Bluetooth hardware of the PC. This unit implements a file transfer protocol (FTP) which at first requests the data logger to send the total number of files that need to be transferred, then the file name, size and the data bytes.

7.3.2   Image decoder

The *Image decoder* decodes or decompresses the compressed image data and stores the images as standard BMP files. The implemented decompression algorithm is similar to the image decoding algorithm implemented in the data logger as described in Section 6.3.3.3. In order to reconstruct a

combined NBI image from two grayscale images, the following steps are performed; (a) the grayscale images are sharpened by increasing the difference between the consecutive pixels, (b) two images are combined by choosing either the maximum, minimum or average value of the pixels of the two images, and then (c) pseudo color is added with the combine image. Parameters for reconstructing NBI images can be set by the user in the decoder module.

7.3.3 Image viewer

The *Image viewer* displays the decoded images. It also contains frame navigation system, zoom in/out feature, marking pen for selecting and marking any special region of the image, and a video player which can display the image sequences as video at any given FPS.

7.4 Results

The software is developed using Microsoft Visual Studio and its operations have been tested. In Figure 7.2, a screenshot of the image viewer unit of the software is shown.

Figure 7.2 Screenshot of the image viewer

7.5 Summary

In this chapter, the architecture of the workstation software for image decoding and viewing is discussed. The software has been developed and tested.

Chapter 8: Animal Testing

8.1   Introduction

In order to validate the performance of the compressor and the developed WCE system in more realistic scenario, the WCE system have been tested in pig's intestine. Pigs intestine is chosen for experiment due to the following reasons.

- Both the pig and the human are mammals. Though there are some differences, pig has relatively similar gastrointestinal functions in comparison to human [138].

- Pigs are widely available from pork industry and animal research centers [139].

- It is less expensive than dog or horse.

It can be mentioned here that, to perform tests in human patients is quite challenging. First of all, it is difficult to design and fabricate an electronic capsule that a human can swallow. A swallowable size capsule should be approximately 26 mm in length and 11 mm in diameter [22]. Miniature multilayer PCB design, fabrication, assembling, packaging processes take significant amount of time, money, and human resource. Secondly, approval from FDA [25] is needed to swallow the capsule in human patient. Getting approval from FDA is a lengthy and expensive process. Finally, it requires approval from hospital, managing a number of patients having gastrointestinal diseases, and involvement of medical stuffs and gastroenterologist to evaluate the performance [94] and measuring the accuracy of their decision (fraction of correct decisions, false

positives, false negatives, etc.) using statistical tools such as receiver operating characteristics (ROC) analysis [95]. All these tasks are beyond the scope of this thesis and left for future exploration.

In this chapter, the experiments with pig's intestine are presented.

8.2 Experiments with pig's intestine

After getting the ethical permission from Animal Research Ethics Board (AREB) [140] for conducting tests involving animal, a portion of pig's small intestine has been collected from Prairie Swine Centre [139]. Two experiments with this tissue have been conducted in the anatomy lab of Western College of Veterinary Medicine [141]. The experiments are briefly described below:

8.2.1 Experiment with generation-1 capsule prototype

8.2.1.1 Objective

The objective of the first experiment is to get an initial assessment on how the developed WCE system works when images of pig's intestine are taken.

8.2.1.2 Method

In this experiment, the generation-1 capsule prototype (PCB's shown in Figure 5.4), the developed data logger and the workstation software are used. Due to the relatively large diameter of the generation-1 capsule prototype, it is not been possible to insert the capsule inside the intestine. So, the intestine is cut open and expanded and then the capsule is placed over the tissue for capturing images. The experimental setup is shown in Figure 8.1 (a) and (b).
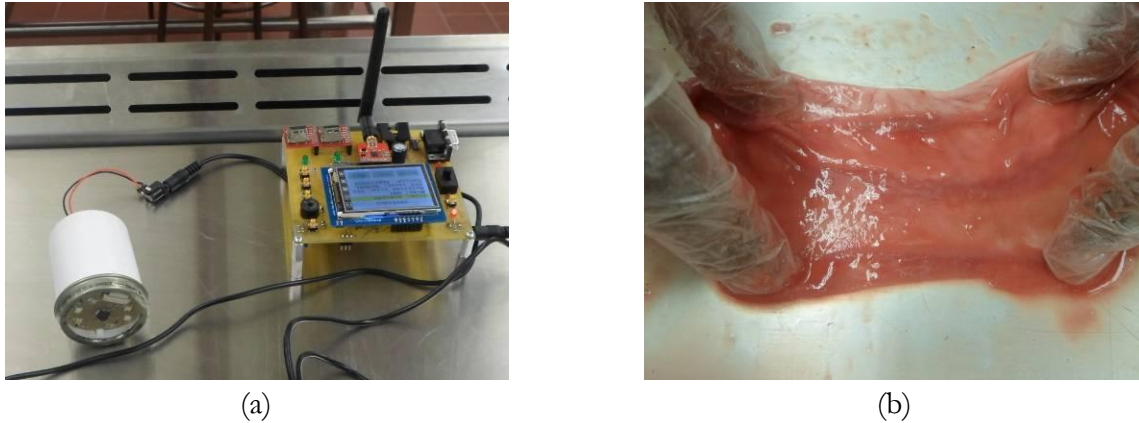
<div align="center">(a)   (b)</div>

Figure 8.1 (a) Photograph of the generation-1 capsule prototype in casing and data logger; (b) Pig's small intestine

dissected and expanded;

8.2.1.3 Results

The capsule captured images of pig's intestine and sent the compressed data wirelessly to the data logger. The images are displayed in real time on the data logger's LCD. These images were later transferred and decoded in PC, an image is shown in Figure 8.2.
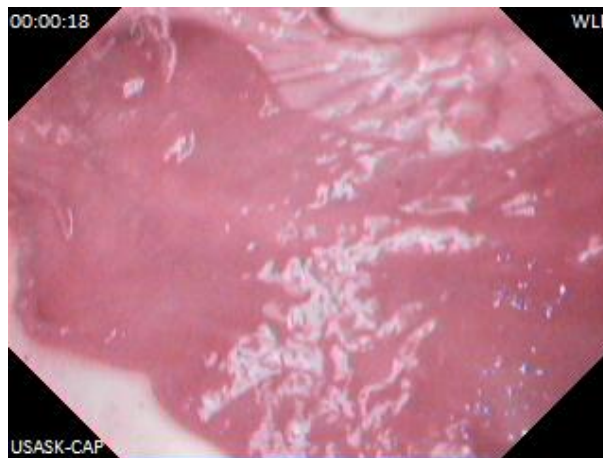

Figure 8.2 A captured WLI image of pig's intestine

8.2.1.4 Discussion

In the experiment, images of intestine are successfully captured by the capsule and the data logger is able to store and show the images in real time. Also, real-time control of lighting mode from the data logger by sending wireless commands to the capsule is done successfully. It is found from the

experiment that the focal length of the lens in front of the image sensor needs to be adjusted in order to get better quality images. Also, it is found that excessive lights can blur the images, so the intensity of the lights need to be controlled more precisely.

8.2.2   Experiment with generation-2 capsule prototype

8.2.2.1 Objective

The objective of this experiment is to see the capsule's performance (such as image quality, RF transmission issues etc.) when it is inserted into the pig's small intestine.

8.2.2.2 Method

In this experiment, the generation-2 capsule prototype (PCB's shown in Figure 5.5), the developed data logger unit and the workstation software are used. Before the experiment, the focal length of the lens and light intensity of the capsule are carefully adjusted. In order to test the performance of the developed WCE system, the capsule prototype is inserted inside the pig's small intestine. The experimental setup is shown in Figure 8.3.

(a)   (b)

Figure 8.3 (a) Capsule PCBs put in casing and inserted inside pig's small intestine; (b) Experimental setup: capsule

inserted in pig's intestine and the data logger is showing real-time inside image of the intestine

8.2.2.3 Results

Images from the capsule are successfully transmitted to the data logger wirelessly through the pig's intestine. After the images are captured by the data logger, they are saved in SD card, decoded and shown in the LCD with time stamp. After capturing several images, the data stored in the SD card of the data logger are transferred to a PC. Using the PC software, the compressed data are decoded and the reconstructed images are saved in the PC. In Figure 8.4, several captured WLI images of QVGA size (320 × 240) using both lossy and lossless compression modes (mode and size selected by sending wireless command from the data logger to the capsule in real time) are shown with compression ratio (CR) mentioned. In Figure 8.5, captured WLI images of QQVGA size (160 × 120) are shown. In Figure 8.6, QVGA size captured NBI images (in lossless mode) are shown.
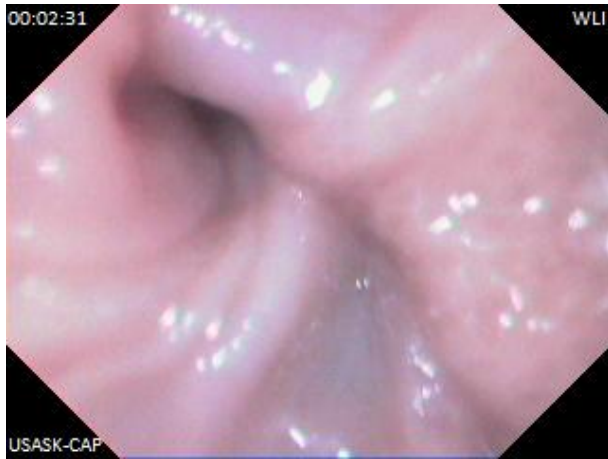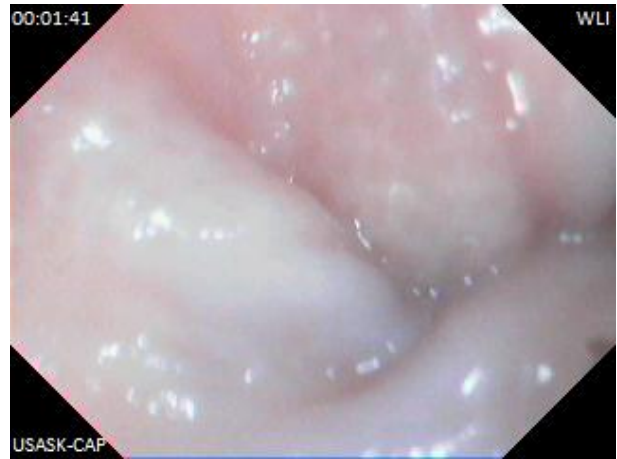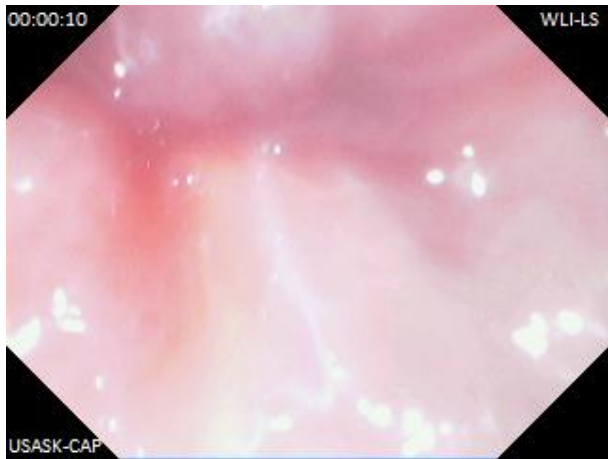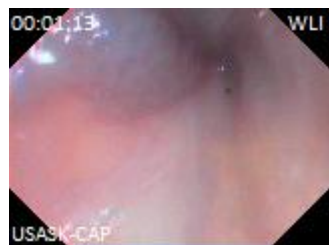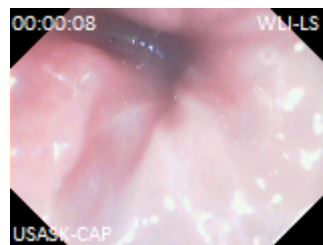
Figure 8.4 Captured QVGA size WLI images from pig's intestine:

(a) lossy compression mode, CR = 81.87%; (b) lossy compression mode, CR = 82.29%;

(c) lossless compression mode, CR = 78.71%; (d) lossless compression mode, CR = 75.61%;

Figure 8.5 Captured QQVGA size WLI images from pig's intestine:

(a) lossy compression mode, CR = 81.19%; (b) lossless compression mode, CR = 75.08%;
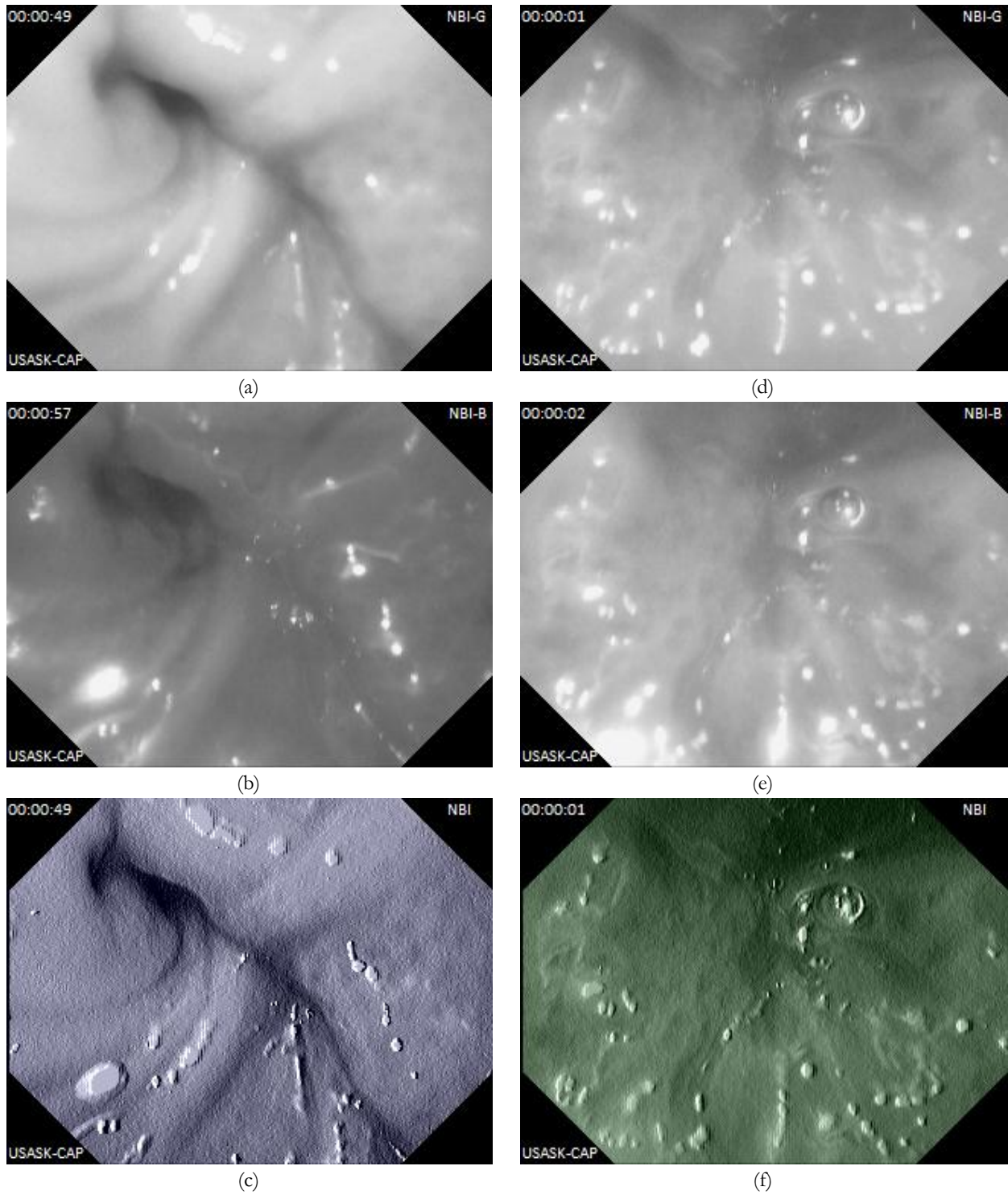
Figure 8.6 Captured NBI images from pig's intestine: (a) grayscale image with green light only, CR = 84.31%; (b) grayscale image with blue light only, CR = 84.11%; (c) Combined pseudo color NBI image from (a) and (b); (d) grayscale image with green light only, CR = 83.95%; (e) grayscale image with blue light only, CR = 83.87%; (f) Combined pseudo color NBI image from (d) and (e)

In the experiment, the capsule prototype is also covered by approximately 40 mm thickness of extra intestine in order to make the scenario of skin and flesh over the intestine. In this scenario, images are also successfully transmitted through the 40 mm thick tissues.

During the experiment, the distance between the capsule and the data logger is varied from 0.3 m to 1 m and images are transmitted successfully. As the data logger is wearable and it is generally worn at one side of the belly, the distance between a swallowed capsule and data logger will be near 0.3 meter for human endoscopy.

8.2.2.4 Discussion

In this experiment, good quality images have been captured by the capsule. The detailed features of the mucosa are visible in both lossy and lossless images. The compression ratio of the images in the real experiments are similar (sometimes slightly higher) than the compression ratio estimated by simulations in Chapter 3 and in Chapter 4.

The hardware components selected for the capsule and data logger prototype worked as expected. However, there were several unknown issues that were identified during experimentation. It has been found that the RF transceiver's [108] application throughput can go low due to environmental condition which affects the FPS of the image transmission. Also, the image sensor in [34] is designed for 15-30 FPS application, however, in capsule endoscopy, 2-4 FPS is required. In order to get low FPS, the sensor is clocked with low frequency clock and for this reason, the captured images can become blured if the capsule is moving as the light exposure time of the image sensor is increased.

8.3   Summary

In this chapter, ex-vivo experiments with pig's small intestine is conducted to verify the performance of the developed WCE system. Good quality images are successfully captured and transmitted by

the capsule, which validates the proposed compressor's performance in realistic scenario. The developed WCE system components (the capsule, data logger and the workstation software) worked properly during the experiments.

Part IV: **Conclusion**

Chapter 9: Summary and Conclusion

9.1   Summary

The works done in this thesis can be summarized as follows:

- Low-complexity image compression algorithms have been developed for capsule endoscopy by identifying the unique properties of endoscopic images. The algorithm consists of a novel color space, referred as YEF, and differential pulse coded modulation (DPCM) followed by optimized Golomb-Rice coding. Based on the nature of endoscopic images, several sub-sampling schemes on the chrominance components are applied. A customized corner clipping algorithm has also been introduced.

- The proposed compressor is tuned to work with both white light imaging (WLI) and narrow band imaging (NBI).

- Both lossy and lossless version of the compression algorithm are constructed.

- In order to visually evaluate the quality of the lossy reconstructed images, subjective evaluation by conducting two surveys among professional medical imaging doctors have been conducted.

- The proposed image compressors have been modeled in HDL and verified in FPGA board. Later, it is implemented in a 0.18 μm CMOS technology and the chip has been fabricated.

- A complete WCE system prototype consisting of an FPGA based electronic capsule, a microcontroller based data logger unit and a Windows based image reconstruction software have been developed.

- Ex-vivo testing in pig's intestine has been conducted to validate the performance of the developed WCE system prototype.

9.2   Discussion and conclusion

The proposed lossy compression algorithm, as discussed in Chapter 3, can produce an average compression ratio of more than 80% and the lossless compressor, as discussed in Chapter 4, can produce an average compression ratio of 75%. By using the proposed the compressors, only 1/5th to 1/4th of the total image data can be transmitted from the capsule, thus data can be fit in the limited bandwidth of the RF transceiver and also RF transmission power can be saved.

For the lossy image compressor, the reconstructed image quality have high PSNR index, over 43.7dB for both WLI and NBI. Moreover, the lossy reconstructed images have been visually verified by several medical imaging doctors and the images have been ranked as "highly acceptable". For the lossless compressor, the reconstructed image is identical with the original input image without any loss or distortion.

The compressor is implemented in hardware in such a way that a single hardware can be configured to produce both lossy and lossless compressed bit stream for both WLI and NBI modes. It can be directly interfaced with commercial image sensors that output pixels in raster scan fashion, eliminating the need of any input buffer memory. The compressor have been synthesized in FPGA board and successfully tested by connecting a commercial image sensor [34]. Due to the low

complexity of the core compressor, it consumes only 43 μW of power and 0.032 mm^2 of area when implemented in 0.18μm CMOS technology.

A miniature field programmable gate array (FPGA) based electronic capsule is designed and developed as discussed in Chapter 5. The capsule contains the proposed low complexity image compressor and can generate both lossy and lossless compressed bit-stream. The capsule prototype also supports both WLI and NBI modes and communicates with the data logger in full duplex fashion, which enables configuring the image size and imaging mode, compression mode, in real time during the examination from the data logger. The capsule is prototype has 4 PCBs, each having a diameter of 16 mm and the prototype has battery life of 8.5 hours.

The data logger presented in Chapter 6 is portable, has high memory capacity of 4 GB micro secure digital (SD) card, graphical display for showing real time endoscopic images, keypad and touch screen based graphical user interface. After logging, the data can be transferred to PC using a SD card reader at a speed of up to 25 MB/sec or using an USB interface. Optionally, the data can also be transferred to PC or Smartphone wirelessly using Bluetooth technology.

The PC software, as described in Chapter 7 is able to decode and show the reinstructed images and can play them as video at any given FPS.

The developed WCE system has been tested in pig's intestine, as discussed in Chapter 8, and good quality images have been captured by the capsule prototype. The compression ratio estimated from simulation results in Chapter 3 and Chapter 4 matched with the real world implementation.

The hardware components selected for the capsule and data logger prototype worked as expected. However, there were several unknown issues that were identified during experimentation such as application throughput of the RF transceiver [108], blurring of images when the capsule moves fast due to lowering the input clock frequency of the image sensor [34], focal length adjustment of the lens, light intensity control etc.

From the above discussion, it can be concluded that the thesis objectives mentioned in Section 1.3 are fulfilled and met.

9.3   Future work

There are several future works that can be done in order to take the research in the next level, they are listed below:

- The size of the capsule can be reduced more to make it swallowable. The design challenges include miniature multilayer PCB design, fabrication, assembling, and packaging processes which take significant amount of time, money, and human resource. After making smaller size capsule prototypes, tests with several human patients need to be performed.

- Dedicated low FPS image sensor and high application throughput RF transceiver for capsule endoscopy can be designed, fabricated and integrated with the existing design.

- Several other bio-sensors such as temperature, pH, etc. can be integrated with the capsule and the data can be wirelessly transmitted and monitored in real time.

- Works can be done on localization of the capsule.

- Integrating hardware for robotic legs, drug delivery, tissue sampling etc. with the capsule can be done.

- Image enhancement and segmentation issues of the reconstructed images in the PC software can be explored.

Part V: **Appendix**

A. List of Publications

A list of publications is shown below, according to the correspondence of the thesis chapters, which are generated from the research during my doctoral program.

A.1   Published peer reviewed journals

Chapter 3: *Lossy Compression Algorithm*

[J1] **T. H. Khan** and K. Wahid, "Low complexity color-space for capsule endoscopy image compression," *IET Electronics Letters,* vol. 47, no. 22, pp. 1217-1218, doi: 10.1049/el.2011.2211, 2011.

[J2] **T. H. Khan** and K. Wahid, "Low power and low complexity compressor for video capsule endoscopy," *IEEE Transactions on Circuits and Systems for Video Technology*, vol. 21, no. 10, pp. 1534-1546, doi: 10.1109/TCSVT.2011.2163985, 2011.

[J3] **T. H. Khan** and K. Wahid, "Subsample-based image compression for capsule endoscopy," *Journal of Real-time Image Processing,* Springer, doi: 10.1007/s11554-011-0208-7, 2011.

Chapter 4: *Lossless Compression Algorithm*

[J4] **T. H. Khan** and K. Wahid, "Lossless and low power image compressor for wireless capsule endoscopy," *VLSI Design, Hindawi Publishing Corporation*, vol. 2011, Article ID 343787, New York, USA, 2011.

[J5] **T. H. Khan** and K. Wahid, "An advanced physiological data logger for medical imaging applications," *EURASIP Journal on Embedded Systems*, *Springer*, 2012:10, doi:10.1186/1687-3963-2012-10, 2012.

Below are some works published during the doctoral program which are not directly related with the thesis:

[J6] **T. H. Khan** and K. Wahid, "A DVP-based bridge architecture to randomly access pixels of high speed image sensors," *EURASIP Journal on Embedded Systems*, *Hindawi Publishing Corporation*, vol. 2011, Article ID 270908, New York, USA, 2011.

[J7] **T. H. Khan** and K. Wahid, "Universal bridge interface for DVP-compatible image sensors," *Microprocessors and Microsystems, Elsevier*, vol. 35, issue. 6, pp. 547-556, 2011.

A.2 Published conference papers

(* indicates related with this thesis)

[C1] A. Mostafa, **T. H. Khan**, K. Wahid, and S. B. Ko, "Efficient color space-based compression scheme for endoscopic images," *In Proc. International Conference on Information Sciences, Signal Processing and their Applications (ISSPA),* pp. 83 - 86, Montreal, QC, Canada, July 2012. *

[C2] **T. H. Khan** and K. Wahid, "Implantable narrow band image compressor for capsule endoscopy," In *Proc. IEEE International Symposium on Circuits and Systems (ISCAS),* pp. 2203 - 2206, Seoul, Korea, May 2012. *

[C3] **T. H. Khan** and K. Wahid, *"*Design of a DVP compatible bridge to randomly access pixels of high speed image sensors," In *Proc. IEEE International Conference on Consumer Electronics (ICCE),* pp. 911-912, Las Vegas, USA, January 2011.

[C4] **T. H. Khan**, G. M. Shahabuddin, and K. Wahid, "Design of a bridge to randomly access high speed image sensor pixels in embedded systems," *In Proc. International Conference on Electrical & Computer Engineering (ICECE),* pp. 450-453, Dhaka, Bangladesh, December 2010.

[C5] **T. H. Khan** and K. Wahid, "Towards design of a bridge to enable high speed image sensors for random access," In *Proc IEEE International Conference on Microelectronics (ICM),* pp. 431-434, Cairo, Egypt, December 2010.

A.3   Published book chapters

[B1] **T. H. Khan** and K. Wahid, "Low-cost VLSI architecture for random block-based access of pixels in modern image sensors", in *Embedded Systems: Hardware, Design, and Implementation*, 1st edition, John Wiley & Sons, Inc, 2013, ch. 4, pp. 107-126, 2012. ISBN: 978-1-1183-5215-1.

B. List of Patent Applications

The following patent applications have been filed, among them [P1] is directly originated from the thesis and [P2] is not directly related with this thesis.

[P1] **T. H. Khan** and K. Wahid, "Methods and apparatus for image processing in wireless capsule endoscopy," *Canadian patent application no: 2,773,795* and *US patent application no: 13/444,222*, filed on Apr 11th, 2012.

[P2] **T. H. Khan** and K. Wahid, "Apparatus, methods and systems for randomly accessing pixel data from streaming image sensor data," *Canadian patent application no: 2,762,356* and *US patent application no: 13/328,503*, filed on Dec 16th, 2011.

C. Survey Questions and Images

C.1   First survey

The first survey contained the original and reconstructed image pairs as shown in Figure C.1 and the following multiple choice question was placed for each image pairs:

Please provide your opinion on the quality of the reconstructed image:

- o   **Excellent (no visual difference)**

- o   **Good (highly acceptable)**
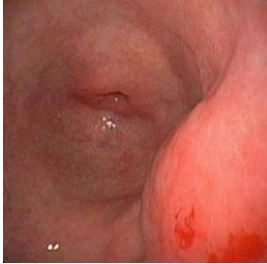
- o   **Average (marginally acceptable)**

- o   **Poor (not acceptable)**
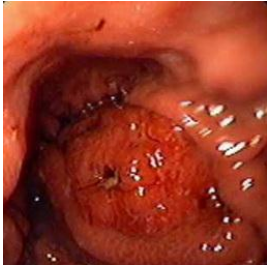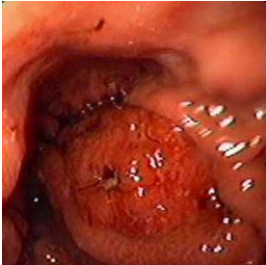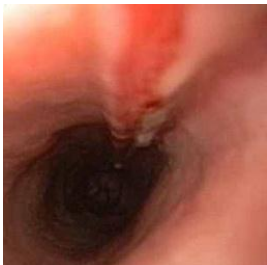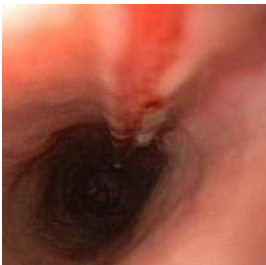
Image No.	Original	Reconstructed (YEF812)
1		
2		
3		
4		
5		

Figure C.1 Original and reconstructed image pairs for the first survey

C.2   Second survey

The second survey contained the original and reconstructed image pairs along with the disease or condition mentioned as shown in Figure C.2 and the following multiple choice question was placed for each image pairs:

Does the reconstructed image (shown in the right) provides sufficient information to detect the above mentioned condition (disease)?

- o   **Yes, no doubt**
- o   **Yes, sufficiently enough information**
- o   **Neutral, unsure**
- o   **No, not enough information**
- o   **No, not at all**
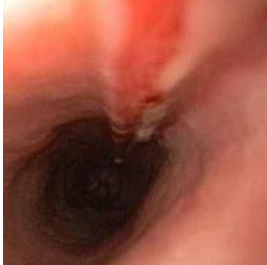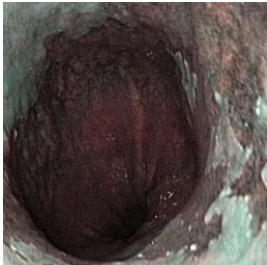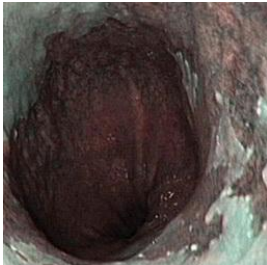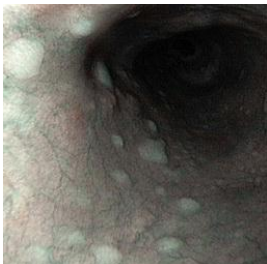
Image No.	Original	Reconstructed (YEF812)	Disease
1			Hyperplastic polyps in the gastric body
2			Oesophageal lesion Caused by a sharp chicken bone
3			Cancer in the Sigmoid Colon
4			Barrets oesophagus
5			Oesophageal glycogenic acanthosis

Figure C.2 Original and reconstructed image pairs for the second survey

REFERENCES

[1] J. L. Toennies, G. Tortora, M. Simi, P. Valdastri and R. J. Webster, "Swallowable medical devices for diagnosis and surgery: the state of the art," *J. Mechanical Engineering Science,* vol. 224, pp. 1397-1414, 2009.

[2] D. Faigel and D. Cave, Capsule Endoscopy, Saunders Elsivier, 2008.

[3] C. McCaffrey, O. Chevalerias, C. O'Mathuna and K. Twomey, "Swallowable-capsule technology," *IEEE Pervasive Computing,* vol. 7, no. 1, pp. 23 - 29, 2008.

[4] A. Moglia, A. Menciassi and P. Dario, "Recent patents on wireless capsule endoscopy," *Recent Patents on Biomedical Engineering,* vol. 1, no. 1, pp. 24-33, 2008.

[5] G. Iddan, G. Meron, A. Glukhovsky and P. Swain, "Wireless Capsule Endoscopy," *Nature,* vol. 405, p. 417, 2000.

[6] F. Gong, P. Swain and T. Mills, "Wireless Endoscopy," *Gastrointestinal Endoscopy,* vol. 51, no. 6, pp. 725-729, 2000.

[7] Z. Fireman and Y. Kopelman, "New frontiers in capsule endoscopy," *Journal of Gastroenterology and Hepatology: Review,* vol. 22, pp. 1174 - 1177, 2007.

[8] P. Swain, "The future of wireless capsule endoscopy," *World Journal of Gastroenterology,* vol. 14, no. 26, pp. 4142 - 4145, 2008.

[9] "Preparing for Capsule Endoscopy," American Gastroenterological Association, 2013. [Online]. Available: http://www.gastro.org/patient-center/procedures/capsule-endoscopy.

[10] L. M. Song, D. G. Adler, J. D. Conway, D. L. Diehl, F. A. Farraye, S. V. Kantsevoy, R. Kwon, P. Mamula, B. Rodriguez, R. J. Shah and W. M. Tierney, "Narrow band imaging and multiband imaging," *Gastrointestinal Endoscopy,* vol. 67, no. 4, pp. 581- 589, 2008.

[11] S. Danese, G. Fiorino, E. Angelucci, S. Vetrano, N. Pagano, G. Rando, A. Spinelli, A. Malesci and A. Repici, "Narrow-band imaging endoscopy to assess mucosal angiogenesis in inflammatory bowel disease: A pilot study," *World J Gastroenterol,* vol. 16, no. 19, pp. 2396 - 2400, 2010.

[12] C. Gheorghe, "Narrow-band imaging endoscopy for diagnosis of malignant and premalignant gastrointestinal lesions," *Journal on Gastrointest Liver Dis,* vol. 15, no. 1, pp. 77-82, 2006.

[13] X. Chen, X. Zhang, L. Zhang, X. Li, N. Qi, H. Jiang and Z. Wang, "A wireless capsule endoscope system with low power controlling and processing ASIC," *IEEE Transactions on Biomedical Circuits and Systems,* vol. 3, no. 1, pp. 11-22, 2009.

[14] M. Quirini, A. Menciassi, C. Stefanini, S. Gorini, G. Pernorio and P. Dario, "Development of a legged capsule for the gastrointestinal tract: an experimental set-up," in *IEEE International Conference on Robotics and Biomimetic*, 2005.

[15] N. Bourbakis, G. Giakos and A. Karargyris, "Design of new-generation robotic capsules for therapeutic and diagnostic endoscopy," in *IEEE Int. Conf. on Imaging Systems and Techniques*, 2010.

[16] M. Meng, T. Mei, J. Pu, C. Hu, X. Wang and Y. Chan, "Wireless robotic capsule endoscopy: state-of-the-art and challenges," in *World Congress on Intelligent Control and Automation*, 2004.

[17] S. Hosseini and M. Khamesee, "Design and control of a magnetically driven capsule-robot for endoscopy and drug delivery," in *IEEE Toronto International Conference Science and Technology for Humanity*, 2009.

[18] O. Alonso, L. Freixas and A. Dieguez, "Advancing towards smart endoscopy with specific electronics to enable locomotion and focusing capabilities in a wireless endoscopic capsule robot," in *IEEE Biomedical Circuits and Systems Conference*, 2009.

[19] A. Kolar, O. Romain, J. Ayoub, S. Viateur and B. Granado, "Prototype of video endoscopic capsule with 3-D imaging capabilities," *IEEE Trans. on Biomedical Cir. and Sys.,* vol. 4, no. 4, pp. 239 - 249, 2010.

[20] Y. Gu, X. Xie, G. Li, T. Sun, Q. Zhang, Z. Wang and Z. Wang, "A new system design of the multi-view micro-ball endoscopy system," in *IEEE Engineering in Medicine and Biology Society (EMBC)*, 2010.

[21] K. Seshadrinathan, R. Soundararajan, A. Bovik and L. K. Cormack, "Study of subjective and objective quality assessment of video," *IEEE Trans. on Im. Pro.,* vol. 19, no. 6, pp. 1427 - 1441, 2010.

[22] "Pillcam," Given Imaging, 2013. [Online]. Available: http://www.givenimaging.com/en-us/.

[23] "MiroCam," Intromedic, 2013. [Online]. Available: http://www.intromedic.com.

[24] "EndoCapsule," Olympus, [Online]. Available: http://www.olympus-europa.com.

[25] "Food and Drug Adminstartion," 2013. [Online]. Available: http://www.fda.gov.

[26] K. Wahid, S. Ko and D. Teng, "Efficient hardware implementation of an image compressor for wireless capsule endoscopy applications," in *Int. Joint Conference on Neural Networks*, 2008.

[27] P. Turcza and M. Duplaga, "Low-power image compression for wireless capsule endoscopy," in *IEEE International Workshop on Imaging Systems and Techniques*, 2007.

[28] M. Lin, L. Dung and P. Weng, "An ultra-low-power image compressor for capsule endoscope," *BioMedical Engineering OnLine,* vol. 5, no. 14, pp. 1 - 8, 2006.

[29]   Y. Gu, X. Xie, G. Li, T. Sun and Z. Wang, "Two-stage wireless capsule image compression with low complexity and high quality," *IET Electronics Letters,* vol. 48, no. 25, pp. 1588 - 1589, 2012.

[30]   M. Lin and L. Dung, "A subsample-based low-power image compressor for capsule gastrointestinal endoscopy," *EURASIP Journal on Advances in Signal Processing,* vol. 2011, no. 257095, 2011.

[31]   L. Dung, Y. Wu, H. C. Lai and P. Weng, "A modified H.264 intra-frame video encoder for capsule endoscope," in *IEEE Biomedical Circuits and Systems Conference*, 2008.

[32]   C. Cheng, Z. Liu, C. Hu and M. Meng, "A Novel Wireless Capsule Endoscope With JPEG Compression Engine," in *IEEE Int. Conf. on Automation and Logistics*, 2010.

[33]   J. Li and Y. Deng, "Fast compression algorithms for capsule endoscope images," in *International Congress on Image and Signal Processing*, 2009.

[34]   "TCM8230MD Image Sensor," Toshiba , 2013. [Online]. Available: https://www.sparkfun.com/products/8667.

[35]   "OVM7692 CameraCube," OmniVisoin, 2013. [Online]. Available: http://www.ovt.com/products/category.php?id=21.

[36]   "MT9V011 Image Sensor," Aptina, 2013. [Online]. Available: http://www.aptina.com/support/documentation.jsp?t=0&q=25.

[37]   "256k × 8 Bit Low Power CMOS SRAM (AS6C2008)," Alliance Memory Inc., 2013. [Online]. Available: http://www.alliancememory.com.

[38]   J. Ziv and A. Lempel, "A universal algorithm for sequential data compression," *IEEE Transactions on Information Theory,* vol. 23, no. 3, pp. 337 - 343, 1977.

[39] R. Tajallipour and K. Wahid, "Efficient data encoder for low-power capsule endoscopy application," in *Int. Conf. on Information Sciences Signal Processing and their Applications*, 2010.

[40] D. Turgis and R. Puers, "Image compression in video radio transmission for capsule endoscopy," *Elsevier Sensors and Actuators A,* pp. 129 - 136, 2005.

[41] S. Rigler, W. Bishop and A. Kennings, "FPGA-based lossless data compression using Huffman and LZ77 algorithms," in *IEEE Canadian Conf. on Elec. and Comp. Engin.*, 2007.

[42] J. Wu and Y. Li, "Low-complexity video compression for capsule endoscope based on compressed sensing theory," in *Int. Conf. of the IEEE Eng. in Medicine and Biology Society*, 2009.

[43] M. Meira, J. Lima and L. Batista, "An FPGA impementation of a lossless electrocardiogram compressor based on prediction and golomb-rice coding," in *Workshop de Informática Médica*, 2005.

[44] S. Golomb, "Run-length encodings," *IEEE Transactions on Information Theory,* vol. 12, no. 3, pp. 399 - 401, 1966.

[45] C. Hu, M. Meng, L. Liu, Y. Pan and Z. Liu, "Image representation and compression for capsule endoscope robot," in *IEEE International Conference on Information and Automation*, 2009.

[46] "Lossless and near-lossless compression of continuous-tone still images - Baseline," ITU-T Recommendation T.87, 1998.

[47] M. Weinberger, G. Seroussi and G. Sapiro, "The LOCO-I lossless image compression algorithm: principles and standardization into JPEG-LS," *IEEE Trans. on Image Proc,* vol. 9, no. 8, pp. 1309 - 1324, 2000.

[48] X. Xiang, L. Guolin, C. Xinkai, L. Xiaowen and Z. Wang, "A low-power digital IC design inside the wireless endoscopic capsule," *IEEE Journal of Solid-State Circuits,* vol. 41, no. 11, pp.

2390 - 2400, 2006.

[49]   A. Savakis and M. Piorun, "Benchmarking and hardware implementation of JPEG-LS," in *International Conference on Image Processing*, 2002.

[50]   M. Papadonikolakis, V. Pantazis and A. Kakarountas, "Efficient high-performance ASIC implementation of JPEG-LS encoder," in *Design, Automation & Test in Europe Conf. & Ex.*, 2007.

[51]   "TCM8240MD CMOS Camera," Toshiba, 2013. [Online]. Available: https://www.sparkfun.com/datasheets/Sensors/Imaging/TCM8240MD_E150405_REV13.pdf.

[52]   "JPEG Color Camera TTL Interface," LinkSprite, 2013. [Online]. Available: https://www.sparkfun.com/products/11610.

[53]   "OmniVision's CameraMate™ ASIC (500/600 Series)," OmniVision, 2013. [Online]. Available: http://www.ovt.com/products/ip_table.php.

[54]   C. Cavallotti, P. Merlino, M. Vatteroni, P. Valdastri, A. Abramo, A. Menciassi and P. Dario, "An FPGA-based versatile development system for endoscopic capsule design optimization," *Sensors and Actuators A: Physical, Elsevier,* vol. 172, no. 1, pp. 301 - 307, 2011.

[55]   D. Covi, C. Cavallotti, M. Vatteroni, L. Clementel, P. Valdastri, A. Menciassi, P. Dario and A. Sartori, "Miniaturized digital camera system for disposable endoscopic applications," *Sensors and Actuators A,* vol. 162, no. 2, pp. 291-296, 2010.

[56]   F. S. Sussman and K. Kulkarni, "Risks of Capsule Endoscopy," *Tech Gastrointest Endosc, Elsevier,* vol. 10, pp. 25 - 30, 2008.

[57]   L. Dung and Y. Wu, "A wireless narrowband imaging chip for capsule endoscope," *IEEE*

Transactions on Biomedical Circuits and Systems, vol. 4, no. 6, pp. 462 - 468, 2010.

[58] K. Kim, S. Yun, S. Lee, S. Nam, Y. J. Yoon and C. Cheon, "A design of a high-speed and high-efficiency capsule endoscopy system," *IEEE Transactions on Biomedical Engineering,* vol. 59, no. 4, pp. 1005 - 1011, 2012.

[59] Y. Chan, M. Q. H. Meng and X. Wang, "A prototype design of a wireless capsule endoscope," in *IEEE International Conference on Mechatronics & Automation*, 2005.

[60] H. Qian, L. Xiao-gang, X. Bin-feng and P. Cheng-lin, "A wireless endoscope based on an embedded system," *Journal of Chongqing University,* vol. 7, no. 3, pp. 241 - 246, 2008.

[61] C. Cavallotti, M. Piccigallo, E. Susilo, P. Valdastri, A. Menciassi and P. Dario, "An integrated vision system with autofocus for wireless capsular endoscopy," *Sensors and Actuators A,* vol. 156, no. 1, pp. 72 - 78, 2009.

[62] G. Cybulski, A. Ksiazkiewicz, W. Lukasik, W. Niewiadomski and T. Palko, "Ambulatory monitoring device for central hemodynamic and ECG signal recording on PCMCI flash memory cards," *Computers in Cardiology 1995,* pp. 505 - 507, 1995.

[63] R. Rieger and Y.-R. Huang, "A custom-design data logger core for physiological signal recording," *IEEE Transactions on Instrumentation and Measurement,* vol. 60, no. 2, pp. 532 - 538, 2011.

[64] B. Hermans and R. Puers, "A portable multi-sensor data-logger for medical surveillance in harsh environments," *Sensors and Actuators A: Physical, Elsevier,* Vols. 123 - 124, pp. 423-429, 2005.

[65] F. S. Jaw, Y. L. Tseng and J. K. Jang, "Modular design of a long-term portable recorder for physiological signals," *Measurement, Elsevier,* vol. 43, no. 10, pp. 1363 - 1368, 2010.

[66] R. K. Kamat, S. A. Shinde, P. K. Gaikwad and H. Guhilot, "Analog front end and FPGA based soft IP core for ECG logger," in *Harnessing VLSI System Design with EDA Tools*, Springer, 2012, pp. 51 - 91.

[67] P. Augustyniak, "Wearable wireless heart rate monitor for continuous long-term variability studies," *Journal of Electrocardiology, Elsevier,* vol. 44, no. 2, pp. 195 - 200, 2011.

[68] F. Ahmed, M. M. Ali and E. Zahedi, "Development of a portable fetal and maternal heart rate recorder for 24 hours," in *IEEE Engineering in Medicine and Biology Society*, 2000.

[69] E. Ryo, K. Nishihara, S. Matsumoto and H. Kamata, "A new method for long-term home monitoring of fetal movement by pregnant women themselves," *Medical Engineering & Physics, Elsevier,* vol. 34, no. 5, pp. 566 - 572, 2012.

[70] R. Luharuka, R. X. Gao and S. Krishnamurty, "Design and realization of a portable data logger for physiological sensing [GSR]," *IEEE Transactions on Instrumentation and Measurement,* vol. 52, no. 4, pp. 1289 - 1295, 2003.

[71] A. Salarian, H. Russmann, F. Vingerhoets, P. Burkhard and K. Aminian, "Ambulatory monitoring of physical activities in patients with Parkinson's disease," *IEEE Transactions on Biomedical Engineering,* vol. 54, no. 12, pp. 2296 - 2299, 2007.

[72] C. Tronstad, S. Grimnes, Ø. G. Martinsen and E. Fosse, "Development of a medical device for long-term sweat activity measurements," in *IFMBE, Springer-Verlag*, 2007.

[73] C. Chao and C. Pomalaza-Raez, "Design and evaluation of a wireless body sensor system for smart home health monitoring," in *IEEE Global Telecommunications Conference*, 2009.

[74] A. Takeuchi, N. Mamorita, F. Sakai and N. Ikeda, "Development of a comprehensive medical recorder on a cellphone," *Computer Methods and Programs in Biomedicine, Elsevier,* vol. 97, no. 1, pp. 28 - 38, 2010.

[75] J. Cunha, M. Coimbra, P. Campos and J. M. Soares, "Automated topographic segmentation and transit time estimation in endoscopic capsule exams," *IEEE Transactions on Medical Imaging,* vol. 27, no. 1, pp. 19 - 27, 2008.

[76] M. Mackiewicz, J. Berens and M. Fisher, "Wireless capsule endoscopy color video segmentation," *IEEE Transactions On Medical Imaging,* vol. 27, no. 12, pp. 1769 - 1781, 2008.

[77] R. Coriat, A. Chryssostalis, J. Zeitoun, J. Deyra, M. Gaudric, F. Prat and S. Chaussade, "Computed virtual chromoendoscopy system (FICE): A new tool for upper endoscopy?," *Gastroentérologie Clinique et Biologique,* vol. 32, no. 4, pp. 363 - 369, 2008.

[78] P. Cosman, R. Gray and R. Olshen, "Evaluating Quality of Com¬pressed Medical Images: SNR, Subjective Rating, and Diagnostic Accuracy," *Proc. of the IEEE,* vol. 82, no. 6, pp. 919 - 932, 1994.

[79] R. Istepanian, N. Philip, M. Martini, N. Amso and P. Shorvon, "Subjective and objective quality assessment in wireless teleultrasonography imaging," in *Int. Conf. of the IEEE Engineering in Medicine and Biology Society*, 2008.

[80] Z. Wang, A. C. Bovik, H. R. Sheikh and E. P. Simoncelli, "Image quality assessment: From error visibility to structural similarity," *IEEE Transactions on Image Processing,* vol. 13, no. 4, pp. 600 - 612, 2004.

[81] H. R. Sheikh and A. Bovik, "Image information and visual quality," *IEEE Trans. on Image Processing,* vol. 15, no. 2, pp. 430 - 444, 2006.

[82] D. M. Chandler and S. S. Hemami, "VSNR: A wavelet-based visual signal-to-noise ratio for natural images," *IEEE Transactions on Image Processing,* vol. 16, no. 9, pp. 2284 - 2298, 2007.

[83] "Gastrolab," 2013. [Online]. Available: http://www.gastrolab.net.

[84] C. Shannon, "A mathematical theory of communication," *Bell Syst. Tech. J.,* vol. 27, pp. 379 - 423, 1948.

[85] D. Salomon, Data Compression: The Complete Reference, 3rd ed., Springer-Verlag, 2004.

[86] "Color Models," Intel® Developer Zone, 2013. [Online]. Available: http://software.intel.com/sites/products/documentation/hpc/ipp/ippi/ippi_ch6/ch6_color _models.html.

[87] H. S. Malvar, G. J. Sullivan and S. Srinivasan, "Lifting-based reversible color transformations for image compression," in *SPIE Applications of Digital Image Processing XXXI*, 2008.

[88] G. Chan, "Towards Better Chroma Subsampling," *SMPTE Journal,* vol. 05/06 May/June, no. 2008, 2008.

[89] S. S. Young, "Alias-free image subsampling using Fourier-based windowing methods," *Opt. Eng.,* vol. 43, no. 4, 2004.

[90] Z. Wang and A. C. Bovik, *Mean Squared Error: Love It or Leave It?,* IEEE Signal Processing Magazine, 2009, pp. 98 - 117.

[91] E. A. Krupinski, "Current perspectives in medical image perception," *Attention, Perception, & Psychophysics,* vol. 72, no. 5, pp. 1205 - 1217, 2010.

[92] E. Krupinski, "The importance of perception research in medical imaging," *Radiation Medicine,* vol. 18, no. 6, pp. 329 - 334, 2000.

[93] R. Bourne, Fundamentals of Digital Imaging in Medicine, Springer-Verlag London Limited, 2010, pp. 87 - 107.

[94] D. Tokuhara, K. Watanabe, Y. Okano, A. Tada, K. Yamato, T. Mochizuki, J. Takaya, T. Yamano and T. Arakawa, "Wireless capsule endoscopy in pediatric patients: the first series

from Japan," *J Gastroenterol, Springer,* vol. 45, pp. 683 - 691, 2010.

[95] T. Fawcett, "An introduction to ROC analysis," *Pattern Recognition Letters - Special issue: ROC analysis in pattern recognition,* vol. 27, no. 8, pp. 861 - 874, 2006.

[96] L. Pillai, "Video compression using DCT," Xilinx Application Note: Virtex-II Series, 2002.

[97] "Introduction to I²C and SPI protocols," 2013. [Online]. Available: http://www.byteparadigm.com/applications/introduction-to-i2c-and-spi-protocols.

[98] "White LED, CMD67-21UWCCT-ND," Chicago Miniature Lighting, 2013. [Online]. Available: http://www.chml.com/products/pdf/1-22.pdf.

[99] "Blue LED, SM1206UV-405-IL," Bivar, Inc., 2013. [Online]. Available: http://www.bivar.com/Images/Cart/SM1206UV-405-IL.pdf.

[100] "Green LED, LNJ624C4CRA," Panasonic Corporation, 2013. [Online]. Available: http://www.semicon.panasonic.co.jp/ds4/LNJ624C4CRA_AEK_discon.pdf.

[101] "MachXO2-2000 FPGA," Lattice Semiconductor, 2013. [Online]. Available: http://www.latticesemi.com/en/Products/FPGAandCPLD/MachXO2.aspx.

[102] J. Kathuria, M. A. Khan and A. Noor, "A review of clock gating techniques," *MIT International Journal of electronics and Communication Engineering,* vol. 1, no. 2, pp. 106 - 114, 2011.

[103] J. L. Shumaker, "Interfacing the TCM8230MD CMOS camera with an ARM7 microcontroller," Army Research Laboratory, 2009.

[104] R. Mahmud, "Techniques to make clock switching glitch free," EE Times, 2013. [Online]. Available: http://www.eetimes.com/story/OEG20030626S0035.

[105] "FCC rules and regulations 47 CFR Part 95, subparts E (95.601-95.673) and I (95.1201-95.1219), Personal Radio Services," 2002.

[106] "ZL70102 MICS transceiver," Microsemi Corporation, 2013. [Online]. Available: http://www.microsemi.com/ultra-low-power-wireless/implantable-medical-transceivers/zl70102.

[107] A. R. Kahn, E. Y. Chow, O. A. Latief and P. P. Irazoqui, "Low-power, high data rate transceiver system for implantable prostheses," *International Journal of Telemedicine and Applications,* vol. 2010, no. 563903, 2010.

[108] "nRF24L01+ transceiver," Nordic Semiconductor, 2013. [Online]. Available: http://www.nordicsemi.com/eng/Products/2.4GHz-RF/nRF24L01P.

[109] P. Valdastri, A. Menciassi and P. Dario, "Transmission power requirements for novel Zigbee implants in the gastrointestinal tract," *IEEE Transactions On Biomedical Engineering,* vol. 55, no. 6, pp. 1705 - 1710, 2008.

[110] "Coin cell battery, 357/303H," Energizer, 2013. [Online]. Available: http://data.energizer.com/PDFs/357-303hz.pdf.

[111] "Low dropout regulator, ADP121," Analog Devices, 2013. [Online]. Available: http://www.analog.com/static/imported-files/data_sheets/ADP121.pdf.

[112] "Micro-Miniature Reed Sensor, MK24-B-2-OE," Meder Electronic, 2013. [Online]. Available: http://www.meder.com/fileadmin/meder/pdf/en/Products/Reed_Sensors/Reed_Sensor_MK24_E.pdf.

[113] Bittele Electronics , 2013. [Online]. Available: http://www.bittele.com/.

[114] Tortai Technologies, 2013. [Online]. Available: http://www.tortai-tech.com/.

[115] "Lattice Diamond," Lattice, 2013. [Online]. Available: http://www.latticesemi.com/LatticeDiamond.

[116] S. Diao, Y. Zheng, Y. Gao, C. H. Heng and M. Je, "A 7.2mW 15Mbps ASK CMOS transmitter for ingestible capsule endoscopy," in *IEEE Asia Pacific Conference on Circuits and Systems (APCCAS)*, 2010.

[117] M. Shen, C. Lee and J. Bor, "A 4.0-mW 2-Mbps programmable BFSK transmitter for capsule endoscope applications," in *IEEE Asian Solid-State Circuits Conference*, 2005.

[118] S. Itoh, S. Kawahito and S. Terakawa, "A 2.6mW 2fps QVGA CMOS one-chip wireless camera with digital image transmission function for capsule endoscopes," in *IEEE International Symposium on Circuits and Systems (ISCAS)*, 2006.

[119] J. Thoné, S. Radiom, D. Turgis, R. Carta, G. Gielen and R. Puers, "Design of a 2 Mbps FSK near-field transmitter for wireless capsule endoscopy," *Sensors and Actuators A: Physical,* vol. 156, no. 1, pp. 43 - 48, 2009.

[120] S. Stoa, R. C. Santiago and I. Balasingham, "An ultra wideband communication channel model for capsule endoscopy," in *International Symposium on Applied Sciences in Biomedical and Communication Technologies (ISABEL)*, 2010.

[121] M. Rasouli, A. P. Kencana, V. A. Huynh, E. K. Ting, J. C. Y. Lai, K. J. Wong, S. L. Tan and S. J. Phee, "Ingestible wireless capsules for enhanced diagnostic inspection of gastrointestinal tract," *Front. Mech. Eng.,* vol. 6, no. 1, pp. 40 - 44, 2011.

[122] P. Corbishley and E. Rodriguez-Villegas, "Breathing detection: Towards a miniaturized, wearable, battery-operated monitoring system," *IEEE Transactions on Biomedical Engineering,* vol. 55, no. 1, pp. 196 - 204, 2008.

[123] T. Deniz and A. Yilmaz, "Design and implementation of a digital ambulatory ECG recorder based on flash MultiMediaCard memory," in *IEEE 46th Midwest Symposium on Circuits and Systems*, 2003.

[124] U. Anliker, J. Ward, P. Lukowicz, G. Troster, F. Dolveck, M. Baer, F. Keita, E. Schenker, F. Catarsi, L. Coluccini, A. Belardinelli, D. Shklarski, M. Alon, E. Hirt, R. Schmid and M. Vuskovic, "AMON: A wearable multi parameter medical monitoring and alert system," *IEEE Transactions on Information Technology in Biomedicine,* vol. 8, no. 4, pp. 415 - 427, 2004.

[125] "AVR Microcontroller," Atmel Corporation, 2013. [Online]. Available: http://www.atmel.com/products/microcontrollers/avr/default.aspx.

[126] "Memory," Atmel Corporation, 2013. [Online]. Available: http://www.atmel.ca/products/memories/default.aspx.

[127] "microSD cards," SanDisk, 2013. [Online]. Available: http://www.sandisk.com/products/memory-cards/microsd.

[128] "Smart GPU," Vizic technologies, 2013. [Online]. Available: http://vizictechnologies.com/#/smart-gpu/4554296549.

[129] "LR series transmitter, TXM-433-LR," Linx Technologies, 2013. [Online]. Available: https://www.linxtechnologies.com/resources/data-guides/txm-xxx-lr.pdf.

[130] "QwikRadio™ UHF ASK Transmitter," Micrel, Inc, 2013. [Online]. Available: http://www.newark.com/pdfs/datasheets/Micrel/MICRF103.pdf.

[131] "XBee RF modules," DiGi, 2013. [Online]. Available: http://www.digi.com/products/wireless-wired-embedded-solutions/zigbee-rf-modules/point-multipoint-rfmodules/xbee-series1-module#overview.

[132] "Class 1 Bluetooth Module, RN-41," Roving Networks, 2013. [Online]. Available: http://www.rovingnetworks.com/products/RN_41.

[133] "TPS61200 boost converter," Texas Instruments, 2013. [Online]. Available:

http://www.ti.com/product/tps61200.

[134] "MCP73831/2 Linear charge management controller," Microchip Technology Inc, 2013. [Online]. Available: http://www.microchip.com/wwwproducts/Devices.aspx?dDocName=en024903.

[135] "AVR-DOS," MCS Electronics, 2013. [Online]. Available: http://www.mcselec.com/index.php?page=shop.product_details&flypage=shop.flypage&product_id=31&category_id=6&option=com_phpshop&Itemid=1.

[136] "2.4GHz dipole antenna," Chang Hong Technology Co., Ltd., 2013. [Online]. Available: http://www.sparkfun.com/datasheets/Wireless/Antenna/DA-24-04.pdf.

[137] E. S. Winokur, M. K. Delano and C. G. Sodini, "A wearable cardiac monitor for long-term data acquisition and analysis," *IEEE Transactions on Biomedical Engineering,* vol. 60, no. 1, pp. 189 - 192, 2013.

[138] M. Kopácová, I. Tachecí, J. Kvetina, J. Bureš, M. Kuneš, S. Špelda, V. Tycová, Z. Svoboda and S. Rejchrt, "Wireless video capsule enteroscopy in preclinical studies: methodical design of its applicability in experimental pigs," *Dig Dis Sci,* vol. 55, no. 3, pp. 626 - 630, 2010.

[139] "Prairie Swine Centre," 2013. [Online]. Available: http://www.prairieswine.com.

[140] "Research Ethics Office," University of Saskatchewan, 2013. [Online]. Available: http://www.usask.ca/research/ethics_review.

[141] "Western College of Veterinary Medicine," University of Saskatchewan, 2013. [Online]. Available: http://www.usask.ca/wcvm/index.php.